Tânia Filipa Gomes Castro

The study of the cardiotoxicity of targeted anticancer drugs: an *in vitro* metabolomic study

Tese incluída no Mestrado em Toxicologia Analítica, Clínica e Forense,

da Faculdade de Farmácia, Universidade do Porto

Trabalho realizado sob a orientação do(s) Professore(s):

Professora Doutora Vera Marisa Costa (Orientadora)

Professora Doutora Paula Guedes de Pinho (Co-orientadora)

Professor Doutor Félix Dias Carvalho (Co-orientador)

Outubro 2022

De acordo com a legislação em vigor, não é permitida a reprodução de qualquer parte desta tese.

According to the legislation in force, the reproduction of any part of this work is not allowed.

Acknowledgments

Após vários meses de trabalho, a conclusão desta dissertação só foi possível graças às muitas pessoas que me foram ajudando, de uma forma ou de outra, e às quais chegou o momento de agradecer.

Em primeiro lugar gostaria de agradecer à minha orientadora, à Professora Doutora Vera Marisa Costa, pelo apoio e dedicação incansável, pela paciência e disponibilidade. Agradeço imenso o seu empenho neste projeto e sobretudo a sua excelente orientação. Ao longo destes meses aprendi mesmo muito consigo e sem si nada disto teria sido possível.

À Professora Doutora Paula Guedes de Pinho, co-orientadora desta tese, muito obrigada pela sua ajuda, por todo o conhecimento transmitido, atenção, disponibilidade e contribuição na elaboração deste trabalho.

Ao professor Doutor Félix Dias Carvalho, co-orientador desta tese, agradeço a oportunidade de integrar o Laboratório de Toxicologia e pela atenção e disponibilidade que sempre demonstrou.

À Margarida, pela imensa ajuda na parte dos estudos metabolómicos e por se ter mostrado sempre disponível para me esclarecer dúvidas e ajudar. Muito obrigada por me teres acompanhado.

À Ana, Filipa e Mariana que desde o primeiro dia me ajudaram imenso e foram pilares essenciais neste ano de trabalho no laboratório.

Agradeço também a todos os meus amigos e colegas do Laboratório de Toxicologia por toda a preocupação, amizade e ajuda em todos os momentos.

Aos meus amigos agradeço o enorme carinho e força que me dão. Obrigada por serem a minha segunda família.

Por último, mas não menos importante, à minha família, agradeço o apoio incondicional, a força para continuar e por acreditarem sempre em mim.

A todos vocês o meu sincero e profundo MUITO OBRIGADA!

The results presented in this master thesis are part of the following scientific communications

POSTER [10/03/2022]

Sorafenib presents higher toxicity than imatinib and pazopanib in AC16 cardiac cells, associated to mitochondrial depolarization and autophagy

Tânia Gomes-Castro, Félix Carvalho, Paula Guedes de Pinho and Vera Marisa Costa. AIMS Meeting 2022.

ORAL PRESENTATION [04/05/2022]

A cardio-oncology study in AC16 cardiac cells involving the new targeted therapies, imatinib, sorafenib and pazopanib

Tânia Gomes-Castro, Mariana Ferreira, Félix Carvalho, Paula Guedes de Pinho and Vera Marisa Costa. 15th Meeting of Young Researchers of U. Porto (IJUP'22), Porto, Portugal.

ARTICLE IN PREPARATION

When anticancer targeted therapy means targeting the heart: a cardio-oncology study in AC16 cells

Tânia Gomes-Castro, Margarida Araújo, Mariana Ferreira, Félix Carvalho, Paula Guedes de Pinho and Vera Marisa Costa.

Abstract

Current cancer treatments have led to a strong reduction in cancer mortality. However, cytotoxic agents have been long known as cardiotoxic. Although targeted therapies used in the treatment of cancer were considered for some more selective, they are not devoid of adverse side effects. Tyrosine kinase inhibitors (TKIs) are pharmacological active molecules that target tyrosine kinases, used in the treatment of different types of cancer, namely chronic myeloid leukaemia, renal cell carcinoma, pancreatic cancer, neuroendocrine tumours and imatinib-resistant gastrointestinal stromal tumour. Imatinib, pazopanib, sorafenib are reported to be cardiotoxic on clinical studies and belong to the TKIs group, being these 3 drugs the focus of this thesis. The work developed in this dissertation aimed to characterize and assess imatinib, pazopanib and sorafenib cytotoxic mechanisms in human differentiated AC16 cardiac cells and to disclosure the impact of these drugs in clinically relevant concentrations in the intracellular metabolome and also the exometabolome of the cells exposed to those targeted drugs.

First, the cells were incubated with crescent concentrations of imatinib (10 to 100μM), pazopanib (1 to 100μM), and sorafenib (0.5 to 50μM). Then, cytotoxicity was studied using the 3-(4,5-dimethylthiazol-2-yl)-2,5-diphenyltetrazolium bromide (MTT) reduction and neutral red (NR) uptake assays at 24h and 48h. Moreover, to disclose the role of autophagy on the cytotoxicity, 3-methyladenine and chloroquine were used at 24h using the NR assay with selected concentrations of the targeted drugs under study. Furthermore, mitochondrial membrane potential using JC-1 probe was also determined to study the effects on the mitochondria of these agents. Finally, the intracellular and extracellular metabolome of differentiated AC16 cells was assessed after a 24-h incubation using clinically relevant concentrations and mostly non-toxic concentrations of the three agents. The cellular metabolome content was analysed using Gas Chromatography/Mass Spectrometry under a non-targeted approach. Multivariate and univariate analysis were used to properly analyse the data acquired.

Regarding the evaluation of imatinib-induced cardiotoxicity by the MTT reduction assay, no significant cytotoxicity was detected up to 100μM after 24h. On the other hand, a time dependent cytotoxicity was observed at 48h. In the NR uptake assay, imatinib elicited a similar cytotoxic profile with a clearly time-dependent cytotoxicity. On the other hand, pazopanib led to a time-dependent toxicity, with no clear dose dependence, according to the MTT reduction assay. Once again, the NR uptake was less sensitive to detect cytotoxicity in the case of this drug, but the lysosomal damage induced by pazopanib also presented a time-dependent profile. In contrast to the other drugs, the cytotoxic profile of sorafenib in differentiated AC16 cells was characterized by a concentration and time-

dependent cytotoxicity, both clearly prominent. At 24h, this drug only caused mitochondrial dysfunction at the concentration of sorafenib 20μM, while at 48h, a significant cardiotoxic effect was observed in all concentrations with the exception of the sorafenib 1μM.

Regarding autophagy, 3-methyladenine increased the cytotoxicity of imatinib and pazopanib in differentiated AC16 cells, whereas it affected differentially the cytotoxicity of sorafenib pending on the concentration of the drug. Chloroquine, in turn, only increased the cytotoxicity of the lowest sorafenib concentration (10μM tested). Finally, both pazopanib and sorafenib caused mitochondrial membrane depolarization in all the tested concentrations, while only the highest concentration of imatinib caused significant changes in the mitochondrial membrane potential.

Therefore, to evaluate possible metabolic disorders, as well as to have an overview of the cardiotoxic mechanisms of the TKIs under study, the metabolome of differentiated human cardiac cells AC16 was analyzed after incubation with the 3 drugs using an early time-point (24h) and clinically relevant concentrations. Metabolome analysis revealed significant differences in the intracellular metabolome of differentiated cells when compared to control cells and the vehicle with the targeted drugs affecting several metabolic pathways. Moreover, the metabolic profiling of volatile carbonyl compounds (VCCs) in cell culture medium showed significant differences after the incubation with pazopanib and sorafenib. The only exception was imatinib that no discriminants metabolites were found, even if there are some differences among groups.

In conclusion, sorafenib was the drug studied herein that caused higher disruption of the several pathways studied, namely autophagy and mitochondrial membrane potential. Moreover, in the metabolomic study it was also the one agent that most impacted on the several routes evaluated, both in the intrametabolome and exametabolome.

Keywords: Imatinib, pazopanib, sorafenib, differentiated AC16 cells, metabolome, cardiotoxicity

Resumo

Atualmente, os tratamentos utilizados contra o cancro levaram a uma forte redução na mortalidade. De facto, os agentes citotóxicos são considerados cardiotóxicos há bastante tempo. Embora as terapias direcionadas utilizadas no tratamento anticancerígeno sejam consideradas mais seletivas, estas podem provocar vários efeitos adversos, entre os quais a cardiotoxicidade. Os inibidores da tirosina quinase (TKIs), moléculas farmacologicamente ativas que têm como alvo as tirosinas quinases, são utilizados no tratamento de diferentes tipos de cancro, nomeadamente leucemia mieloide crónica, carcinoma de células renais, cancro do pâncreas, tumores neuroendócrinos e tumor estromal gastrointestinais resistentes ao imatinib. Em estudos clínicos, existem relatos de cardiotoxicidade associados ao imatinib, pazopanib e sorafenib, fármacos pertencentes ao grupo dos TKIs, sendo estes 3 fármacos o foco principal nesta tese. O trabalho desenvolvido nesta dissertação teve como objetivo caracterizar e avaliar os mecanismos citotóxicos do imatinib, pazopanib e sorafenib em células cardíacas humanas diferenciadas AC16 e perceber o impacto destes fármacos, quando usados em concentrações clinicamente relevantes, tanto no metaboloma intracelular como no exometaboloma das células AC16.

Em primeiro lugar, as células foram incubadas por 24 ou 48horas com concentrações crescentes de imatinib (10 a 100μM), pazopanib (1 a 100μM) e sorafenib (0,5 a 50μM). Em seguida, a fim de estudar a citotoxicidade dos compostos, foram usados os ensaios de redução de brometo de 3-(4,5-dimetiltiazol-2-il)-2,5-difeniltetrazólio (MTT) e incorporação de vermelho neutro (NR). Além disso, para perceber o papel da autofagia na citotoxicidade induzida por estes fármacos, a 3-metiladenina e cloroquina foram testados usando o ensaio de NR com concentrações selecionadas e após 24 horas de incubação. Ademais, o potencial de membrana mitocondrial também foi determinado para avaliar os efeitos desses agentes sobre as mitocôndrias, usando a sonda JC-1. Finalmente, o metaboloma intracelular e extracelular de células AC16 diferenciadas foi avaliado após uma incubação de 24 horas usando concentrações clinicamente relevantes e principalmente não tóxicas dos três agentes. O conteúdo do metaboloma celular foi analisado usando Cromatografia Gasosa/Espectrometria de Massa, optando por uma abordagem não direcionada. Por fim, a análise multivariada e univariada foram utilizadas para analisar adequadamente os dados.

Em relação à avaliação da cardiotoxicidade induzida pelo imatinib, usando o ensaio de redução do MTT, observou-se que não foi detetada citotoxicidade significativa até 100μM após uma exposição de 24 horas. Por outro lado, uma citotoxicidade dependente do tempo foi observada às 48 horas. No ensaio de captação de NR, o imatinib apresentou um perfil citotóxico claramente dependente do tempo. Além disso, de acordo com o ensaio de redução do MTT, o pazopanib causou uma toxicidade dependente do tempo, sem dependência clara da dose. Mais

uma vez, o ensaio de captação do NR foi menos sensível para detetar citotoxicidade no caso deste fármaco, no entanto, o dano lisossomal induzido pelo pazopanib também apresentou um perfil dependente do tempo. Em contraste com os outros fármacos, o perfil citotóxico de sorafenib em células diferenciadas AC16 foi caracterizado por uma citotoxicidade dependente da concentração e do tempo, ambas claramente proeminentes. Às 24 horas, esse fármaco causou disfunção mitocondrial apenas na concentração de 20μM, enquanto às 48 horas, um efeito cardiotóxico significativo foi observado em todas as concentrações, com exceção do sorafenib 1μM.

Ao nível da autofagia, a 3-metiladenina aumentou a citotoxicidade do imatinib e do pazopanib nas células diferenciadas AC16, enquanto que com o sorafenib foi observada uma citotoxicidade dependente da concentração do mesmo. A cloroquina, por sua vez, apenas aumentou a citotoxicidade da menor concentração testada de sorafenib (10μM). Por fim, tanto o pazopanib quanto o sorafenib causaram despolarização da membrana mitocondrial em todas as concentrações testadas, enquanto que o imatinib apenas causou alterações significativas no potencial de membrana mitocondrial na concentração mais alta testada.

Para avaliar os possíveis distúrbios metabólicos, bem como para ter uma visão geral dos mecanismos cardiotóxicos dos TKIs em estudo, o metaboloma de células cardíacas humanas diferenciadas AC16 foi analisado após incubação com concentrações clinicamente relevantes dos três fármacos após 24 horas. A análise do metaboloma revelou diferenças significativas no metaboloma intracelular das células diferenciadas quando comparadas às células controlo/veículo. Além disso, o perfil metabólico dos compostos carbonílicos voláteis (VCCs) em meio de cultura celular mostrou diferenças significativas após a incubação com pazopanib e sorafenib. A única exceção foi o imatinib, onde não foram encontrados metabólitos discriminantes, apesar da análise multivariada mostrar significância.

Em conclusão, neste estudo, o sorafenib foi o fármaco que causou maior perturbação das várias vias avaliadas, nomeadamente autofagia e potencial de membrana mitocondrial. Além disso, no estudo do metaboloma, tanto a nível do intrametaboloma quanto no exametaboloma, este fármaco também foi que mais impactou as diversas vias estudadas.

Palavras chave: Imatinib, pazopanib, sorafenib, células AC16 diferenciadas, metaboloma, cardiotoxicidade

Index

Acknowledgments i

Abstract iii

Resumo v

Figure Index x

Table Index xiv

Abbreviation list xvi

1. Introduction 1

1.1. Heart diseases and cancer 1

1.2. Cardiotoxicity caused by anticancer drugs 3

1.3. New targeted therapies against cancer 8

1.4. Tyrosine kinase inhibitors 9

1.4.1. Cardiotoxicity of TKIs 10

1.4.2. Clinical data 11

1.4.3. Pre-clinical and in vitro studies 19

2. Material and Methods 35

2.1. Materials and reagents 35

2.2. Cell culture procedures 35

2.3. Cytotoxicity assays 36

2.3.1. The MTT reduction assay 37

2.3.2. The NR uptake assay 37

2.4. Mitochondrial membrane potential 38

2.5. Statistical analysis 38

2.6. Metabolome analysis 39

2.6.1. Sample preparation 40

2.6.2. Chromatographic and mass spectrometry procedures to analyze intracellular samples 41

2.6.3. HS-SPME/GC-MS procedures to analyze extracellular samples 42

2.6.4. GC-MS pre-processing data 42

2.6.5. Multivariate analysis (MVA) 43

2.6.6. Identification process 44

2.6.7. Univariate analysis 45

3. Results 46

3.1. Imatinib caused a time-dependent cytotoxicity in differentiated AC16 cells, according to the MTT reduction assay 46

3.2. Imatinib caused impairment of lysosome function in differentiated AC16 cells as early as 24h, according to the neutral red uptake assay 47

3.3. Pazopanib led to time-dependent toxicity, with no clear dose dependence, according to the MTT reduction assay 48

3.4. Pazopanib affected lysosomal uptake ability in AC16 cells at pharmacological relevant concentrations 49

3.5. Sorafenib presented a concentration and time-dependent mitochondrial impairment in AC16 cells, according to the MTT reduction assay 50

3.6. Clinically relevant concentrations of sorafenib caused impact in lysosome function of AC16 cells in a dose and time-dependent manner 51

3.7. 3-Methyladenine, an autophagy inhibitor, increased the cytotoxicity of imatinib and pazopanib in differentiated AC16 cells, when it affected differentially the cytotoxicity of sorafenib 52

3.8. The autophagy inhibitor, chloroquine, increased the cytotoxicity of only the lowest concentration of sorafenib 53

3.9. Sorafenib and pazopanib caused mitochondrial membrane depolarization in all the tested concentrations, while only the highest concentration of imatinib caused significant changes in mitochondrial membrane potential 54

3.10. Evaluation of the metabolic changes after targeted therapies 55

3.11. Imatinib caused a strong effect on the metabolome intracellular of AC16 cells 73

3.12. Pazopanib changed the metabolome intracellular of AC16 cells 76

3.13. A clinically relevant concentration of sorafenib causes the strongest impact on the intracellular metabolites of AC16 cells 79

3.14. The vehicle used did not caused relevant changes in the metabolome of cells 82

3.15. Exometabolome of AC16 cells was significantly changed by imatinib but no discriminative metabolites were found 85

3.16. Pazopanib altered the exometabolome of AC16 cells 87

3.17. Sorafenib at pharmacological relevant concentrations caused significant differences on the volatile carbonyl compounds of AC16 cells 89

3.18. The vehicle did not change the exometabolome of AC16 cells 92

4. Discussion 96

4.1. Cytotoxicity assays 96

4.2. Metabolomic profiling 101

5. Conclusions 111

6. References 112

Figure Index

Figure 1. Schematic representation of the main moleculares targets of the compounds sorafenib and sunitinib and their main consequences in the cardiovascular system. The TKIs sorafenib and sunitinib primarily target VEGFR and PDGFR. Inhibition of VEGF has as its main consequence the induction of hypertension and deleterious effects at the cardiac level, due to its interference with blood flow, angiogenesis and vascular integrity. Moreover, inhibition of PDGFR and AMPK are associated with impairments in energy homeostasis, targeting mostly mitochondria, and affecting cell survival, which may lead to heart failure (14, 42). 11

Figure 2. Derivatization reaction of carbonyls with PFBHA. 41

Figure 3. Imatinib (IMA) cytotoxicity assessed through the MTT reduction assay in differentiated AC16 cells following a 24-h (A) or 48-h (B) incubation**.** Results are presented as mean ± standard deviation from 2-8 independent experiments (N=8 to 32). Statistical analysis was performed using one-way ANOVA followed by Tukey's post hoc test. ***p<0.001, ****p<0.0001 vs. control (CTL); $^{\#}$p<0.05, $^{\#\#\#}$p<0.001, $^{\#\#\#\#}$ p<0.0001 vs. the immediate lower concentration tested in the same time point. 46

Figure 4. Imatinib (IMA) cytotoxicity evaluated through the NR uptake assay in differentiated AC16 cells following a 24-h (A) or 48-h (B) incubation. Results are presented as mean ± standard deviation from 2-10 independent experiments (N=8 to 40). Statistical analysis was performed using one-way ANOVA followed by Tukey's post hoc test. ****p<0.0001 vs. control (CTL); $^{\#\#\#}$p<0.001, $^{\#\#\#\#}$p<0.0001 vs. the immediate lower concentration tested in the same time point. 47

Figure 5. Pazopanib (PAZ) cytotoxicity evaluated by the MTT reduction assay in differentiated AC16 cells following a 24-h (A) or 48-h (B) incubation. Results are presented as mean ± standard deviation from 2-8 independent experiments (N=7 to 32). Statistical analysis was performed using one-way ANOVA followed by Tukey's post hoc test. ***p<0.001, ****p<0.0001 vs. control (CTL); $^{\#\#\#}$p<0.001, $^{\#\#\#\#}$ p<0.0001 vs. the immediate lower concentration tested at the same time point. 48

Figure 6. Pazopanib (PAZ) cytotoxicity, in differentiated AC16 cells following a 24-h (A) or 48-h (B) incubation, assessed by the NR uptake assay. Results are presented as mean ± standard deviation from 3-10 independent experiments (N=12 to 40). Statistical analysis was performed using one-way ANOVA followed by Tukey's post hoc test. *p<0.05, ****p<0.0001 vs. control (CTL); $^{\#}$p<0.05, $^{\#\#\#}$p<0.001, $^{\#\#\#\#}$ p<0.0001 vs. the immediate lower concentration tested in the same time-point. 49

Figure 7. Sorafenib (SOR) cytotoxicity, evaluated through the MTT reduction assay, in differentiated AC16 cells following a 24-h (A) or 48-h (B) incubation. Results are presented

as mean ± standard deviation from 3-5 independent experiments (N=12 to 20). Statistical analysis was performed using one-way ANOVA followed by Tukey's post hoc test. ****p<0.0001 vs. control (CTL); ##p<0.01, ###p<0.001, #### p<0.0001 vs. the immediate lower concentration tested. 50

Figure 8. Sorafenib (SOR) cytotoxicity regarding the NR uptake assay in differentiated AC16 cells following a 24-h (A) or 48-h (B) incubation. Results are presented as mean ± standard deviation from 2-8 independent experiments (N=4 to 32). Statistical analysis was performed using one-way ANOVA followed by Tukey's post hoc test. ****p<0.0001 vs. control (CTL); #p<0.05, ##p<0.01, ####p<0.0001 vs. the immediate lower concentration tested in the same time-point. 51

Figure 9. Effect of an autophagy inhibitor (3-methyladenine, 3-MA) on the cytotoxicity of imatinib (IMA) (A), pazopanib (PAZ) (B) and sorafenib (SOR) (C) in differentiated AC16 cells at 24-h. The assay used herein for cytotoxicity assessment was the NR uptake assay. Results are presented as mean ± standard deviation from 3-4 independent experiments (N=12 to 16). Statistical analyses were performed using the one-way ANOVA followed by Tukey's post hoc test. *p<0.05, **p<0.01, ****p<0.0001 vs. control (CTL), $p<0.05, $$$$p<0.0001 vs. condition without 3-MA. 52

Figure 10. Effect of an autophagy inhibitor (chloroquine, CHLOR) on the cytotoxicity of imatinib (IMA) (A), pazopanib (PAZ) (B) and sorafenib (SOR) (C) in differentiated AC16 cells at 24-h. The assay used herein for cytotoxicity assessment was the NR uptake assay. Results are presented as mean ± standard deviation from 4-8 independent experiments (N=14 to 32). Statistical analyses were performed using the one-way ANOVA followed by Tukey's post hoc test. *p<0.05, ****p<0.0001 vs. control (CTL), $$$p<0.001 vs. condition without CHLOR, ##p<0.01, ####p<0.0001 vs. condition with CHLOR. 53

Figure 11. Mitochondrial membrane potential evaluation using the JC-1 dye in differentiated AC16 cells exposed to imatinib (IMA), pazopanib (PAZ) and sorafenib (SOR) for 24-h. Results are presented as mean ± standard deviation from 4 independent experiments (N=7 to 16). Statistical analyses were performed using the one-way ANOVA followed by Tukey's post hoc test. ****p<0.0001 vs. control (CTL). 54

Figure 12. PCA scatter plots obtained through GC-MS data to evaluate the reproducibility of the methods for (A) Intracellular metabolic profiling and (B) Volatile carbonyl compounds (VCC) profiling through the QCs. Each sample is represented by a gray sphere as a single variable, while the QCs are represented in burgundy spheres. 56

Figure 13. PCA scatter plots acquired from the analysis of the intracellular content of: (A) AC16 differentiated control cells (n=9; PC2 R2X=0.43); (B) exposed to DMSO 0.05 (n=10; PC2 R2X=0.403); (C) DMSO 0.25 (n=10; PC2 R2X=0.404); (D) imatinib (n=10; PC2

R^2X=0.487); (E) pazopanib (n=10; PC2 R^2X=0.568) or (F) sorafenib (n=10; PC2 R^2X=0.468). 57
Figure 14. PCA scatter plots acquired from the analysis of the VCC content of: (A) AC16 differentiated control cells (n=9; PC2 R2X=0.58); (B) exposed to DMSO 0.05% (n=10; PC2 R2X=0.531); (C) DMSO 0.25% (n=10; PC2 R2X=0.53); (D) imatinib (n=9; PC2 R2X=0.561); (E) pazopanib (n=10; PC2 R^2X=0.512) or (F) sorafenib (n=10; PC2 R^2X=0.495). 58
Figure 15. (A) PLS-DA score scatter plots of the differentiated control cells (n=9; blue circle), against the differentiated cells incubated with imatinib (n=10; red circle), in the intracellular metabolome; (B) PLS-DA models statistical validation by 500 permutations of the PLS-DA model of the differentiated AC16 cells incubated with imatinib. 74
Figure 16. (A) PLS-DA score scatter plots of the differentiated control cells (n=9; blue circle), against the differentiated cells incubated with pazopanib (n=10; yellow circle), in the intracellular metabolome; (B) PLS-DA models statistical validation by 500 permutations of the PLS-DA model of the differentiated AC16 cells incubated with pazopanib. 77
Figure 17. (A) PLS-DA score scatter plots of the differentiated control cells (n=9; blue circle), against the differentiated cells incubated with sorafenib (n=10; turquoise circle), in the intracellular metabolome; (B) PLS-DA models statistical validation by 500 permutations of the PLS-DA model of the differentiated AC16 cells incubated with sorafenib. 80
Figure 18. (A) PLS-DA score scatter plots of the differentiated control cells (n=9; blue circle), against the differentiated cells incubated with DMSO 0.05% (n=10; violet circle), in the intracellular metabolome; (B) PLS-DA models statistical validation by 500 permutations of the PLS-DA model of the differentiated AC16 cells incubated with DMSO 0.05%. 83
Figure 19. (A) PLS-DA score scatter plots of the differentiated control cells (n=9; blue circle), against the differentiated cells incubated with DMSO 0.25 (n=10; orange circle), in the intracellular metabolome; (B) PLS-DA models statistical validation by 500 permutations of the PLS-DA model of the differentiated AC16 cells incubated with DMSO 0.25. 85
Figure 20. (A) PLS-DA score scatter plots of the differentiated control cells (n=9; blue circle), against the differentiated cells incubated with imatinib (n=9; red circle) after GC-MS analysis of VCCs; (B) PLS-DA models statistical validation by 500 permutation of the PLS-DA model of the differentiated AC16 cells incubated with imatinib. 86
Figure 21. (A) PLS-DA score scatter plots of the differentiated control cells (n=9; blue circle), against the differentiated cells incubated with pazopanib (n=10; yellow circle), after GC-MS analysis of VCCs; (B) PLS-DA models statistical validation by 500 permutations of the PLS-DA model of the differentiated AC16 cells incubated with pazopanib. 88
Figure 22. (A) PLS-DA score scatter plots of the differentiated control cells (n=9; blue circle), against the differentiated cells incubated with sorafenib (n=10; turquoise circle), after

GC-MS analysis of VCCs; (B) PLS-DA models statistical validation by 500 permutations of the PLS-DA model of the differentiated AC16 cells incubated with sorafenib. 90
Figure 23. (A) PLS-DA score scatter plots of the differentiated control cells (n=9; blue circle), against the differentiated cells incubated with DMSO 0.05 (n=10; violet circle), after GC-MS analysis of VCCs ; (B) PLS-DA models statistical validation by 500 permutations of the PLS-DA model of the differentiated AC16 cells incubated with DMSO 0.05. 93
Figure 24. (A) PLS-DA score scatter plots of the differentiated control cells (n=9; blue circle), against the differentiated cells incubated with DMSO 0.25 % (n=10; orange circle), after GC-MS analysis of VCCs; (B) PLS-DA models statistical validation by 500 permutations of the PLS-DA model of the differentiated AC16 cells incubated with DMSO 0.25 %. 94
Figure 25. Heatmaps showing the metabolic alterations occurred on the endometabolome of AC16 differentiated cells after exposure to A) imatinib 50 μM; B) pazopanib 10 μM, C) sorafenib 10 μM, both compared to control cells. The scale is color-coded as a function of the ES, from maximum decrease (dark blue) to maximum increase (red). Statistically significant differences are indicated (*p < 0.05, **p < 0.01, ***p < 0.001, ****p < 0.0001). 104
Figure 26. Overview of the dysregulated metabolic pathways of the intracellular metabolites alterations in differentiated AC16 cells after exposure to A) imatinib 50 μM; B) pazopanib 10 μM, C) sorafenib 10 μM, both compared to control cells. The node color is based on the p value, where a dark circle color indicates a more significant change of the pathway. The node radius corresponds to the pathway impact value. Pathways were annotated when p < 0.05 and pathway impact > 0.05. 106
Figure 27. Boxplots illustrating the metabolites changing in differentiated AC16 cells after exposure to A) PAZ 10 μM or B) SOR 10 μM both compared to control cells (*p < 0.05; ** p < 0.01). 108

Table Index

Table 1. Cardiac adverse effects of classic chemotherapeutic drugs. 6
Table 2. Clinic studies that highlight the incidence of cardiotoxicity of the main compounds in the TKIs class. 15
Table 3. Incidence of cardiac effects of the main compounds in the TKIs class in preclinic studies. 23
Table 4. Reports of cardiotoxicity of several TKIs class compounds in in vitro studies. 28
Table 5. Parameters used in the MZmine software for the pre-processing of the chromatographic data. RT: retention time 43
Table 6. List of all intracellular metabolites TMS-derivatized detected from the PLS-DA models (data normalized by total area of the chromatogram) with VIP>1. 60
Table 7. List of all VCC PFBHA-derivatized metabolites detected from the PLS-DA models (data normalised by total area of the chromatogram) with VIP>1. 68
Table 8. Parameters of cross-validation obtained for the PLS-DA models of the metabolome intracellular analysis of control differentiated AC16 cells and the respective cells incubated with imatinib. 74
Table 9. Intracellular metabolites selected for integration of the PLS-DA model of differentiated AC16 cells incubated with imatinib (VIP>1). 74
Table 10. Parameters of cross-validation obtained for the PLS-DA models of the endometabolome analysis of control differentiated AC16 cells and the respective cells incubated with pazopanib. 77
Table 11. Intracellular metabolites selected for integration of the PLS-DA model of differentiated AC16 cells incubated with pazopanib (VIP>1). 78
Table 12. Parameters of cross-validation obtained for the PLS-DA models of the endometabolome analysis of control differentiated AC16 cells and the respective cells incubated with sorafenib. 80
Table 13. Intracellular metabolites selected for integration of the PLS-DA model of differentiated AC16 cells incubated with sorafenib (VIP>1). 81
Table 14. Parameters of cross-validation obtained for the PLS-DA models of the endometabolome analysis of control differentiated AC16 cells and the respective cells incubated with DMSO 0.05%. 83
Table 15. Parameters of cross-validation obtained for the PLS-DA models of the endometabolome analysis of control differentiated AC16 cells and the respective cells incubated with DMSO 0.25. 85

Table 16. Parameters of cross-validation obtained for the PLS-DA models regarding the VCC content, by comparison of control differentiated AC16 cells and the respective cells incubated with imatinib. 86
Table 17. Parameters of cross-validation obtained for the PLS-DA models regarding the VCC content, by comparison of control differentiated AC16 cells and the respective cells incubated with pazopanib. 88
Table 18. VCC metabolites selected for integration of the PLS-DA model of differentiated AC16 cells incubated with pazopanib (VIP>1). 88
Table 19. Parameters of cross-validation obtained for the PLS-DA models regarding the VCC content, by comparison of control differentiated AC16 cells and the respective cells incubated with sorafenib. 90
Table 20. VCC metabolites selected for integration of the PLS-DA model of differentiated AC16 cells incubated with sorafenib (VIP>1). 91
Table 21. Parameters of cross-validation obtained for the PLS-DA models regarding the VCC content, by comparison of control differentiated AC16 cells and the respective cells incubated with DMSO 0.05. 93
Table 22. Parameters of cross-validation obtained for the PLS-DA models regarding the VCC content, by comparison of control differentiated AC16 cells and the respective cells incubated with DMSO 0.25 %. 95

Abbreviation list

3-MA - 3-Methyladenine

AA - Amino acids

ANP - Atrial natriuretic peptide

AMPK - adenosine monophosphate-activated protein kinase

BNP - brain natriuretic peptide

CK - creatine kinase

c-KIT - stem cell factor receptor

CML - chronic myeloid leukaemia

CVD - cardiovascular diseases

DMSO - dimethyl sulfoxide

DNA - deoxyribonucleic acid

ECG - electrocardiogram

ErbB2 - erythroblastic leukemia viral oncogene homolog 2

FBS - heat inactivated foetal bovine serum

FDA - food and drug administration

GC-MS - gas chromatography coupled to mass spectrometry

GIST - gastrointestinal stromal tumour

HBSS - hank's balanced salt solution

HER2 - human epidermal growth factor receptor 2

HF - heart failure

HS - horse serum

HS-SPME - headspace solid-phase microextraction

IMA - imatinib

LC - L-carnitine

LDH - lactate dehydrogenase

LVD - left ventricular dysfunction

LVEF - left ventricular ejection fraction

LVF - left ventricular function

MMP, $\Delta\Psi m$ - Mitochondrial membrane potential

MPs - microparticles

MTT - 3-(4,5-Dimethylthiazol-2-yl)-2,5-diphenyl tetrazolium bromide

$^{\bullet}NO$ - nitric oxide

NR - neutral red

NRVMs - neonatal rat ventricular myocytes

PAZ - pazopanib

PBS - phosphate buffered saline-Dulbecco

PDGFR - platelet-derived growth factor receptor

Pen-Strep - penicillin/streptomycin

QCs - control samples

RCC - renal cell carcinoma

RNA - ribonucleic acid

ROS - reactive oxygen species

SOR - sorafenib

TKIs - tyrosine kinase inhibitors

VEGF - vascular endothelial growth factor

VEGFRs - vascular endothelial growth factor receptors

VEGFRi - vascular endothelial growth factor receptors inhibitor

1. Introduction

1.1. Heart diseases and cancer

According to estimates from the World Health Organization (WHO), in 2019 heart diseases and cancer were the two main causes of mortality and important barriers to the increasing life expectancy worldwide (1). In addition to demographic characteristics such as age, family history, hypertension, there are other risk factors related to lifestyle and environment, such as smoking, alcohol consumption, obesity and sedentary lifestyle that influence these diseases (1, 2). Indeed, heart circulatory system diseases (CVD) are responsible for over 3.9 million deaths a year, or 45% of all deaths worldwide. In fact, CVD accounts for 1.8 million deaths and 2.1 million deaths, which means 40% and 49% of all deaths, in men and woman, respectively.

By comparison, cancer, the next most common cause of death in the world, accounts for under 1.1 million deaths (24%) in men and just under 900,000 deaths (20%) in women, respectively (3). In the year 2020, statistics regarding cancer estimated 19.3 million new cases of cancer and almost 10.0 million deaths from cancer globally. The most commonly diagnosed cancers in the whole world were female breast cancer with 2.26 million new cases, followed by lung and prostate cancer with 2.21 and 1.41 million new cases, respectively. However, lung, liver, and stomach cancers are the most lethal cancers (4). According to the American Cancer Society, in 2022, in the United States of America alone, are expected 1.9 million new cancer cases and 609,360 cancer deaths, including about 350 deaths a day from lung cancer, the leading cause of death from cancer in that country (5).

Briefly and in a simplistic fashion, cancer is considered a dysregulation of cell differentiation mainly focused in a disequilibrium between cell division and cell death resulting in a limitless replicative potential and uncontrolled and massive multiplication (6). Moreover, unlike healthy cells, tumor cells have a great capacity to acquire resistance to apoptosis and senescence, as well as autonomy related to growth factors. In addition, tumor cells also have the potential to trigger and maintain angiogenesis, that is, to lead to the formation of new capillary blood vessels growth from pre-existing vasculature, allowing tumor increase. The process begins when an endothelial cell of a small vessel is activated by an angiogenic stimulus, such as vascular endothelial growth factor (VEGF). In response to the stimulus, the endothelial cell becomes motile and extends a development of a capillary sprout, forming a tube and creating a single lumen shared by many cells. Hence, a tumor must stimulate the formation of new blood vessels that supports its growth and VEGF is a key activator of angiogenesis in both normal cells and tumors. When cells within

a tumor become oxygen deficient, they begin to express VEGF, which diffuses through the tissues activating endothelial cells on nearby vessels (7). That is why some new cancer therapies are targeted to block the action of VEGF. On the other hand, the cancer can spread more rapidly due to the activity of certain kinases that are more active in some types of cancer cells. Tyrosine kinases are essential mediators of the signaling cascade, which determine important roles in various biological processes such as growth, differentiation, metabolism and apoptosis in response to both external and internal stimuli. Although their activity is heavily regulated in normal cells, they can acquire transformative functions due to mutation(s), overexpression and autocrine paracrine stimulation and so on, leading to malignancy (8). However, constitutive oncogenic activation in cancer cells can be blocked by selective tyrosine kinase inhibitors (TKIs) such as small molecule inhibitors and monoclonal antibodies, which will be discussed later on.

To fight cancer, several strategies may be pursued according to the type of cancer, its staging but also to the patients' characteristics. Regarding treatment, a patient may undergo several anticancer treatments, such as chemotherapy, radiotherapy, surgery, targeted therapies, or most commonly their combination. The use of combination therapy increases clinical efficacy, but also increases the risk of adverse effects (9). One of the most limiting effects of anticancer therapy is cardiotoxicity that will be discussed further in this work.

The heart is a vital organ, as it promotes blood circulation, thus allowing the arrival of nutrients, oxygen, hormones and other substances indispensable to all body cells. In addition, the heart contributes to internal homeostasis by controlling body temperature and tissue pH, through the pumped blood. However, cellular homeostasis may be called into question, since this organ is also a target for toxicity of several agents, among them antineoplastic agents that have a big role in clinical cardiotoxicity (10). In fact, the cardiotoxicity inflicted by anticancer agents led to a new field of expertise: cardio-oncology also called onco-cardiology or chemo-heart.

Heart diseases associated to cancer therapies can manifest themselves in a number of ways, including myocardial infarction or cardiac arrhythmias; however, one of the most common cardiotoxic manifestations associated with the antineoplastic agents are hypertension and the development of left ventricular dysfunction (LVD), namely decreased left ventricular ejection fraction (LVEF), which may progress to heart failure (HF). HF is a severe debilitating disease that can result from any functional or structural cardiac disorder that can disrupts the ventricular ability to fill or eject blood. Fluid retention, which leads to pulmonary congestion and peripheral edema may be cardiac manifestations of HF, and can result, in a few years, on the death of the majority of the diagnosed patients (11, 12).

Chemotherapy is a very aggressive treatment that can cause immediate adverse effects like nausea and vomiting. Moreover, this treatment can also cause short but also long-term cardiac toxicity (2). The anticancer group of drugs most described as cardiotoxic is anthracyclines. Their mechanisms of cardiotoxicity are wide, and seem to be mostly a result of multiple forms of cellular injury to cardiac myocytes and endothelial cells provided by the excess of reactive species production induced by the quinone group of anthracyclines, inhibition of cardiac topoisomerase, mitochondrial damage among other mechanisms (13-15). The resistance to common cancer treatment, the wide incidence of adverse effects, such as cardiotoxicity, and also the fact that some cancers still have poor survival rate, made clear the need to explore new effective alternatives to improve the conventional chemotherapy or radiotherapy. With the growing need for the discovery of new pharmacologically active substances capable of improving the survival rate of patients and ideally being devoid of toxicity, new avenues have emerged in anticancer therapies, with the introduction of the so-called 'new targeted therapies' (16). Targeted therapy is a type of cancer treatment that targets specific cancer cells receptors or pathways, which control how cancer cells grow, divide and spread. Different types of cancer cells have different gene changes, which reflect in different functions of proteins or enzymes. Targeted therapies were made to target those proteins and block the messages, causing the cancer cells to stop growing, to destroy themselves or change angiogenesis, for instances (16). The targeted therapies include human epidermal growth factor receptor 2 (HER2) antibodies, tyrosine kinase inhibitors (TKIs), monoclonal antibodies against VEGF and proteasome inhibitors (13, 17).

1.2. Cardiotoxicity caused by anticancer drugs

Chemotherapy that targets cells at different phases of the cells' life cycle is still the most frequent anticancer therapy, currently. It works by stopping or slowing down the cancer cells from multiplying and it has contributed to the significant decrease of morbidity and mortality in several types of cancer observed throughout the XXth century (18). The chemotherapeutic agents can be grouped according both to their mechanism of action but also their chemical structure. The various groups of antineoplastic agents that can compromise the synthesis of DNA, RNA and, consequently, protein formation, are: antimetabolites (e.g. 5-fluorouracil), topoisomerase II inhibitors (e.g. anthracyclines), alkylating agents (e.g. cyclophosphamide) and agents interfering with tubulin (e.g. paclitaxel) among others (2). All the groups mentioned can cause cardiotoxicity and it should be added that the cardiovascular effects of antineoplastic drugs depend significantly

on the group of drugs mentioned, but also the biological variability of the patient and his/her state of health, during and after treatment. Even so, as conventional chemotherapy drugs are not selective, they can affect normal cells. Moreover, they have a great potential to develop resistance to cancer treatment and cause serious adverse effects (19). As stated, one of the most serious and frequent adverse effect of anticancer therapy and, in particular chemotherapy and mediastinal radiotherapy, is cardiotoxicity (19).

Although there are other classes, anthracyclines and anthracenediones, which include doxorubicin, mitoxantrone, epirubicin, idarubicin and daunorubicin, still remain the most broadly used class in therapeutics due to its effectiveness. They exhibit strong anti-neoplastic features due to four main mechanisms: (i) disruption of DNA and RNA synthesis by intercalating between base pairs; (ii) inhibition of topoisomerase II, leading to DNA breaks and blocking ligase repair; (iii) impairment of histones, which diminish DNA repair and (iv) increase in iron-related reactive species, damaging to the DNA (14, 15).

Several factors affect the response to cancer therapies, so the choice of adequate treatments depends on factors like the type of cancer and its characteristics, dose, drug interactions and resistance, personal medical history of the patient, potential synergism after co-administration or sequential administration of chemotherapeutic cardiotoxic drugs or the application of other therapeutics with potential cardiac toxicity, among others (19). Over the last decades, improved aspects of cancer prevention and its treatment have led to an increase in the number of cancer survivors, but on the other hand, the heart has limited potential for regeneration, therefore, anticancer treatments applied to those survivors, cause adverse effects that affect the cardiovascular system and lead to deterioration of cardiac function (9), with great economic and social burden. Hence, one of the top priorities nowadays is the life-quality of cancer survivors. At present, the goal is not just to treat cancer, but also to insure that the adverse effects in the future are fewer for easier adjustment in patients' lives after treatments (20), being that the cardiovascular system is key on that aspect.

The cardiotoxicity resulting from antineoplastic therapy is a growing concern for oncologists and cardiologists (21), being acknowledged for more than 50 years. Cardio-oncology is an emerging field that focuses on the prevention and management of heart disease in cancer patients (22), whether cardiotoxicity results from chemotherapy and/or radiotherapy (21), being nowadays also enforced on new targeted therapies. Cardiotoxicity can be manifested as acute/subacute or chronic cardiotoxicity: the first type is observed at the beginning of the treatment up to two weeks after it ended (short-term), it is rare and not dose-related, while chronic toxicity can occur within one year or more after treatment ended (long-term) and it is dose-related (19, 21, 23). This classification has been mostly used for chemotherapy agents. Other classifications have been used, considering the wide range of

possible cardiotoxic effects. On one hand, the antineoplastic drugs used in anticancer therapy predominantly cause dose-related cardiotoxicity and irreversible lesions and have been classified as type I agents (e.g. the anthracycline doxorubicin and other chemotherapeutic drugs). In these cases, myocardial dysfunction is associated with a high degree of propensity for cell death after exposure. Instead, there are type II agents that do not cause irreversible cellular destruction and not present dose-dependent cardiotoxicity (e.g. the antibody trastuzumab). The latter causes a cardiac dysfunction that is reversible; however, when administered associated with anthracyclines, some degree of cell death may occur (24).

In summary, from a clinical point of view, antineoplastic drugs can cause severe cardiovascular complications, which may or may not be permanent, such as permanent loss of contractile function, rhythm formation and/or conduction abnormalities, as well as vascular effects, including vasospasm, blood pressure changes and thromboembolic injury (21). In Table 1, a brief summary will be given regarding the effects of the classic chemotherapeutic agents on the cardiovascular system. The new targeted agents and their cardiotoxicity will be reviewed in the next section, as they are the main subject of this work.

Table 1. Cardiac adverse effects of classic chemotherapeutic drugs.

Cardiotoxic agents		ANTICANCER Mechanism of action	Cardiac adverse effects	References
TOPOISOMERASE II INHIBITORS	<u>Anthracyclines and anthracenediones:</u> Doxorubicin Epirubicin Idarubicin Daunorubicin Mitoxantrone	DNA intercalating agents, which cause oxidative stress. They have alkylating properties and cause direct effects on the cell membrane; they are inhibitors of helicase, DNA polymerase and topoisomerase II and consequently induce apoptosis as a result of inhibition of topoisomerase II	Reduction of left ventricular contractility, arrhythmias and cardiomyopathy, which may ultimately lead to congestive heart failure	(14, 15, 18, 25)
ALKYLATING AND METALATING AGENTS	Cyclophosphamide and ifosfamide Platinum agents (e.g. cisplatin)	Highly reactive compounds that disturb DNA synthesis and cell division. They cause direct DNA damage, causing inhibition of the replication process, fragmentation, cross-linking strands, and mispairing of the nucleotides (causing mutations)	A combination of symptoms and signs of myopericarditis can result in congestive heart failure, arrhythmias, hypertension, cardiac tamponade, myocardial depression and left ventricular dysfunction	(2, 15, 18)

ANTIMETABOLITES	5-Fluorouracil and its oral prodrug, capecitabine	Interference with the DNA and RNA formation inhibits thymidylate synthase and incorporates its metabolites into RNA and DNA, causing nucleotide depletion and consequent inhibition of DNA replication	Chest pain, rhythm disturbances, hypotension, dyspnea, myocardial infarction, cardiac ischemia and endothelial dysfunction	(2, 15, 18, 26)
ANTIMICROTUBULE AGENTS	Taxanes (e.g. docetaxel and paclitaxel)	Inhibit microtubule formation with consequent inhibition of the process of cell division, and freezing mitosis (mitotic inhibition)	Arrhythmias, bradycardia and cardiac ischemia	(14, 22, 26)

1.3. New targeted therapies against cancer

To treat cancer patients, researchers have continued to investigate the DNA changes and proteins that drive to cancer, with the aim of designing treatments that target these proteins and to find new ways to be precise in the therapies against cancer. The targeted therapies are based on precision medicine, and as mentioned above, they are drugs or other substances that block the growth and spread of cancer by interfering with specific receptors or cancer cells proteins, among others. They differ from standard chemotherapy because they are designed to act on specific molecular targets and attack cancer cells, hopefully without harming healthy cells (27). Like other cancer treatments, targeted therapies can be given orally as a pill or capsule, or intravenously, and they are administered in cycles with a period of treatment followed by a period of rest (28).

Targeted therapies can be divided in two types of treatments: small molecule therapies, which, as the name suggests, comprises molecules that are small enough to enter cells easily, being used for intracellular targets. On the other hand, there are treatments using monoclonal antibodies designed to change cancer cells in different ways (16, 27).

At the beginning of era of targeted therapies, trastuzumab, also known as Herceptin™, was seen as a revolution in the scientific and clinical world. Trastuzumab was first approved by the Food and Drug Administration (FDA) to treat HER2+ metastatic breast cancer in the United States in September 1998 and in the European Union in August 2000. The FDA also approved trastuzumab to treat HER2+ early breast cancer in 2006, and HER2+ metastatic stomach cancer in 2010 (29). Before trastuzumab, most HER2+ breast cancers were considered incurable. Doctor Dennis Slamon worked on the development of trastuzumab, the first HER2 targeted agents, and the first clinical study will be described next (28).

Monoclonal antibodies are used to particularly target extracellular and cell surface proteins, activating cellular apoptosis and/or inhibiting tumor proliferation. One of the most ground-breaking work with targeted therapies was done by Slamon and colleagues as stated. Knowing that the HER2 gene is overexpressed in aggressive and metastatic forms of breast cancers, targeting this receptor has become a way to explore this new therapeutic target, with several monoclonal antibodies being developed against the extracellular domain of the HER2 protein. These antibodies inhibit the proliferation of human cancer cells that overexpressed HER2 both *in vitro* and *in vivo* (28). In the first study performed by Slamon *et al.*, the effectiveness and safety of trastuzumab, a recombinant monoclonal

antibody against HER2, was evaluated in women with metastatic breast cancer that overexpressed HER2. They were randomly divided: 234 patients received standard chemotherapy (anthracycline, cyclophosphamide, paclitaxel) alone versus 235 patients to receive standard chemotherapy (anthracycline, cyclophosphamide, paclitaxel) plus trastuzumab. Patients who had not previously received adjuvant (postoperative) therapy with an anthracycline were treated with doxorubicin (or epirubicin in the case of 36 women) and cyclophosphamide with (143 women) or without trastuzumab (138 women). Patients who had previously received adjuvant anthracycline were treated with paclitaxel alone (96 women) or paclitaxel with trastuzumab (92 women). The main findings of this study highlight the clinical benefits of the treatment with the antibody, observable mainly by a longer time required for disease progression, a lower rate of death at one year and a 20% reduction in the risk of death. Meanwhile, unexpectedly, the study also revealed increased cardiotoxicity inherent to the use of the monoclonal antibody, with cardiac dysfunction occurring in about: (i) 27% of women receiving an anthracycline, cyclophosphamide, and trastuzumab; (ii) 8% of the group given an anthracycline and cyclophosphamide alone; (iii) 13% of the group taken paclitaxel and trastuzumab and (iv) 1% of the group given paclitaxel alone. Despite being considered specific and being a huge breakthrough when added to conventional chemotherapy, with proved to benefits patients with metastatic breast cancer that overexpresses HER2 (28), trastuzumab causes significant increases in clinical cardiotoxicity and at that time a new avenue appeared in cardio-oncology, now featuring the new targeted therapies.

1.4. Tyrosine kinase inhibitors

After trastuzumab, new drugs emerged such as tyrosine kinase inhibitors (TKIs) to tackle other cancer targets. TKIs are pharmacological active molecules that target tyrosine kinases, enzymes responsible for the activation of several proteins in the signaling transduction cascade by phosphorylation (30, 31). The anticancer mechanism of action of this class of agents encompasses competitive binding, followed by inhibition of ATP binding pocket of tyrosine kinases. Since their approval by the FDA in 2006, they are used in the treatment of different types of cancer that include chronic myeloid leukemia (CML), renal cell carcinoma (RCC), pancreatic cancer, neuroendocrine tumors and imatinib-resistant gastrointestinal stromal tumor (GIST) (30, 31). TKIs are composed by several drugs, such as imatinib (IMA), sunitinib, sorafenib (SOR), pazopanib (PAZ), lapatinib, axitinib among others. Axitinib is an orally bioavailable TKI selective for VEGFRs -1, -2 and -3 that are used in the therapy of advanced RCC. Axinitib reduces the blood supply to the tumor and slows the growth of cancer and is used in adults, when another drug like sunitinib or a cytokine is

no longer preventing the progression of the tumor (32). In this work, IMA, sunitinib, PAZ and SOR will be mentioned in more detail and some of the data obtained are from scientific publications, case reports or abstracts.

Since May 2001, when the FDA approved IMA mesylate, a small-molecule inhibitor of multiple tyrosine kinases, for the treatment of CML, it has become a standard first-line therapy that revolutionized its treatment (33). This drug was designed against a specific molecular target known to be the cause for the establishment and maintenance of the malignant phenotype. In fact, IMA is a rationally designed oral signal transduction inhibitor that specifically targets several protein tyrosine kinases, Abl, Arg (Abl-related gene), the stem cell factor receptor (c-KIT), platelet-derived growth-factor receptors (PDGFRs), and their oncogenic forms, most notably BCR-ABL (33). As another example of a compound from this class of anticancer agents, is the multi-target receptor TKI sunitinib (administrated by oral via), that prolongs survival in patients with GIST and RCC after disease progression or with intolerance to IMA (31, 34). Sunitinib inhibits cancer and angiogenesis as amongst its targets are VEGFRs, mast/stem cells growth factor receptor (SCFR, c-KIT or CD117), PDGFRs, the *ret* oncogene product, RET and adenosine monophosphate-activated protein kinase (AMPK), among others (30, 35). PAZ is a small molecule selective for VEGFRs -1, -2 and -3 that is used in the therapy of advanced RCC and soft tissues sarcomas. In turn, PAZ inhibits the angiogenesis in tumors in which VEGFRs -1, -2 and -3, c-KIT and PDGFRs are upregulated (36). Finally, SOR is an anticancer drug approved by the FDA for the treatment of unresectable hepatocellular carcinoma and advanced RCC. Like sunitinib, SOR is not very selective as well. SOR can decrease tumor cell proliferation by inhibiting tyrosine kinase receptors like RAF/MEK/ERK, VEGFR, PDGFR, c-KIT and several other kinases (37, 38).

1.4.1. Cardiotoxicity of TKIs

Despite strong anti-cancer effects, surprisingly these targeted therapies also suffer for the lack of selectivity and also inhibit tyrosine kinases in non-cancer cells, leading to the appearance of toxicity and adverse side effects. These small-molecules, multi-targeted receptors tyrosine kinase inhibitors, are often associated with adverse effects, such as, muscle cramps, diarrhea, nausea, stomatitis, nasal bleeding and skin rashes. Nonetheless, the treatment with IMA is generally well tolerated with a low incidence of severe side effects (30, 35). However, over the last decade, evidence shows that these therapies are not completely safe for the cardiovascular system. The TKIs are frequently associated with cardiac dysfunction, generally linked to inhibition of key signaling pathways for cardiomyocyte survival and homeostasis (30, 39-41). HF, QT prolongation, hypertension,

LVEF, among others have been seen after TKIs administration (30) (Figure 1), as will be discussed later.

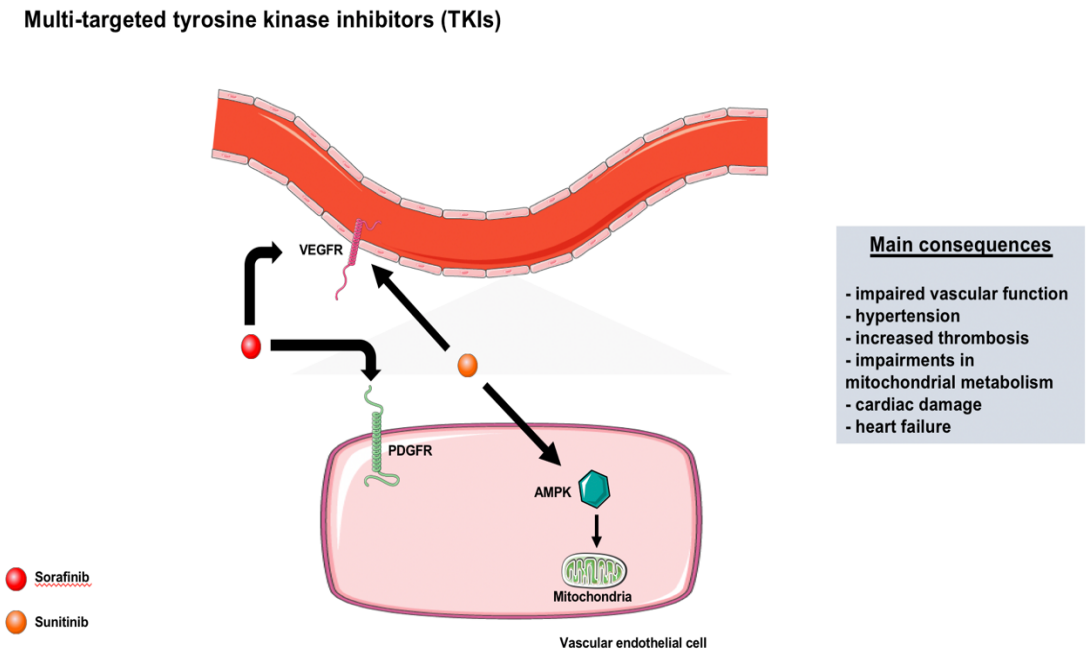


Figure 1. Schematic representation of the main molecular targets of the compounds sorafenib and sunitinib and their main consequences in the cardiovascular system. The TKIs sorafenib and sunitinib primarily target VEGFR and PDGFR. Inhibition of VEGF has as its main consequence the induction of hypertension and deleterious effects at the cardiac level, due to its interference with blood flow, angiogenesis and vascular integrity. Moreover, inhibition of PDGFR and AMPK are associated with impairments in energy homeostasis, targeting mostly mitochondria, and affecting cell survival, which may lead to heart failure (14, 42).

1.4.2. Clinical data

Clinical data regarding TKIs cardiotoxicity are recent and even more difficult to assess for the new TKIs recently used in therapy. Even so it is clear that the heart is an off target. Effectively, there is in the literature a wide list of adverse effects associated with cardiotoxicity of these compounds. Initially, in the case of IMA, according to a report by Kerkela *et al.*, 10 patients developed congestive HF after taking IMA mesylate. Using cultured cardiomyocytes of mice and humans, the authors showed that IMA is cardiotoxic and, in humans, can lead to severe LVD and HF. In addition, the authors also presented experimental evidence for a causal role of the inhibition of c-Abl in the pathogenesis of congestive HF and suggested that the cardiotoxic effects of IMA are mediated via inhibition of c-Abl signaling pathways (43). However, these results were questioned by several

authors who eventually came to different conclusions. Effectively, several studies have proven that the incidence of IMA-induced cardiotoxicity was very low and that cardiotoxic adverse side effects could occur preferentially in patients with pre-existing heart disease. Thus, IMA may precipitate pre-existing heart disease rather than inducing cardiotoxicity in most reported patients (44). Still, IMA and potentially also other Abl kinase inhibitors can in fact cause HF. This potential side effect justifies careful monitoring, which should be started immediately after initiation of treatment (44).

After several reports, researchers began to be more interested in the cardiotoxicity of these new compounds and adopted a monitoring strategy as a way to address new studies. Cardiotoxicity was not observed in a medium-sized sample of "real world" patients under long-term therapy with IMA. In fact, median brain natriuretic peptide (BNP) blood levels and echocardiographic indices of systolic and diastolic LV function were not different in patients who used and did not use the drug. Most of the included patients had been taking the drug for at least 2 years, which suggested that cardiotoxicity did not develop even with long-term use (33). However, despite the absence of systematic cardiac toxicity in that study, there is still the possibility of isolated cases of cardiotoxicity associated with IMA. Cardiomyopathy leading to HF is a serious adverse effect of treatment in various classes of TKIs. For IMA, the risk was reported to be 1-2% for clinically significant HF in patients with hematologic malignancies (43, 45, 46).

After IMA, several compounds were also used for cancer treatments such as sunitinib and SOR; however, both have also been shown to cause cardiotoxicity. In fact, in a retrospective study by Chu and colleagues, two of 75 participants with GIST had a cardiac infarction and six (8%) developed congestive HF. For patients treated with the dose approved by the FDA, LVEF declined progressively during sunitinib treatment from a baseline of 64.5% to 59.4% after the fourth cycle, 19% of patients had a LVEF of 15 percentage points or more during treatment and 47% of patients developed hypertension. Other findings by Schmidinger and colleagues also suggested that sunitinib has clinically relevant cardiotoxicity. In that study, 73 patients with normal serum creatine kinase and cardiac troponin-T concentrations at baseline were treated with sunitinib or sorafenib. Upon treatment, creatine kinase (myocardial-band isoenzyme) rose in 23% of patients, accompanied by clinical cardiac symptoms in 10%. Six of the 17 evaluated patients had abnormal echocardiographical findings, such as reduced LVEF (47). Of note, cardiac adverse effects associated with SOR seem similar to those related to sunitinib. Furthermore, a trial investigating the use of adjuvant sunitinib in patients with RCC showed hypertension in 44.7% of patients vs. 13.1% in the placebo group (48). In a phase III clinical trial regarding metastatic RCC, 17% of the 903 participants receiving SOR developed hypertension, when compared to 1% in the placebo group (49). In a phase II trial comparing

axitinib and SOR, axitinib showed higher toxicity, with 40% of patients showing any grade of hypertension (vs. 29% in the sorafenib group). However, this adverse event led to treatment discontinuation in only one patient in the axitinib group (50). Moreover, hypertension after treatment with TKIs is a predictor of treatment responses, since data suggest that patients who develop hypertension during TKI therapy have a longer median overall survival and progression-free survival compared with those who do not develop this type of cardiovascular adverse effect (31). Nonetheless, the former group requires adequate and effective cardiovascular therapy. However, in addition to hypertension these compounds also cause other adverse side effects. Sunitinib and SOR have been reported to cause conduction disturbances that lead to electrocardiogram (ECG) abnormalities, like QTc prolongation, an effect that seems to be dose dependent (47, 51). A meta-analysis that included 6548 patients from 18 clinical trials showed a significant risk of QTc prolongation for sunitinib but not for PAZ or axitinib and SOR (51).

Moreover, TKIs drugs are also associated with the risk of HF and thromboembolic events. A large meta-analysis with almost 7000 patients receiving sunitinib showed a 4.1% incidence of HF of any grade (52). However, data from clinical trials and retrospective studies revealed a decrease in LVEF in 21-28% of patients, with a HF incidence of 3-15% (52). Lastly, a systematic review with a meta-analysis of 10,000 patients included 10 phase II and III studies on sunitinib and SOR revealed a prevalence of arterial thromboembolic events of 1.4%, with no meaningful difference between the drugs (53). In addition, another meta-analysis that included prospective phase II and III trials of a total of 14 studies (4,430 patients) that evaluated PAZ, sunitinib, SOR and axitinib showed that the incidence of thromboembolic events related to VEGFR-TKIs was 3%, and there was no statistically significant increase in the risk of thromboembolic events for VEGFR-TKIs *versus* controls in overall population (54). None of the two meta-analyses confirmed an elevated risk of venous thromboembolic events in patients treated with sunitinib, SOR, axitinib or PAZ (54). Moreover, in the study performed by Kerkela *et al*., they identified severe mitochondrial structural abnormalities in the heart of a patient with sunitinib-induced HF. This patient had a B-type natriuretic peptide (BNP) of 79 pg/mL (normal 80 pg/mL) and a LVEF of 65% compared to a BNP that increased to 2,300 pg/mL and LVEF decreased to 20-25% after the patient had HF, that is, before and after treatment with sunitinib, respectively (55).

Based on this findings, it can be concluded that this class of targeted therapy is quite associated with various cardiotoxicity adverse effects manifested as hypertension, HF, cardiac arrhythmias (bradyarrhythmias, tachyarrhythmias, QTc prolongation), thromboembolic events, fluid retention and exacerbation of coronary artery disease, as can be seen in Table 2. Despite what has been mentioned they are excellent drugs for inhibition

of certain cancer pathways and can therefore be considered great drugs for cancer treatment.

Table 2. Clinic studies that highlight the incidence of cardiotoxicity of the main compounds in the TKIs class.

NUMBER OF PATIENTS	TYPE OF CANCER	ANTICANCER TREATMENT	CARDIAC EFFETCS	STUDY
48 patients	Renal cell carcinoma (85%) Gastrointestinal stromal tumor (15%)	Sunitinib	15% with symptomatic HF Hypertension 17% Coronary artery disease 6% Congestive HF/Cardiomyopathy 6%	(56)
86 patients	Renal cell carcinoma	Sunitinib and sorafenib	Among 74 assessable patients, 33.8% experienced a cardiovascular event (sunitinib, n = 11; sorafenib, n = 14) Electrocardiogram (ECG) changes were found in 12 of 25 event patients (changes in rhythm, conduction disturbances, in axis, in QRS amplitude, ST segment depression and elevation, T wave, and QT prolongation) Echocardiograms that were obtained in 22 patients were abnormal in 10 patients; reduced LVEF (n = 9), regional contractile dysfunctions (n = 7), relaxation disturbances greater than grade 1 (n = 1), and pericardial effusion (n = 1)	(47)

75 patients	Gastrointestinal stromal tumor	Sunitinib	11% of patients had a cardiovascular event, with congestive heart failure recorded in 8% Ten of 36 (28%) patients had absolute LVEF reductions in ejection fraction (EF) of at least 10%, and seven of 36 (19%) had LVEF reductions of 15 EF% or more Sunitinib induced increases in mean systolic and diastolic blood pressure, and 47% individuals developed hypertension	(31)
723 patients	Renal cell carcinoma	Axinitib (N=361) Sorafenib (N=362) Of these, 54% patients had previously received sunitinib, 35% cytokines, 8% bevacizumab, and 3% temsirolimus	Hypertension: axinitib (40%) and sorafenib (29%)	(32)

750 patients	Renal cell carcinoma	Sunitinib (N= 375) Or interferon alfa (N= 375)	Hypertension: Sunitinib (24%) and interferon alfa (1%) LVEF: Sunitinib (2%) and interferon alfa (1%)	(57)
1110 patients	Renal cell carcinoma	Pazopanib (N= 557) Sunitinib (N= 553)	Hypertension: Pazopanib (46%) and sunitinib (41%) Cardiac dysfunction: Pazopanib (13%) and sunitinib (11%) Myocardial infarction or ischemia: Pazopanib (2%) and sunitinib (4%) Fatal adverse events: Pazopanib (2%) and sunitinib (3%)	(58)
369 patients	Metastatic soft-tissue sarcoma	Pazopanib (N=246) or placebo (N=123)	Hypertension: Pazopanib (41%) and placebo (7%)	(59)
861 patients	Renal cell carcinoma	Pembrolizumab and axitinib (N= 432) Or sunitinib (N= 429)	Death: 2.6% in the pembrolizumab–axitinib group and 3.5% in the sunitinib group. Hypertension: Pembrolizumab and axitinib (44.5%) and sunitinib (45.4%)	(60)

1 patient (case report)	Renal cell carcinoma	Developed acute decompensated systolic heart failure after 11 months of sunitinib treatment (37.5 mg daily of 4 weeks on treatment/2 weeks off treatment)	B-type natriuretic peptide (BNP) of 79 pg/mL (normal < 80 pg/mL) and an LVEF of 65%. When the patient presented with heart failure, BNP was 2,300 pg/mL and LVEF had decreased to 20–25%	(55)

Abbreviations: B-type natriuretic peptide (BNP); Doxorubicin and cyclophosphamide followed by docetaxel (AC-T); Doxorubicin and cyclophosphamide (AC); Ejection fraction (EF); Heart failure (HF); Left ventricular ejection fraction (LVEF); Number (N); Corrected QT interval (QTc).

1.4.3. Pre-clinical and *in vitro* studies

With the longer-term clinical experience of some of TKIs, their use has been shown to result in cardiotoxicity, as was seen with the monoclonal antibody tyrosine kinase-targeted anticancer drugs trastuzumab (Herceptin) and bevacizumab (Avastin). While, many new targeted small molecule anticancer kinase inhibitors are actively being developed, there are several pre-clinical and *in vitro* studies featuring the cardiotoxicity of TKIs, which will be discussed next.

As already mentioned throughout the work, IMA and sunitinib, among others, are TKIs inhibitors that prolong survival rate in cancer patients. In terms of mechanisms, in a mouse model, the authors found that sunitinib caused mitochondrial damage and apoptosis in cardiomyocytes (31). In the studies performed by Kerkela and colleagues, two types of experiments were done: i) C57B7/6 mice were treated with sunitinib (25 mg/kg/day) mixed with chow for 5 weeks and ii) in cultured cardiomyocytes of neonatal rat ventricular myocytes (NRVMs) isolated from 2- to 3-day old Sprague-Dawley rats. In the *in vitro* study, they tested the loss of mitochondrial membrane and the ATP content and the cells were treated with vehicle (H_2O) or 1μM sunitinib for 12h or sunitinib for 8h, respectively (55). The main findings of this study highlight the myocyte loss and cardiomyocyte hypertrophy without an accompanying increase in cardiac mass in the sunitinib-treated hearts when compared to vehicle treated (H_2O) and a loss of mitochondrial membrane potential and energy rundown occurred in cardiomyocytes after sunitinib exposure. Surprisingly, based on determination of the concentration of a drug or inhibitor needed to inhibit a biological process or response by 50% (IC50) for sunitinib versus AMPK in kinase assays *in vitro*, they found that AMPK was directly target by sunitinib, since it inhibited AMPK with an IC50 of 216 ± 58nM. These data suggest that sunitinib is a potent inhibitor, particularly of activated AMPK. In summary, AMPK activity, which should be increased in the setting of energy compromise, is reduced in cardiomyocytes in culture, and this is due to direct inhibition of AMPK by sunitinib (55). Thus, the mechanisms of the cardiotoxicity of sunitinib have been ascribed to the inhibition of AMP-activated protein kinase, an essential kinase in the maintenance of metabolic homeostasis in the heart, especially in the environment of energy stress.

In addition, on the study performed by Hasinoff *et al.*, they aimed to correlate binding constants and binding selectivity scores of the kinase inhibitor with damage induced by kinase inhibitors in neonatal cardiac myocytes isolated from 2–3 days old Sprague–Dawley rats. For this, they studied 8 approved FDA-tyrosine kinase inhibitors and 10 other kinase inhibitors and related the toxicity with a panel of 317 kinases. Hence, the 18 kinase inhibitors

studied were: canertinib, dasatinib, dovitinib, erlotinib, flavopiridol, gefitinib, IMA, lapatinib, midostaurin, motesanib, PAZ, SOR, staurosporine, sunitinib, tandutinib, tozasertib, vandetanib and vatalanib. According to the results obtained, the kinase inhibitors caused a time dependent damage to neonatal cardiac myocytes (61), according to the lactate dehydrogenase (LDH) release assay. Lapatinib and gefitinib caused the least amount of myocyte damage, measured by LDH release (0.6% and 2.8%, respectively, after 72h), and in the case of lapatinib, this only reached a significant different value to the untreated control ($p = 0.048$) with 5μM after 72h. In contrast, flavopiridol and staurosporin caused the highest LDH (39.6% and 66.2%, respectively). Both results were determined after a 72h treatment with 5μM. In addition, the binding of the kinase inhibitor was directly related to myocyte damage in the specific case of 12 kinases (61). In conclusion, the cardiotoxicity of these agents may derive from the general lack of specificity of binding to tyrosine and serine-threonine kinases and not from specific binding of any group (61).

Several studies suggested a role for the aryl hydrocarbon receptor (AhR) and its regulated genes such as cytochrome P4501A1 (CYP1A1) in the pathogenesis of HF and cardiac hypertrophy (62). To test the hypothesis that sunitinib induces cardiac hypertrophy through the modulation of AhR, Maayah *et al*., treated adult male Wistar albino rats weighing 230–250g for 15 and 30 days with increasing doses (25, 50, and 100mg/kg). Thereafter, cardiac hypertrophy parameters were determined at the biochemical, histopathology, and gene expression levels. In more details, on the one hand, 8 groups of 6 rats each were created : i) groups 1 and 2: controls (normal saline 2.5ml/kg/day) for 15 and 30 days, respectively, ii) groups 3 and 4: injected with sunitinib (25mg/kg/day) for 15 and 30 days, respectively, iii) groups 5 and 6: received sunitinib (50mg/kg/day) for 15 and 30 days, respectively and iv) groups 7 and 8: injected with sunitinib (100mg/kg/day) for 15 and 30 days, respectively. All drugs were injected intraperitoneally. The results show that, when compared to the control group, the administration of sunitinib (100mg/kg) generated large increases in serum creatine kinase (CK), approximately 441%, and in the MB fraction of creatine kinase (CK-MB), approximately 318%. Moreover, there was also a significant alteration of cardiac hypertrophic markers, Atrial natriuretic peptide (ANP), BNP and iron-corrected T1 mapping (CT-1), in a dose-dependent manner, in the treatment with sunitinib. The differences caused by these markers during the 15 and 30 days period was approximately 16, 3 and 2 folds, compared to 85, 23 and 160 folds respectively, at the highest dose tested. Likewise, sunitinib treatment caused four times the induction of CYP1A1 gene expression at a dose of 100mg/kg, after 15 days of treatment against 55 times after 30 days. Sunitinib also induced CYP1A1 mRNA in a dose and time-dependent manner. *In vitro,* the authors of the previous studied used the rat H9c2 cells that were

incubated for 24h to wide concentrations range of sunitinib (0, 0.5, 1, 2.5, 5, 25, 50, and 100μM). The effect of sunitinib on ANP and CT-1 gene expression or CYP1A1 mRNA was studied, when H9c2 cells were treated for 12h with various concentrations of sunitinib (0, 1, 2.5, and 5μM). Furthermore, other effects were tested. For instances, the effect of the antagonist Ahr, resveratrol (RES), on sunitinib-mediated induction of hypertrophic genes was studied, where H9c2 cells were simultaneously treated with sunitinib (5μM) for 12h. On the other hand, the effect on CYP1A1 expression of the Ahr agonist (SB, 10μM), was tested (203) when cells were cells incubated with sunitinib (5μM) for 12h (62). With regard to *in vitro* experiences, the authors concluded that sunitinib 25, 50, and 100μM significantly decreased the cell viability by approximately 35, 50, and 70%, respectively with the MTT reduction assay. This drug also caused a significant induction of the cardiac hypertrophic markers, ANP and CT-1, at 5μM. In addition, sunitinib induced CYP1A1 mRNA in H9c2 cells in a time and concentration-dependent manner. In that, sunitinib treatment for 12h induced CYP1A1 mRNA levels by approximately 2- and 10.5-fold at 2.5 and 5μM concentration, respectively (62). In conclusion, treatment with sunitinib pathophysiological damage to the heart and increased various hypertrophic markers. AhR and the CYP1A1 directly involvement in sunitinib induced cardiac hypertrophy in H9c2 cells was supported by the ability of RES, to block sunitinib-induced hypertrophy and the ability of SB potentiate hypertrophic genes induced by the sunitinib (62).

Besides the cardiac hypertrophy caused by sunitinib, this drug is also involved in inflammatory and fibrotic processes (63). The mechanisms involved in the cardiotoxicity, as well the potential cardioprotective effects of L-carnitine (LC) caused by sunitinib were studied in male Wistar rats (6–8 weeks old), that were divided into 4 groups of 6 animals each: i) Control group (no treatment, free access to tap water); ii) rats treated with LC (400mg/kg body weight/day dissolved in the drinking water); iii) rats treated with sunitinib (25mg/kg body weight/day also dissolved in the drinking water); iv) rats treated with LC and sunitinib (at the above-indicated doses). Treatment with sunitinib was initiated 2 weeks later than that with LC, and was maintained for 8 weeks, so, treatment with LC lasted a total of 10 weeks. The authors demonstrated that the gene expression of IL-1β, IL-6 and nuclear factor kappa B (NF-κB) was significantly increased (2.2-, 3.8- and 3.2-fold, respectively), in rats treated with sunitinib. However, simultaneous treatment with LC decreased these values, reaching those observed in control rats. The authors then proceeded with *in vitro* studies. And the myoblast cell line, H9c2 cell line, was treated with sunitinib (5μM; 24h incubation) and an inhibitor of NF-κB, SN50 (5μM) (63). Acute exposure of H9c2 cells to sunitinib led to an activation of NF-κB (76%) after 40 min of incubation, with greater translocation of the NF-κB complex to the nucleus. Nevertheless, this effect of sunitinib was

abolished by pre-incubation with LC. As in the *in vivo* experiments, the exposure of H9c2 cells to LC alone had no effect when compared to the control group, untreated. Further, in cells treated with sunitinib in the presence of SN50, the results revealed that the SN50 attenuated the effect of sunitinib regarding the content of NOX2, IL-6, CTFG and MMP9 (63). To conclude, these data showed that inflammatory and fibrotic processes are involved in sunitinib-induced cardiotoxicity, while LC exerts protective effect against cardiac damage secondary to sunitinib treatment. Moreover, NF-κB might play an important role in the cardiotoxicity of sunitinib (63).

To finish, Neves *et al*., demonstrated how microparticles (MPs) of cancer patients treated with inhibitors of the VEGF (VEGFi), such as PAZ, sunitinib, or SOR mediate the endothelial cell injury, comparing the effects of isolated MPs before and after treatment with VEGFi. Herein, human aortic endothelial cells (HAECs) were stimulated with isolated plasma MPs, which were isolated from 39 cancer patients before and after treatment with VEGFi. HAEC cells were pre-treated with BQ123 (ETA receptor antagonist; 1mmol/L) or BQ788 (ETB receptor antagonist; 1mmol/L) and are stimulated with vatalanib, another VEGFi (64). Furthermore, NADPH stimulated O_2^- production was assessed by lucigenin assay. The HAEC cells were exposed to total pre-treatment and post-treatment MPs for 5, 15, 30, and 60min (n = 5–6) or to post-treatment MPs for 5, 30, and 60min in presence or absence of BQ123 or BQ788 (n = 5–9). After these experiences, the authors highlight an increase in NADPH-dependent O_2^- generation after treatment with VEGFi. Additionally, MPs from VEGFi-treated patients caused an increase in endothelial reactive oxygen species (ROS) production that promotes endothelial dysfunction and inflammation in HAEC, effects attenuated by ETA and ETB receptor blockers. Furthermore, they show that post-VEGFi treatment endothelial cell-derived microparticles (ECMPs) induced an increase in pre-pro-ET-1 mRNA expression, corroborating the increase in endothelin-1 (ET-1) production in HAEC stimulated with vatalanib. These results define a new mechanism involving interplay between microparticles, the ET-1 system and endothelial cell pro- inflammatory and redox signaling, which may be important in cardiovascular toxicity and hypertension associated with VEGFi anti-cancer treatment (64)

To further reinforce the role of TKIs at the level of cardiotoxicity, in addition to the vast examples described above, several preclinical and *in vitro* studies characterizing are illustrated in the following tables.

Table 3. Incidence of cardiac effects of the main compounds in the TKIs class in preclinical studies.

ANIMALS	TREATMENT	CARDIAC EFFETCS	STUDY
Male Sprague-Dawley Rats (150–180 g)	Test the effects of the 4 TKIs on basal and ADP-stimulated respiration in rat heart-derived mitochondria: Dasatinib, sunitinib, and imatinib were tested up to a concentration of 250 nmol/mg, whereas sorafenib was tested up to 100 nmol/mg protein	None of the four drugs had a statistically significant effect on basal respiration at the highest dose tested; Sorafenib inhibited ADP-stimulated respiration > 80% at 100 nmol/mg protein; Only sorafenib directly impaired mitochondrial function at clinically relevant concentrations, potentially contributing to the cytotoxic effect of the drug.	(65)
Male Wistar rats (6–8 weeks old)	They were divided into 4 groups of 6 animals each: Control group (no treatment, free access to tap water); Rats treated with L-Carnitine (400 mg/kg body weight/day dissolved in the drinking water); Rats treated with sunitinib (25 mg/kg body weight/day also dissolved in the drinking water);	Inflammatory and fibrotic processes are involved in sunitinib-induced cardiotoxicity; L-Carnitine exerts protective effect against cardiac damage secondary to sunitinib treatment	(63)

	Rats treated with L-Carnitine and sunitinib (at the above-indicated doses); Treatment with Sunitinib was initiated 2 weeks later than that with L-Carnitine, and was maintained for 8 weeks (that is, treatment with L-Carnitine lasted 10 weeks)		
Sprague–Dawley rats (2–3 days old)	Myocytes were continuously treated with either 2 μM and 5 μM with the kinase inhibitors (imatinib mesylate, lapatinib ditosylate, sunitinib, pazopanib, sorafenib and so on) for 24, 48 and 72h	Kinase inhibitor-induced myocyte damage; Cardiotoxicity may derive from the general lack of specificity of tyrosine binding and serine-threonine kinases and not from specific binding of any group; The binding of the kinase inhibitor was directly related to myocyte damage in the specific case of 12 kinases and of these 12, only MEK1 and MEK2 were previously clearly identified as having a role in which their inhibition may result in cardiotoxicity	(61)
Male 129S1/SvlmJ mice (18 male 8-week-old mice)	Vehicle or Sunitinib (40 mg/kg/day) or Sunitinib + trimetazidine (TMZ) (20 mg/kg/day) via oral gavage for 28 days Mice were randomized into 3 groups of 6:	Sunitinib induces hypertension (28.33 ± 5.00 mmHg) and left ventricular dysfunction (11.16 ± 2.53%);	(66)

	Group sunitinib received 40 mg/kg/day of sunitinib Co-administration group sunitinib + TMZ received 40 mg/kg/day of sunitinib and 20 mg/kg/day of TMZ Control groups received daily administration of the vehicle of the corresponding volume	Sunitinib + TMZ reverses sunitinib induced cardiotoxicity and activates the AMPK/mTOR/autophagy pathway	
Zebrafish Embryos	Sunitinib and vehicle control (0.1% DMSO) Zebrafish embryos exposed to sunitinib (2 μM) at 8h post-fertilization for 12h or injected with fibroblast growth factor 2 (FGF2) mRNA	Zebrafish embryos injected with FGF2 mRNA, producing low molecular weight FGF2, displayed less cardiotoxicity than treated with sunitinib alone FGF2 prevented sunitinib-induced cardiotoxicity	(67)
Female FVB mice, 14 to 16 weeks old	Mice had gavage with Vehicle (n=4), sorafenib (n=5, 30 mg/kg per day), sunitinib (n=5, 40 mg/kg per day) or erlotinib (n=5, 50 mg/kg per day), once daily for 2 weeks	Heart weight indexed to body weight was higher in erlotinib- and sorafenib-treated mice (45% and 46%) when compared with vehicle (40%). Treatment with sorafenib and sunitinib, but not erlotinib, led to increased indexed lung weight, consistent with left heart failure Erlotinib had no significant effect on any echocardiographic parameters. Sunitinib and sorafenib both caused variable decreases in fractional shortening and increases in left ventricular end systolic volume	(68)

		MIB-MS and RNAseq both indicated that cardiac STAT3 activity was upregulated by erlotinib treatment	
Mice were 10-week old FVB/N females (10/group)	Erlotinib 50 mg/kg/day or sunitinib 40 mg/kg/day or vehicle daily for 2 weeks	Sunitinib-treated mice had decreases in systolic function, elevation in liver cholesterol levels, elevated ethanolamine in the serum; Erlotinib did not affect contractile function	(69)
C57B7/6 mice	Vehicle (H_2O) and Sunitinib (25 mg/kg/day) mixed with chow for 5 weeks	Myocyte loss and cardiomyocyte hypertrophy without an accompanying increase in cardiac mass in the sunitinib-treated hearts 5' adenosine monophosphate-activated protein kinase (AMPK) activity, which should be increased in the setting of energy compromise, is reduced in hearts of sunitinib-treated, and this is due to direct inhibition of AMPK by sunitinib	(55)
Adult male Wistar albino rats, weighing 230–250 g (n=48)	8 groups of 6 rats each and animals were injected intraperitoneally:	Sunitinib induces cardiac hypertrophy in a dose-dependent manner;	(62)

	Groups 1 and 2: controls (normal saline 2.5 ml/kg/day) for 15 and 30 days, respectively; Groups 3 and 4: injected with sunitinib (25 mg/kg/day) for 15 and 30 days, respectively; Groups 5 and 6: received sunitinib (50 mg/kg/day) for 15 and 30 days, respectively; Groups 7 and 8: injected with sunitinib (100 mg/kg/day) for 15 and 30 days, respectively	Administration of sunitinib (100 mg/kg) resulted in significant increases in serum creatine kinase (CK) and creatine kinase MB fraction (CK-MB) by approximately 441 % and 318 %, respectively, as compared with the control group; Sunitinib treatment induced CYP1A1 mRNA in a dose- and time-dependent manner	
Wild-type C57BL6 mice	Treated healthy mice with vehicle or imatinib for 3 or 6 weeks at a dose of 50, 100 or 200 mg/kg/d; Hearts from mice treated with intraperitoneal injections of vehicle or imatinib (50 mg/kg/d) for 3 weeks; Mitochondria were isolated from hearts of mice treated with either imatinib (200 mg/kg/d) or vehicle for 5 weeks	Imatinib was sufficient by itself to induce cardiotoxicity, culminating in left ventricular contractile dysfunction and dilatation (ejection fraction was 49% against 35.9% for vehicle or treatment with sunitinib 200 mg/kg/d, respectively)	(43)

Abbreviations: 5’ adenosine monophosphate-activated protein kinase (AMPK); creatine kinase (CK); creatine kinase MB fraction (CK-MB); fibroblast growth factor 2 (FGF2); trimetazidine (TMZ)

Table 4. Reports of cardiotoxicity of several TKIs class compounds in *in vitro* studies.

ANIMALS	TREATMENT	CARDIAC EFFETCS	STUDY
H9c2 cells were grown in either high-glucose or galactose-containing medium and kept in 5% CO_2 at 37°C	Cells were incubated for 24h with the four TKIs (imatinib, sunitinib, sorafenib and dasatinib) at concentrations up to 100 μM in media containing either glucose (glycolytic conditions) or galactose (mitochondrial-dependent conditions)	According to the CellTiter-Glo Luminescent Cell Viability Assay, sorafenib was significantly more toxic to galactose-grown cells than glucose-grown cells, demonstrating a greater than fourfold shift in the IC_{50} (10.1 μM vs. 44.7 μM respectively); In contrast, imatinib, dasatinib, and sunitinib were equally cytotoxic to both glucose and galactose-grown cells	(65)
Rat cardiomyocytes (H9c2 cell line)	Cells were treated with sunitinib (5 μM; 24h incubation) in the presence or absence of an NF-κB inhibitor, SN50	Inflammatory and fibrotic processes are involved in sunitinib-induced cardiotoxicity by the expression of pro-fibrotic factors, nitrotyrosine and NOX 2 subunit of NADPH oxidase; and by a decrease in that of collagen degradation factor; Cardiotoxic effects of sunitinib were blocked by NF-kB inhibition	(63)

Rat cardiomyocyte derived cell line H9c2	H9c2 cells were treated with sunitinib (0.16–100.00 μM) for 48h	Sunitinib inhibited the proliferation of rat H9c2 cardiomyocytes (IC_{50} value was 6.53 μM, and the survival fraction of 20 μM sunitinib group was 14.23%) and induced apoptosis;	(70)
Adult cardiac myocytes were freshly isolated from 8–12-week-old male C57BL/6 mice HL-1 cell line	Sunitinib and vehicle (DMSO 0.1%) HL-1 cells were incubated either with 1 μg/mL sunitinib, 0.1 μg/mL sunitinib or empty vehicle (DMSO) for 24h. All experiments were performed in triplicate.	Sunitinib exposure significantly decreased sarcomere shortening and Ca2+ transients; Myofilament Ca^{2+} sensitivity was not altered, while reactive oxygen species (ROS) levels were significantly increased after exposure to the drug; MicroRNAs (miR-684_2, let-7b_1, miR-39c, miR-467f_1, miR-296_3p, miR-673_5p, miR-341, miR-451) expression patterns were not altered by sunitinib	(71)
H9c2 cardiomyocytes	Vehicle or Sunitinib (2-10μM) or Sunitinib + trimetazidine (TMZ) (40-120μM) for 48h	Sunitinib reduces cell viability and inhibits the AMPK/mTOR/autophagy pathway; Sunitinib + TMZ alleviates cell viability loss in H9c2 cardiomyocytes and activates the AMPK/mTOR/autophagy pathway	(66)

Human aortic endothelial cells (HAECs) were stimulated with isolated microparticles (MPs)	Plasma MPs were isolated from 39 cancer patients before and after treatment with VEGFi (pazopanib, sunitinib, or sorafenib) To assess effects of patients microparticles on endothelial cell signaling and function they used HAEC: cells were pre-treated with BQ123 (ETA receptor antagonist; 1 mmol/L) or BQ788 (ET_B receptor antagonist; 1 mmol/L) and are stimulated with vatalanib (VEGFi)	Post-VEGFi treatment endothelial cell-derived microparticles (ECMPs) induced an increase in pre-pro-ET-1 mRNA expression, corroborating the increase in endothelin-1 (ET-1) production in HAEC stimulated with vatalanib; MPs from VEGFi-treated patients caused an increase in endothelial ROS production that promotes endothelial dysfunction and inflammation in HAEC, effects attenuated by ETA and ETB receptor blockers	(64)
The human iPSC-derived “iCell Cardiomyocytes” (iPSC-CMs)	Sunitinib and DMSO-treated control groups After the iPSC-CMs were cultured for 5–6 d, they were stimulated with sunitinib (0.3 μM, 1 μM, or 3 μM) with or without XMU-MP-1 a small molecule inhibitor of kinases MST1/2, homologs of Hippo, (0.3 μM, 1 μM, or 3 μM) for 72h To evaluate the effect of drug washout on sarcomere structure, the sunitinib-containing medium was removed and replaced with fresh drug-free medium after 72h of sunitinib stimulation for another 72h (they have two different	iPSC-CMs have the ability to recover from sunitinib-induced sarcomere disruption, suggesting that can mimic the reversibility of LVEF decreases observed in sunitinib- treated patients; Hippo pathway is involved in the process of sunitinib-induced disruption of sarcomere and its recovery after drug washout; Inhibition of the Hippo pathway with XMU-MP-1 suppressed the sunitinib-induced disruption of sarcomere	(72)

	time points 72h and 144h for sarcomere analysis after sunitinib washout)		
Cardiomyoblast H9c2 cells, Caki-1 and OS-RC-2 renal cell carcinoma cells	For the measurement of cell viability, cells were seeded for 12h. Sunitinib (10 μM) with or without FGF2 was then added to the cells for another 12h	FGF2 Protects Against Sunitinib-Induced Cardiotoxicity Without Compromising its Antitumor Activity *in vitro;* FGF2 Reversed Sunitinib-Induced Decrease in PLC-c/ c-Raf Protein levels in H9c2 Cells	(67)
Neonatal rat ventricular myocytes (NRVMs) were isolated from 2- to 3-day old Sprague-Dawley rats	Cells were treated with vehicle (Control) or 1μM sunitinib for 12h ATP content: cells were treated with vehicle (control) or sunitinib for 8h	Sunitinib induces loss of mitochondrial membrane potential and energy rundown; Sunitinib indirectly inhibits the mTOR 1 complex (mTORC1); AMPK activity, which should be increased in the setting of energy compromise, is reduced in cardiomyocytes in culture, and this is due to direct inhibition of AMPK by sunitinib	(55)
Rat cardiomyocyte H9c2 cells	Cells viability: cells were exposed for 24h to wide concentrations range of sunitinib (0, 0.5, 1, 2.5, 5, 25, 50, and 100μM)	Sunitinib 25, 50, and 10 μM significantly decreased the cell viability by approximately 35, 50, and 70 %, respectively; Sunitinib caused a significant induction of the cardiac hypertrophic	(62)

	Effect of sunitinib on ANP and CT-1 gene expression or CYP1A1 mRNA: H9c2 cells were treated for 12h with various concentrations of sunitinib (0, 1, 2.5, and 5μM) Effect of the AhR antagonist, resveratrol (RES), on sunitinib mediated induction of hypertrophic genes: H9c2 cells were treated with sunitinib (5μM) in the absence or presence of SB (10μM) for 12h Effect of the AhR agonist, SB203580 (SB), on sunitinib induced CYP1A1 and ANP mRNA: H9c2 cells were treated with sunitinib (5μM) in the absence or presence of SB (10μM) for 12h	markers, ANP and CT-1, only at the highest concentration (5μM); Sunitinib induced CYP1A1 mRNA in H9c2 cells in a concentration-dependent manner. In that, sunitinib treatment for 12 h induced CYP1A1 mRNA levels by approximately 2- and 10.5-fold at 2.5 and 5μM concentration, respectively AhR and the CYP1A1 are directly involved in sunitinib induced cardiac hypertrophy	
Human myocardium muscle strips isolated from right atrial appendages (*n* = 26 from six hearts) of patients undergoing heart surgery	Sunitinib and vehicle (DMSO 0.1%) Sunitinib was added to the organ bath to a final concentration of 0.1, 1 or 10 μg/mL. To test the reversibility of the effects, they measured the developed force reached within 5 min after removing sunitinib from the perfusate. Control muscle strips obtained from the same hearts were treated with DMSO at a concentration of 0.1%	Higher concentrations of sunitinib (1 and 10μg/mL) decreased developed force at 30 minutes 76.9 + 2.8 and 54.5 + 6.3%, compared to 96.1 + 2.6% in controls ($P < 0.01$); Administration of vehicle alone (0.1% DMSO) did not affect developed force or diastolic tension	(71)

Neonatal rat ventricular myocyte (NRVM) were prepared from 2-4 days old Sprague-Dawley rats	NRVMs were treated with vehicle or imatinib (2, 5 or 10μM) for 24h	Imatinib induces activation of the endoplasmic reticulum (ER) stress response, loss of mitochondrial membrane potential, cytochrome c release and cell death in a dose-dependent manner; cardiotoxic effects of imatinib are mediated via inhibition of c-Abl signaling pathways	(43)

Abbreviations: cell-derived microparticles (ECMPs); endothelin-1 (ET-1); Human aortic endothelial cells (HAECs); iPSC-derived “iCell Cardiomyocytes” (iPSC-CMs); microparticles (MPs); mTOR 1 complex (mTORC1); Neonatal rat ventricular myocyte (NRVM); reactive oxygen species (ROS); resveratrol (RES); SB203580 (SB); trimetazidine (TMZ)

Overall, the cardiotoxicity of TKIs has been more studied to try to clarify how these drugs, such as IMA, PAZ, SOR, sunitinib among others, act in the body when associated with these cardiac damages. As illustrated in the two tables mentioned above, several authors have performed innumerable experiments both in humans, animals or *in vitro*, testing various methods, combinations between the drugs and so on in order to be able to elucidate the involved processes resulting in cardiotoxicity. Thus, the objective of our work was to understand the cardiotoxicity induced by IMA, PAZ and SOR, in AC16 cardiac model cells and which are the altered metabolomic pathways following this toxicity.

2. Material and Methods

2.1. Materials and reagents

The human cardiomyocytes AC16 cell line was obtained from Sigma Aldrich (St. Louis, MO, USA). All plastic sterile material used in cell culture, like 6-multiwell plates, 48-multiwell plates, and 75 cm^2 flasks was obtained from Corning Star (United States of America).

SOR (sc-220125) and IMA (sc-202180A) were acquired from Santa Cruz Biotechnology (United States of America). 3-Methyladenine (3-MA), neutral red (NR) solution, sodium bicarbonate, chloroquine, gelatin from bovine skin, trypan blue solution 0.4% (w/v), dimethyl sulfoxide (DMSO), sodium chloride, sodium bicarbonate, N-methyl-N-(trimethylsilyl) trifluoroacetamide (BSTFA) with 1% trimethylchlorosilane (TMCS), O-(2,3,4,5,6- pentafluorobenzyl) hydroxylaminemhydrochloride (PFBHA), desmosterol, pyridine, and all of the standards used in gas chromatography coupled to mass spectrometry (GC-MS) were purchased to Merck (United States of America). 3-(4,5-Dimethylthiazol-2-yl)-2,5-diphenyl tetrazolium bromide (MTT) was acquired to Alfa Aesar (United States of America). Penicillin/streptomycin (10 000 U/mL / 10 mg/mL) (Pen-Strep), heat inactivated fetal bovine serum (FBS) and Hank's balanced salt solution with Ca^{2+} and Mg^{2+} (HBSS+/+) were obtained from Pan Biotech (Aidenbach, Germany). Carbonyl cyanide 3-chlorophenylhydrazone (CCCP), PAZ (cds023580), *N*,*O*-Bis(trimethylsilyl)trifluoroacetamide (BSTFA), 3-chloro-2-methylbenzaldehyde and trypsin-EDTA solution were purchased to Sigma-Aldrich (St. Louis, MO, USA). Phosphate buffered saline-Dulbecco without Ca^{2+} and Mg^{2+} (PBS -/-) was obtained from Biochrom GmbH (Berlin, Germany). Heat inactivated horse serum (HS), DMEM/F12 (1:1) medium and fibronectin bovine plasma were acquired to Gibco (United States of America). Methanol, glacial acetic acid and absolute ethanol were purchased from Fisher Scientific (United States of America). The lipophilic cationic dye, 5,5′,6,6′-tetrachloro-1,1′,3,3′-tetraethyl-benzamidazolyl carbocyanine iodide (JC-1, ab141387) was acquired to Abcam (UK).

2.2. Cell culture procedures

The AC16 cells are used as a cardiac model and they were obtained by the fusion of SV40 transformed, uridine auxotroph human fibroblasts, devoid of mitochondrial DNA with human ventricular cardiomyocytes. The fused cells have cardiomyocytes specific

markers and retain nuclear and mitochondrial DNA from the primary cardiomyocytes (73). In the present work, they were maintained and grown in proliferative medium (DMEM/F12 + 12.5% FBS + 1% Pen-Strep) at 37ºC with continuous flow of 5% CO_2 in an incubator. AC16 cells were used until the passage 10 as recommended (73), for all experiments. Trypsinization for subculture was done when cells reached at least 90% confluence. For experiments, the cells were seeded in 48- or 6-well plates previously coated with gelatin 0.02% (*w/v*) and fibronectin 0.0005% (*w/v*). The coating was done for at least 1h at 37ºC. The cells were seeded at a density of $32.5x10^4$cells per cm^2 in proliferative medium and they were given 24h to attach to the plates. To start differentiation, AC16 cells were exposed to differentiation medium (DMEM/F12 + 2% HS + 1% Pen-Strep) for 24h. Twenty four hours after the beginning of differentiation, new warm differentiation medium was given to cells, while they were exposed to several concentrations of the three compounds under study: IMA, PAZ or SOR at concentrations lower than 100μM. These concentrations are in the range of plasma concentrations found for these targeted drugs on the plasma of cancer patients (74-76). The drugs were dissolved in DMSO (IMA: 11.79mg/mL; PAZ: 8.75mg/mL; SOR: 9.3mg/mL) and the aliquots of the stock solutions were frozen at -20ºC for a maximum period of 6 months. Before each incubation and after thawing, the aliquots of the stock solutions were diluted in differentiation medium and cells were exposed to different drug concentrations. Moreover, differentiated cells were exposed to DMSO in the highest concentration used for the drugs mentioned. As in the concentration of 100μM (maximal concentration used in experiences with IMA and PAZ) the percentage of DMSO in the well was 0.5% and for a concentration of 50μM (maximal concentration used in experiences with SOR) the percentage of DMSO in the well was 0.25%, the two percentages of DMSO were used as vehicle wells and their cytotoxicity tested as any other drugs.

Finally, the incubation period of differentiated AC16 cells never surpassed more than 48h after the start of the differentiation, as they undergo cell death as described (73).

2.3. Cytotoxicity assays

In 48-well plates and after cell differentiation protocol, the compounds were incubated in new differentiation medium and two time-points were chosen (24 and 48h) for the two cytotoxicity assays: the lysosomal NR uptake assay and the MTT reduction assay. Furthermore, at the 24h time point an autophagy inhibitors, 3-MA and

chloroquine, were also tested to determine their role on the cytotoxicity of the anticancer drugs, as described (77). The two cytotoxicity assays will be described next.

2.3.1. The MTT reduction assay

The MTT assay relies on the ability of dehydrogenases, mostly mitochondrial, to transform the soluble yellow tetrazolium dye, MTT, into an insoluble blue formazan product, measured spectrophotometrically (78). At the end of the incubation time, the cell medium was removed and to each well was added 200µL of warmed new differentiation medium and 20µL of the 5mg/mL MTT solution previously done in PBS (final well concentration of MTT was 0.5mg/mL). Subsequently, cells were incubated for 3h at 37ºC in a 5% CO_2 flow. The reaction was stopped by adding 200µL of 100% DMSO to cause cellular lysis and solubilize the formazan crystals meanwhile formed. A 15 minutes agitation protected from light followed (79). Finally, the absorbance was then read at 570 and 690nm (reference wavelength) in a multi-well plate reader [Biotech Synergy HT (Winooski, VT, USA)]. The values are expressed as percentage of control cells that were set to 100%, after subtracting the absorbance reference value of each well.

2.3.2. The NR uptake assay

For this assay, AC16 cells were also seeded in 48-well plates, where they were differentiated and incubated with the anticancer drugs under study. In brief, the NR dye incorporated in the cells may stand for lysosomal functionality, as it enters easily the viable cell membranes and accumulates in lysosomes, where it suffers a charge modification at lower pH (80). The protocol for this assay has been described within the group for these cells (79) and will be described next. At the end of each incubation time (24 or 48h), the medium was rejected and 250µL/well of NR solution in warm differentiation medium (33µg/mL of NR in DMEM/F12 + 2% Horse Serum Heat Inactivated + 1% Pen-Strep) were added. Afterwards, plates were placed for 3h at 37ºC under 5% CO_2, while protected from light. Then, the medium was again removed, and the cells washed with 250µL of previously warmed HBSS (+/+). The HBSS solution was rejected and 200µL *per* well of desorption solution (comprising 50% ethanol 100%, 49% deionized water and 1% glacial acetic acid) was added to burst the cells and release the hitherto NR dye imprisoned with the viable cells. Finally, the 48-well plates were placed

in a microplate shaker for 15 min, at room temperature and protected from light until a homogeneous solution was obtained. Absorbance was measured at 540 and 690 nm wavelength (reference wavelength), in a plate reader [Biotech Synergy HT (Winooski, VT, USA)]. The values are expressed as percentage of control cells, which were set to 100%, after subtracting the reference absorbance obtained in each well.

2.4. Mitochondrial membrane potential

Since the cardiotoxicity of several anticancer drugs often involves mitochondrial dysfunction, the mitochondrial membrane potential (MMP) was assessed in this dissertation. For this assay, AC16 cells were also seeded in 48-well plates. The cells were incubated 24h with the drugs (IMA 10, 30 and 50μM; PAZ 10, 30 and 50μM; SOR 5, 10 and 20μM) and JC-1 probe was used as described for MMP determination (81). In that sense, after the 24-h incubation, 7.5μL of JC-1 of a stock solution was used to each well (well final concentration was 20μM). In parallel, a positive control for mitochondrial membrane depolarization was used and 10μL of stock solution of 100μM of the protonophore CCCP known as an uncoupler of mitochondrial potential was added to some wells. All the aforementioned conditions were placed in a CO_2 incubator at 37ºC for 15 minutes protected from light. Next, the plate was centrifuged 5 minutes at 400 × *g* at room temperature, the supernatant aspirated and 250μL of warm HBSS (+/+) were carefully added to each well. Centrifugation for 5 minutes at 400 × *g* at room temperature was done and HBSS rejected. This washing step was repeated once more. Finally, 250μL of warm HBSS (+/+) was added to each well and the cells were ready for analysis in a fluorescent plate reader (Biotech Synergy HT, Vermont, USA). Two fluorescent readings were done: excitation and emission at 535 nm and 595 nm, for determination of JC-1 forms J-aggregates, and excitation and emission at 485 nm and 535 nm for determination of JC-1 forms monomers. In healthy cells, JC-1 forms J-aggregates yielding a red colored emission (82, 83). In apoptotic or unhealthy cells, JC-1 forms monomers (due to low $\Delta\Psi m$) and shows green fluorescence. The data on MMP was presented as the ratio of fluorescent intensity of J-aggregates to fluorescent intensity of monomers.

2.5. Statistical analysis

In this section, results are expressed as mean ± standard deviation (SD). One Way ANOVA statistical analysis was done, followed by Tukey's *post hoc* test when a

significant *p* was reached ($p < 0.05$). The GraphPad Prism 9 software (San Diego, CA, USA) was used. Further information regarding statistical analysis can be found in each figure legends.

2.6. Metabolome analysis

For simplification and more clarity, the metabolome analysis will be described in a different section. The heart homeostasis is strongly related with the cardiac metabolic flexibility. As done before in our group with cyclophosphamide and its metabolites (79), a metabolomic study was performed in AC16 cells to determine the effects of IMA, PAZ and SOR on this *in vitro* model. The concentrations selected in this study comprise two premises: reflect mainly the early stage of cardiac effects (24h) on the cytotoxicity assays and be within the range of plasma concentrations found in cancer treated patients. Regarding the latter point, in several case reports or clinical studies, the blood plasma concentrations found were 2, 4 and 5μM until 14μM for IMA (75, 84), 40, 44.5 and 45μM for PAZ (74, 85, 86) and 8, 10 and 42μM for SOR (76, 87).

To begin the metabolomic study, the cells were incubated for 24h with 50μM IMA, 10μM PAZ, 10μM SOR, DMSO 0.25%, DMSO 0.05% and control (PBS) and then samples were taken for intracellular metabolome and exometabolome evaluation, as it will be described next. The differentiated AC16 cells were seeded in previously gelatin 0.02% (*w/v*) and fibronectin 0.0005% (*w/v*) coated 6 well plates, using 2 wells *per* condition. The medium, FBS, HS and Pen-Strep were used from the same lots transversely throughout all experiments to avoid bias or confounding factors related to the medium and its supplements.

Thus, at 24h, samples for the analysis of intracellular (n=10) and extracellular (n=10) metabolome were collected according to a protocol already described (79). For the extracellular metabolome, culture medium was collected on ice and centrifuged at 2000 x *g* for 5 minutes at 4°C to remove cellular debris. These samples were frozen immediately at -80°C in a 10mL headspace solid-phase microextraction (HS-SPME) glass vial capped with a polytetrafluoroethylene (PTFE) septum and a screw cap. For the intracellular metabolome, the same cells were washed twice with 0.9% *w/v* NaCl. As the metabolism changes rapidly, it is imperative to rapidly quench the cellular metabolism as soon as possible and extract the intracellular metabolites, to have a reliable screenshot of the cells metabolism. The extraction solution chosen for the analysis of the intracellular metabolome was ice-cold methanol:water solution (80:20 proportion, *v/v*), being this extraction procedure tested before in AC16 cells (79). After adding the

extraction solution, cells were scraped, gathered, and centrifuged for 10 minutes at 3000 x *g* at 4°C. The supernatant was used for the evaluation of the intracellular metabolome and the pellet rejected. Moreover, quality control samples (QCs) were a pool with the same volume of all samples analyzed both for exometabolome and endometabolome to assess analytical reproducibility of the different GC-MS methods used. These QCs were aliquoted to avoid more the than three freeze/thaw cycles, since freeze/thaw cycles can affect the metabolome (88). All the samples were stored at -80°C until analysis.

2.6.1. Sample preparation

For the intracellular metabolome analysis, 1mL of extraction solvent was relocated to a glass vial, where 10µL of desmosterol (0.5mg/mL dissolved in methanol) were added as internal standard. After vortexing, the samples were evaporated at room temperature to dryness under a stream of nitrogen gas. A derivatization step was followed aimed to increase volatility (89). First, the evaporated samples suffered oximation by adding 50µL of methoxyamine hydrochloride (15mg/mL) in pyridine, first derivatization procedure. That reaction occurs at 70°C for 1h. Methoxyamine inhibits ring formation of reducing sugars by protecting the aldehyde and ketone groups, making them available to the second derivatization step. In this second step, metabolites reacted with 100µL of BSTFA with 1% TMCS, for 1h at room temperature. BSTFA allocates trimethylsilyl groups to carboxylic acids, alcohols, amines, amides, phenols and all other groups with available -OH, -NH and NH_2 (89). The derivatized samples were then placed in an autosampler and injected in the GC-MS apparatus.

In the extracellular media, the volatile carbonyl compounds (VCCs) were determined by GC-MS. This procedure was been previously performed in the group (79, 90) and will be described next. The method used for volatile components detection in the cells' culture medium is based on HS-SPME coupled to a GC-MS system. The VCCs (aldehydes and ketones) analysis requires a derivatization step with PFBHA to guaranty thermal stability and volatility of the compounds with carbonyl groups. As can be seen in **Figure 2,** in the case of some metabolites, after analysis, despite being the same, appear in two forms, *trans* and *cis*, since they are detected after reaction with PFBHA. To perform this derivatization, and after thawing slowly the samples of culture medium samples in order to minimize loss of volatile metabolites (90), 5µL of a methanolic solution with 3-chloro-2-methylbenzaldehyde (internal standard, with a stock concentration of 1mg/mL) and 47µL of PFBHA (stock concentration of 40g/L) were

added. A 30 minutes derivatization step at room temperature followed. After that, the derivatized samples were placed in an autosampler for GC-MS analysis.

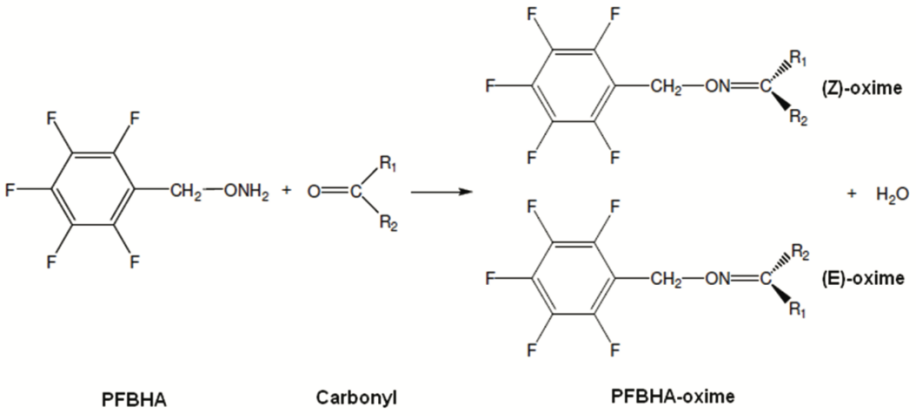


Figure 2. Derivatization reaction of carbonyls with PFBHA.

2.6.2. Chromatographic and mass spectrometry procedures to analyze intracellular samples

For the analysis of the intracellular metabolites, an EVOQ 436 GC system (Bruker Daltonics, Fremont, CA) was used. The system was coupled to a SCION Triple Quadrupole mass detector, using a capillary column Rxi-5Sil MS (30 m x 0.25 mm x 0.25 µm) from RESTEK. The high purity helium C-60 was the carrier gas (Gasin, Portugal) and a constant flow rate of 1.0 mL/minute was used. Per sample, two microliters were injected in split mode (ratio 1:20) with an injector temperature of 250°C held for 20 minutes. A temperature gradient was used: the oven temperature was set at 70°C for 2 minutes, followed by heating until 250°C (15°C/minute), set for 2 minutes and an additional heating was done until 300°C (10°C/minute) and the temperature was maintained for 5 minutes. The separation run was taken for 26 minutes. The electron ionization (EI) mode (70 eV) was selected in the MS detector and the EI temperature was 270°C, with a manifold temperature of 40°C and 280°C in the transfer line. Data was collected in a *full scan* mode with mass ranging from 50 to 500 *m/z*. To increase quality and avoid bias, GC-MS data acquisition and sample preparation were done randomly. The analytical reproducibility of the method was assessed by analyzing, in the same conditions, the internal standards and a QC sample every seven samples (88).

2.6.3. HS-SPME/GC-MS procedures to analyze extracellular samples

For the analysis of the VCCs metabolites, the HS-SPME/GC-MS analysis was executed with a CombiPAL autosampler (Varian Pal Autosampler, Switzerland) and the Cycle Composer software, (CTC Analytics System Software, Switzerland) as previously described and according to an optimized procedure (90). The VCCs were analyzed with a SCION Triple Quadrupole mass detector. For these procedure, helium C-60 (Gasin, Portugal) was used with a constant flow rate of 1.0mL/min. The column used for chromatographic separation was a Rxi- 5Sil MS (30m x 0.25mm x 0.25µm) capillary column (RESTEK).

The temperature of the oven was held at 40°C for 1 minute, then increased until 250°C (set for 5 minutes) with a rate of 5°C/minute. A further increase to 300°C with the same rate (5°C/minute) was deemed. Injection was performed in splitless mode at 250°C (maintained for 20 minutes). The separation run lasted 58 minutes and the EI mode (70 eV) was selected in the MS detector at 250°C. Manifold temperature was held at 40°C and the transfer line temperature was fixed at 230°C. For data acquisition, a full scan mode with a mass range between 40 and 450 *m/z* was performed, with a scan rate of 6 scans *per* second.

As mentioned before for the analysis of the intracellular metabolome, sample order was also random, and a QC sample was injected every eleven samples (88).

2.6.4. GC-MS pre-processing data

Raw data files acquired from the GC-MS analysis were turned into a universal format (net.cdf file extension) using the MASSTransit software version 3.0.1.16 (Palisade Corp, Newfield, NY). Data were then pre-processed to turn data sets into manageable formats, exclusion of any bias noise-related and retention time variations were taken into account. This procedure was executed using the MZmine 2.23 software (91) and consisted of baseline correction, detection of peaks of interest, deconvolution of the chromatograms, and alignment (parameters used are shown in **Table 5**). After pre-processing, artefact peaks derived from GC contaminants (such as phthalates, siloxanes, and cyclosiloxanes) and peaks with a signal to noise ratio lower than three were deleted from the matrix. Then, data were normalized by total area of the chromatogram when comparing control *versus* drug under study. All peaks with a relative

standard deviation (RSD) higher than 30% across all QCs were also removed from data matrices. Sample names, normalized peak areas, and the remaining *m/z*-RT pairs were uploaded to SIMCA 13.0.1 (Metrics Umea, Sweden) and a multivariate analysis (MVA) was used to analyze the data.

Table 5. Parameters used in the MZmine software for the pre-processing of the chromatographic data. RT: retention time

Parameter		Intracellular metabolome analysis	Extracellular metabolome analysis (VCCs)
Crop filtering	***m/z***	50 – 500	40 – 450
	RT (minutes)	5.8 – 25.0	14.4 – 36.0
Peak detection	**Noise level**	$5.7x10^4$	$1.5x10^4$
Chromatogram deconvolution	**Peak range (minutes)**	0.02 – 0.25	0.02 – 0.28
	Min peak height	$8x10^4$	$1x10^5$
	Baseline level	$6x10^4$	$4x10^4$
Alignment	***m/z* tolerance**	0.5	0.5
	RT tolerance (minutes)	0.05	0.05

2.6.5. Multivariate analysis (MVA)

Prior to any statistical analysis, the data set were scaled to different models for comparison effects (Pareto, unit variance [UV] and centered scaling). Pareto provided

the best model in intracellular data, while UV provided the best models in VCCs data. A Principal Component Analysis (PCA) was the first step of the MVA workflow, which is the adequate process for data trends overview and outlier identification (92).

QC samples distribution/clustering was also analyzed in this point to assess and guarantee the analytical reproducibility of the method. In this step, the approach is unsupervised, meaning that no information about the data's group class (control or drug-exposed) is provided to better evaluate both data quality and homogeneity without any confounding or subjectivity factors.

The remaining analysis included the use of a supervised method, with well-defined and identified groups to assess the existence, or not, of data separation from groups. The MVA supervised model utilized was the Partial Least Squares discriminant analysis (PLS-DA). The PLS-DA output leads to scatter plots where each point represents an individual sample projected in a plane. Samples from the same group are clustered by color to improve visual inspection of the model. The quality of the models was validated quantitatively, as visual inspection can often be misleading regarding data separation as it has a subjectivity factor inherent to it. Normally, the Q^2 (capability of the model to predict group separation) and R^2 (original data fraction that can be explained by the model) cumulative values are used, as the definitions of excellent models *per se* is a value equal or greater than 0.5, for both parameters (92). Additionally, the quality of the fit of the original model (Q^2 and R^2) was compared to the quality of the fit of several models in which the Y-observations order was permutated randomly (500 permutations). By fitting the model in random order, the Q^2 and R^2 should decrease to ensure that group separation is not due to chance. After assessment of the PLS-DA loading plots, the features responsible for group separation were analyzed. A Variable Importance in Projection (VIP) higher than 1 was used for possible distinctive feature selection (92).

2.6.6. Identification process

Identification of discriminant metabolites assessed as possible distinctive features was performed in agreement to the chemical analysis minimum reporting standards of Metabolomics Standard Initiative (MSI) (93). The process comprised the comparison between the compound mass spectrum of samples with the spectra from the National Institute of Standards (NIST14) library, Kovats retention index (RI) and retention time (RT). Regarding spectra comparison with the libraries, the identification

process was only considered for similarity match higher than 70% for forward and reverse percentages. Metabolites RI values were calculated using the RT obtained for a series of *n*-alkanes (C8-C40), which were injected in the same chromatographic conditions to obtain the respective RTs. These values were used to calculate the metabolites RI. Whenever possible, theoretical metabolites identification was confirmed with standards. Finally, unidentified metabolites were named according to the respective RT value (*e.g.,* Unk11.0 is the unidentified metabolite with the chromatographic peak on minute 11.0). Lastly, the Human Metabolome Database (http://www.hmbd.ca, HMBD) and Kyoto Encyclopedia of Genes and Genomes (http://www.kegg.jp, KEGG) databases were consulted to assist the identification process.

2.6.7. Univariate analysis

Apart from the MVA workflow to determine which metabolites are or not important for group separation, a univariate statistical analysis of potentially relevant compounds (VIP>1) was also applied to confirm the importance of metabolite's discrepancies between groups. Metabolites that characteristically had more than one chromatographic peak due to the derivatization reactions were summed (e.g., simple carbohydrates like glucose or aldehydes like methylglyoxal), as previously reported (94). The univariate approach consisted first in a Shapiro-Wilk normality test to evaluate if the data followed a normal distribution. In case of normal distributed data, an unpaired Student's *t* test was performed. Otherwise, the unpaired Mann-Whitney test was used. All statistical analysis was performed in GraphPad Prism Version 7.0a (GraphPad Software, San Diego, CA, USA). Metabolites were considered statistically different when $p<0.05$. A False Discovery Rate (FDR) was applied to correct *p* values from the univariate analysis, using the Benjamini-Hochberg correction (95, 96). Moreover, for each relevant compound, the effect size (ES) was calculated accordingly to equations thoroughly described in (97) and a positive ES value shows that the metabolites increased in cells exposed to the drug (IMA, PAZ or SOR), while a negative ES value indicates a decrease comparatively to control.

3. Results

3.1. Imatinib caused a time-dependent cytotoxicity in differentiated AC16 cells, according to the MTT reduction assay

To evaluate IMA cytotoxicity, differentiated AC16 cells were exposed to a wide range of concentrations (10 to 100μM). After the drugs' incubation, the MTT reduction assay was performed at two time-points (24 and 48h) as referred in the methods section.

In AC16 differentiated cells **(Figure 3A)** at 24h, IMA had significantly higher values of MTT reduction at 10μM (115.67 ± 8.01%), 30μM (124.26 ± 8.84%), or 50μM (112.58 ± 10.58%) of what existed in control cells (100.00 ± 2.94%). On the other hand, a time dependent cytotoxicity was observed at 48h, beginning at 30μM, with a significant decrease of MTT reduction observed when compared to control cells. Moreover, the values of MTT reduction for 30μM (84.76 ± 4.41%) were significantly higher than for 40μM (68.81 ± 4.45%), which were, on the other hand higher than 50μM (58.26 ± 2.52%), that were higher than the values of MTT reduction of 100μM (35.94 ± 11.23%) **(Figure 3B)**. At 48h, the maximum value of DMSO used (0.5%) caused a slight cytotoxicity (88.6 ± 3.67%), when compared to control cells (100.00 ± 1.85%).

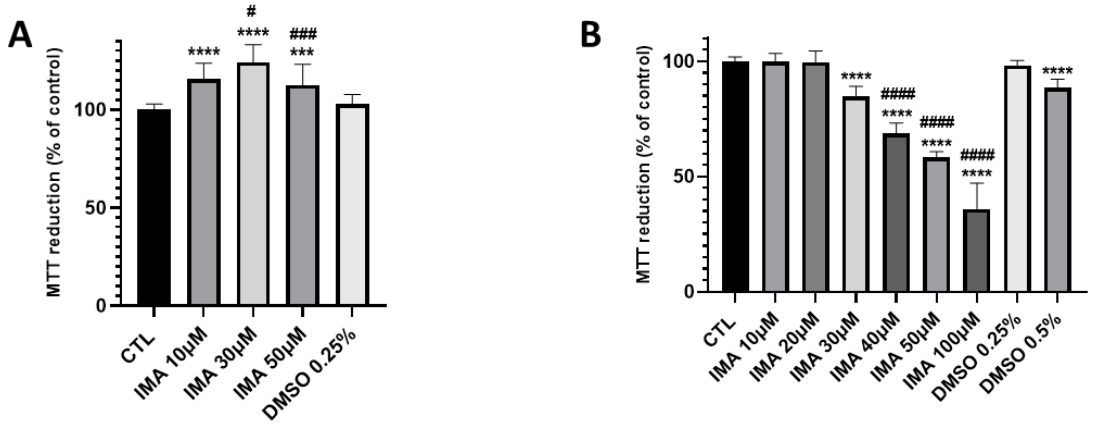


Figure 3. Imatinib (IMA) cytotoxicity assessed through the MTT reduction assay in differentiated AC16 cells following a 24-h (A) or 48-h (B) incubation. Results are presented as mean ± standard deviation from 2-8 independent experiments (N=8 to 32). Statistical analysis was performed using one-way ANOVA followed by Tukey's *post hoc* test. ***p<0.001, ****p<0.0001 *vs.* control (CTL); $^{\#}p$<0.05, $^{\#\#\#}p$<0.001, $^{\#\#\#\#}p$<0.0001 *vs.* the immediate lower concentration tested in the same time point.

3.2. Imatinib caused impairment of lysosome function in differentiated AC16 cells as early as 24h, according to the neutral red uptake assay

Another classical cytotoxicity assay was performed: the NR uptake assay at two time-points (24 and 48h). IMA clearly caused a time-dependent cytotoxicity in the NR uptake assay in AC16 cells exposed to a wide range of concentrations (10 to 100μM). At 24h **(Figure 4A)**, there was not a rise in cytotoxicity with increased concentrations, since IMA 10μM had values of 95.67 ± 6.93%, IMA 20μM had values of 54.96 ± 4.49%, while in the cells exposed to 30μM there was a decrease in the cytotoxicity observed (65.26 ± 5.76%). The IMA 50μM condition had values of 34.48 ± 5.85%, when compared to control at 24h (100.00 ± 3.31%). At 48h, a wider range of concentrations was tested with the following values in the NR uptake assay: 10μM (97.46 ± 4.48%), 20μM (78.76 ± 14.15%), 30μM (33.36 ± 5.6%), 40μM (19.45 ± 5.65%), 50μM (21.53 ± 10.33%) and 100μM (5.01 ± 1%), being all the last meaningful different when compared to control at 48h (100.00 ± 2.48%) **(Figure 4B)**.

DMSO did not cause any significant toxicity in both concentrations and time-points tested in this assay.

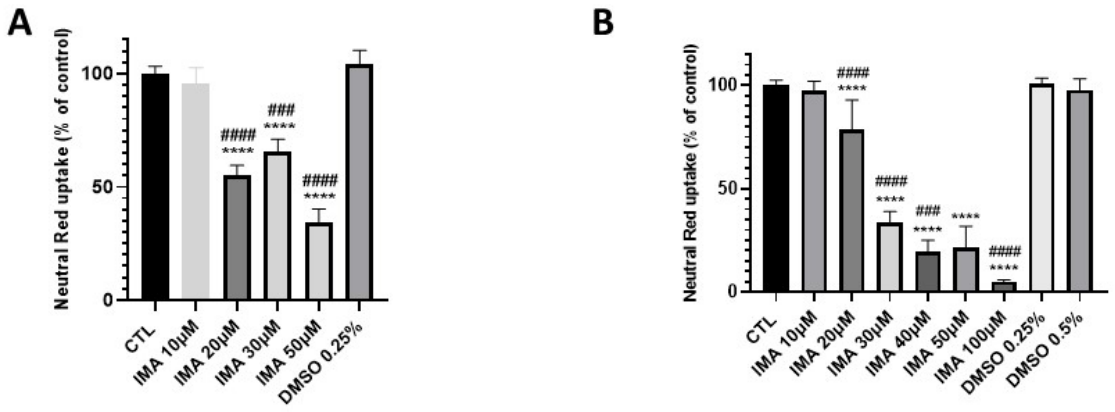


Figure 4. Imatinib (IMA) cytotoxicity evaluated through the NR uptake assay in differentiated AC16 cells following a 24-h (A) or 48-h (B) incubation. Results are presented as mean ± standard deviation from 2-10 independent experiments (N=8 to 40). Statistical analysis was performed using one-way ANOVA followed by Tukey's *post hoc* test. ****p<0.0001 vs. control (CTL); ###p<0.001, ####p<0.0001 vs. the immediate lower concentration tested in the same time point.

3.3. Pazopanib led to time-dependent toxicity, with no clear dose dependence, according to the MTT reduction assay

To evaluate mitochondrial activity, AC16 cells were exposed to growing concentrations of the drug PAZ (1 to 100μM) and the MTT reduction assay was performed at several time-points (24 and 48h). Regarding AC16 cells at 24h, a significantly impaired MTT reduction was found for 5, 10, 30 and 50μM (5μM: 89.37 ± 8.02%, 10μM: 86.82 ± 6.27%, 30μM: 67.89 ± 9.36%, 50μM: 64.25 ± 5.28%), when compared to control cells (100.00 ± 2.44%), being that impairment was significantly higher in the highest concentration **(Figure 5A)**. After 48h, the impact on the cells' ability to reduce MTT by the aforementioned drug **(Figure 5B)** was significant at concentrations of 1μM and above (1μM: 85.68 ± 2.62%, 5μM: 55.37 ± 8.08%, 10μM: 55.37 ± 8.08%, 20μM: 54 ± 3.92%, 50μM: 60.94 ± 2.96%, 100μM: 56 ± 4.23%). With these results, a time-dependent cytotoxicity profile, with no clear dose dependence, was seen. At 48h, the vehicle used, DMSO, was also tested and in the highest concentration tested (0.5%), it caused a slight but meaningful cytotoxicity (84.78 ± 2.86%), when compared to control cells (100.00 ± 2.04%).

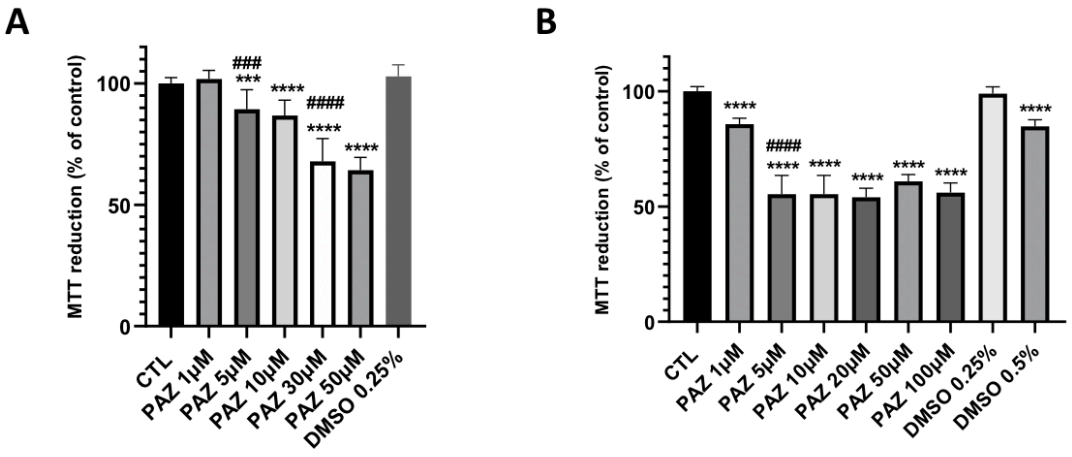


Figure 5. Pazopanib (PAZ) cytotoxicity evaluated by the MTT reduction assay in differentiated AC16 cells following a 24-h (A) or 48-h (B) incubation. Results are presented as mean ± standard deviation from 2-8 independent experiments (N=7 to 32). Statistical analysis was performed using one-way ANOVA followed by Tukey's *post hoc* test. ***p<0.001, ****p<0.0001 vs. control (CTL); $^{###}p$<0.001, $^{####}p$<0.0001 vs. the immediate lower concentration tested at the same time point.

3.4. Pazopanib affected lysosomal uptake ability in AC16 cells at pharmacological relevant concentrations

Likewise, the lysosomal integrity was evaluated by the NR uptake assay after PAZ exposure. The NR uptake assay was performed at two time-points (24 and 48h). In AC16 cells, a 24-h incubation with PAZ led to significant cytotoxicity as soon as 5μM and higher concentrations with the following values registered: 5μM (96 ± 3.22%), 10μM (88.49 ± 3.41%), 30μM (90.73 ± 3.55%), 50μM (90.73 ± 5.46%), when compared to control cells (100.00 ± 2.69%) **(Figure 6A)**. A time-dependent cytotoxicity was observed, for this drug. At 48h, a wider range of concentrations was tested with the following values: 5μM (88.14 ± 3.46%), 10μM (79.56 ± 11.42%), 20μM (84.83 ± 6.40%), 50μM (89.89 ± 5.68%), 100μM (90.05 ± 2.12%) **(Figure 6B)**, all significantly different to control cells (100.00 ± 1.37 %).

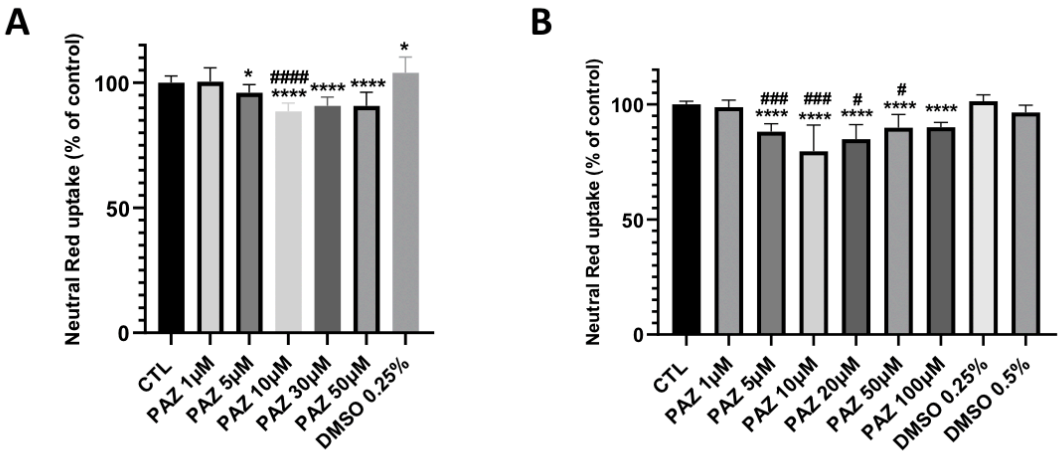


Figure 6. Pazopanib (PAZ) cytotoxicity, in differentiated AC16 cells following a 24-h (A) or 48-h (B) incubation, assessed by the NR uptake assay. Results are presented as mean ± standard deviation from 3-10 independent experiments (N=12 to 40). Statistical analysis was performed using one-way ANOVA followed by Tukey's *post hoc* test. **p*<0.05, *****p*<0.0001 vs. control (CTL); #*p*<0.05, ###*p*<0.001, #### *p*<0.0001 vs. the immediate lower concentration tested in the same time-point.

3.5. Sorafenib presented a concentration and time-dependent mitochondrial impairment in AC16 cells, according to the MTT reduction assay

Similarly to the previous compounds tested, AC16 cells were incubated with growing concentrations of SOR (0.5 to 50μM) to evaluate cellular mitochondrial activity using the MTT reduction assay at several time-points (24 and 48h). At the 24h incubation time, only the 20μM concentration of SOR had a significant impact in the cells' capability of reducing MTT (20μM: 48.05 ± 16.06%), when compared to control cells (100.00 ± 1.86%) **(Figure 7A)**. The other 2 concentrations had no meaningful difference (5μM: 93.52 ± 10.18%, 10μM: 105.68 ± 9.63%) towards control cells. At 48h, a concentration-dependent cytotoxicity was seen, being the values obtained in the MTT reduction assay: 0.5μM (106.01 ± 2.49%), 1μM (99.86 ± 3.08%), 2μM (91.07 ± 4.15%), 5μM (68.85 ± 8.16%), 10μM (63.61 ± 3.3%), 20μM (20.18 ± 3.98%), 30μM (3.81 ± 2%), 40μM (2.42 ± 0.45%), 50μM (2.16 ± 0.33%), all significantly different regarding control cells (100.00 ± 1.59%), with the exception of 1μM condition. DMSO 0.25% had no impact on cells ability to reduce MTT **(Figure 7B)**. These data clearly demonstrate a time-dependent cytotoxicity for SOR in AC16 cells.

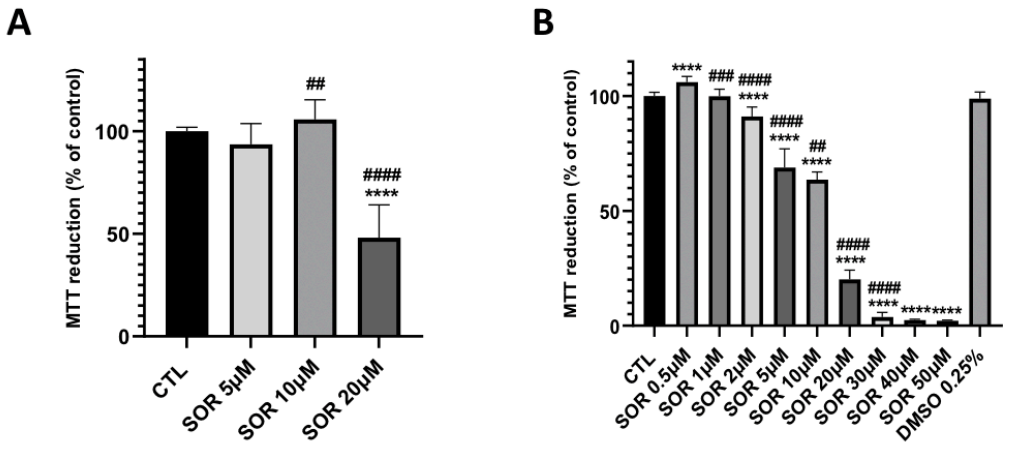


Figure 7. Sorafenib (SOR) cytotoxicity, evaluated through the MTT reduction assay, in differentiated AC16 cells following a 24-h (A) or 48-h (B) incubation. Results are presented as mean ± standard deviation from 3-5 independent experiments (N=12 to 20). Statistical analysis was performed using one-way ANOVA followed by Tukey's *post hoc* test. ****p<0.0001 vs. control (CTL); $^{\#\#}p$<0.01, $^{\#\#\#}p$<0.001, $^{\#\#\#\#}p$<0.0001 vs. the immediate lower concentration tested in the same time-point.

3.6. Clinically relevant concentrations of sorafenib caused impact in lysosome function of AC16 cells in a dose and time-dependent manner

AC16 cells were exposed to SOR (0.5 to 50μM) and an indirect measure of lysosome function was done by the NR uptake assay. This assay was performed at two time-points (24 and 48h). When exposed to several concentrations of SOR for 24h, AC16 cells ability to uphold NR was diminished at concentrations higher than 5μM (5μM: 83.3 ± 6.93%, 10μM: 57.09 ± 4.74%, 20μM: 22.22 ± 8.12%), when compared to control cells (100.00 ± 1.86%) **(Figure 8A)**. After 48h, a cytotoxic effect was also observed with the following values: 2μM (93.53 ± 4.06%), 5μM (78.17 ± 2.55%), 10μM (49.14 ± 8.66%), 20μM (8.73 ± 1.39%), 30μM (4.01 ± 0.75%), 40μM (2.85 ± 0.68%), 50μM (2.74 ± 1.29%), when compared to control cells (100.00 ± 1.92%) **(Figure 8B)**. In both time-points, a concentration dependent cytotoxicity was found.

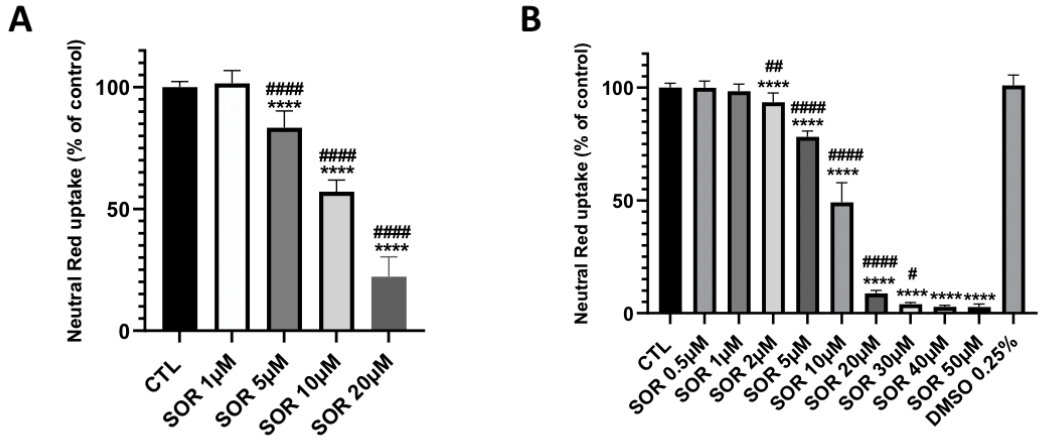


Figure 8. Sorafenib (SOR) cytotoxicity regarding the NR uptake assay in differentiated AC16 cells following a 24-h (A) or 48-h (B) incubation. Results are presented as mean ± standard deviation from 2-8 independent experiments (N=4 to 32). Statistical analysis was performed using one-way ANOVA followed by Tukey's *post hoc* test. ****p<0.0001 vs. control (CTL); $^{\#}p$<0.05, $^{\#\#}p$<0.01, $^{\#\#\#\#}p$<0.0001 vs. the immediate lower concentration tested in the same time-point.

3.7. 3-Methyladenine, an autophagy inhibitor, increased the cytotoxicity of imatinib and pazopanib in differentiated AC16 cells, when it affected differentially the cytotoxicity of sorafenib

To assess the effect of an autophagy inhibitor on the cytotoxicity of the drugs under study, concentrations around the concentration effective in producing 50% of the maximal toxic response (TC50) for IMA and SOR were used because they are clinically relevant, while in the case of PAZ, concentrations similar to plasmatic levels of patients were used since the concentrations tested never reached TC50 in the NR uptake assay. Regarding IMA, the autophagy inhibitor significantly increased its cytotoxicity in the 30μM condition (50.88 ± 7.06%), when compared to IMA 30μM alone (64.85 ± 6.24%). 3-MA did not cause any meaningful change when concomitant with IMA 50μM (29.06 ± 5.99%), when compared to IMA 50μM alone (32.37 ± 6.64%). On the other hand, 3-MA increased the cytotoxicity in both PAZ concentrations tested (PAZ 30μM: 95.67 ± 2.75%; PAZ 30μM + 3-MA: 87.85 ± 3.25% and PAZ 50μM: 91.38 ± 2.76%; PAZ 50μM + 3-MA: 81.56 ± 3.23%).

For SOR, a concentration dependent response existed: in the NR uptake assay, the 3-MA increased the cytotoxicity of SOR 10μM (3-MA + SOR 10μM: 47.04 ± 3.71%) when compared to SOR 10μM alone (56.47 ± 2.48%); on the other hand, 3-MA partially reverted the cytotoxicity of SOR 20μM (3-MA + SOR 20μM: 24 ± 5.8%) when compared to SOR 20μM alone (19.68 ± 4.79%).

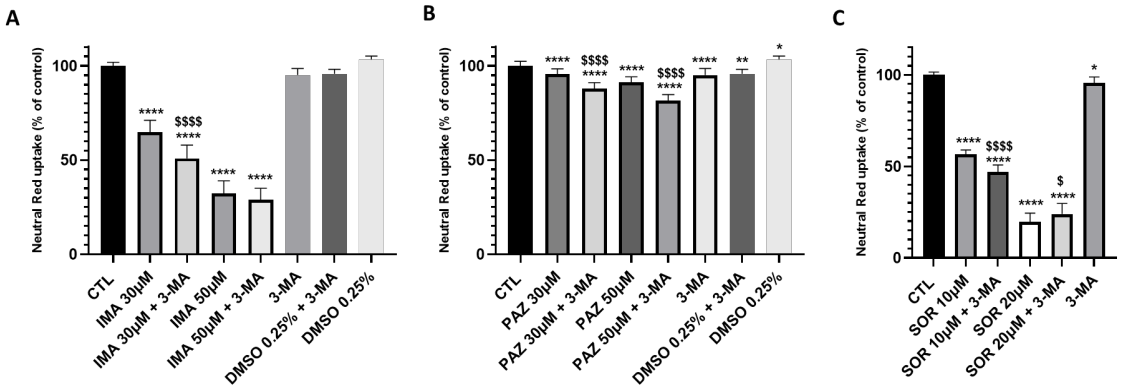


Figure 9. Effect of an autophagy inhibitor (3-methyladenine, 3-MA) on the cytotoxicity of imatinib (IMA) (A), pazopanib (PAZ) (B) and sorafenib (SOR) (C) in differentiated AC16 cells at 24-h. The assay used herein for cytotoxicity assessment was the NR uptake assay. Results are presented as mean ± standard deviation from 3-4 independent experiments (N=12 to 16). Statistical analyses were performed using the one-way ANOVA followed by Tukey's *post hoc* test. **p*<0.05, ***p*<0.01, *****p*<0.0001 vs. control (CTL), $^{\$}p$<0.05, $^{\$\$\$\$}p$<0.0001 vs. condition without 3-MA.

3.8. The autophagy inhibitor, chloroquine, increased the cytotoxicity of only the lowest concentration of sorafenib

To assess the effect of another autophagy inhibitor, chloroquine (CHLOR), on the cytotoxicity of the drugs under study, the same concentrations of the targeted drugs of the least subsection were used. Regarding IMA, the autophagy inhibitor had no meaningful impact on the cytotoxicity of the two concentrations tested being the values: IMA 30μM (51.84 ± 10.45%); IMA 30μM + CHLOR (46.39 ± 16.23%); IMA 50μM (25.83 ± 10.25%) and IMA 50μM + CHLOR (22.25 ± 8.50%).

Similarly, CHLOR did not cause any meaningful change to the cytotoxicity of PAZ 30μM (93.91 ± 3.73%) when compared to PAZ 30μM alone (98.58 ± 7.18%). In addition, no significant differences were seen between PAZ 50μM (90.78 ± 4.26%) and PAZ 50μM + CHLOR (88.09 ± 5.26%). Finally, CHLOR increased the cytotoxicity of SOR 10μM (SOR 10μM + CHLOR: 48.14 ± 9.83%) when compared to SOR 10μM alone (56.35 ± 10.40%), while making no difference in the higher concentration tested being the results: SOR 20μM with CHLOR: 15.15 ± 6.07% and SOR 20μM alone: 18.83 ± 6.91%.

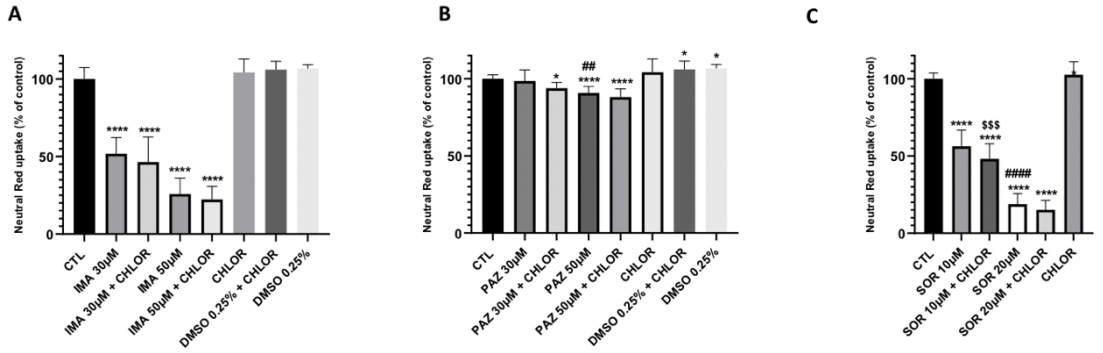


Figure 10. Effect of the autophagy inhibitor, chloroquine (CHLOR) on the cytotoxicity of imatinib (IMA) (A), pazopanib (PAZ) (B) and sorafenib (SOR) (C) in differentiated AC16 cells at 24-h. The assay used herein for cytotoxicity assessment was the NR uptake assay. Results are presented as mean ± standard deviation from 4-8 independent experiments (N=14 to 32). Statistical analyses were performed using the one-way ANOVA followed by Tukey's *post hoc* test. *$p<0.05$, ****$p<0.0001$ vs. control (CTL), $^{\$\$\$}p<0.001$ vs. condition without CHLOR, $^{\#\#}p<0.01$, $^{\#\#\#\#}p<0.0001$ vs. condition with CHLOR.

3.9. Sorafenib and pazopanib caused mitochondrial membrane depolarization in all the tested concentrations, while only the highest concentration of imatinib caused significant changes in mitochondrial membrane potential

Mitochondrial membrane potential **(**MMP, ΔΨm) can be assessed using the lipophilic cationic dye, JC-1. JC-1 is concentrated within mitochondria and responds according to the ΔΨm. IMA only caused changes in MMP in the highest concentration tested, IMA 50μM (11.50 ± 1.55), while all conditions with PAZ, 10μM (11.45 ± 2.93), 30μM (10.86 ± 3.7), or PAZ 50μM (9.73 ± 3.11) caused a mitochondrial depolarization compared to the values observed in control and healthy cells (16.88 ± 4.17). On the other hand, SOR caused an impressive MMP depolarization (5μM: 3.87 ± 0.36; 10μM: 3.65 ± 0.38 and 20μM: 3.30 ± 0.29), being the most powerful mitochondrial toxin drug used.

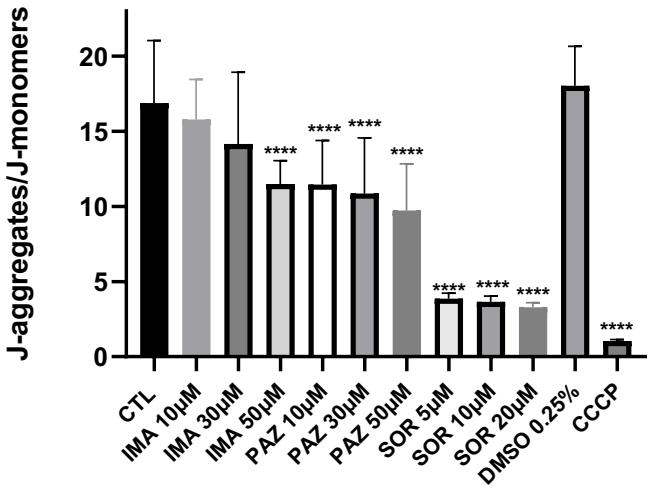
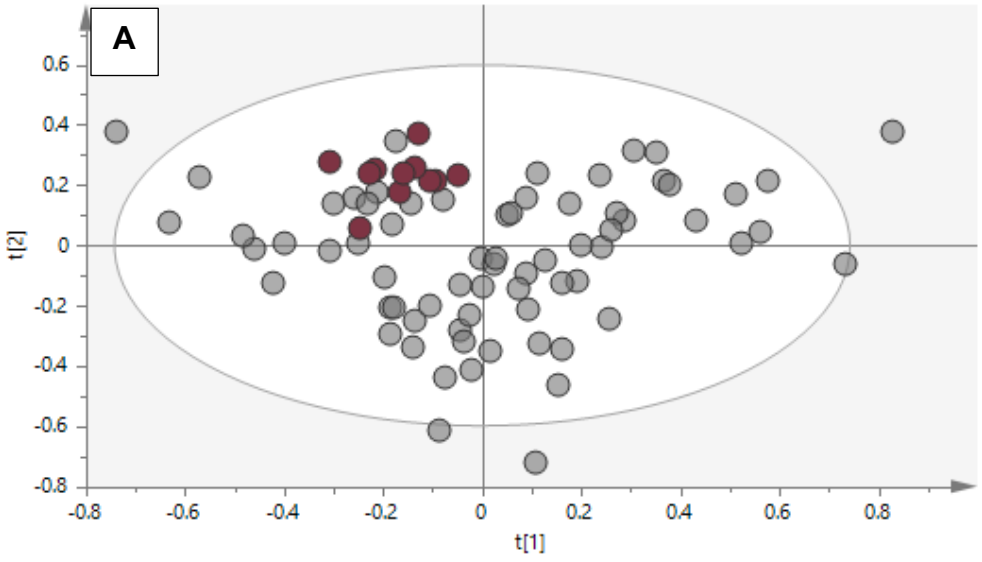


Figure 11. Mitochondrial membrane potential evaluation using the JC-1 probe in differentiated AC16 cells exposed to imatinib (IMA), pazopanib (PAZ) and sorafenib (SOR) for 24h. Results are presented as mean ± standard deviation from 4 independent experiments (N=7 to 16). Statistical analyses were performed using the one-way ANOVA followed by Tukey's *post hoc* test. ****p<0.0001 vs. control (CTL).

3.10. Evaluation of the metabolic changes after targeted therapies

To identify possible discriminant metabolites involved on metabolic changes caused by targeted anticancer drugs, different GC-MS methodologies were used. In this dissertation, both the intracellular metabolome or endometabolome and the extracellular metabolome or exometabolome were analyzed. The endometabolome was previously extracted and the residue derivatized with the MSTFA. Regarding the exometabolome, namely the VCCs, it was analyzed directly by HS-SPME after derivatization with PFBHA (see material and methods section 2.6.1.). Both methods undertaken in metabolomic studies included quality control samples in order to attain high quality and reliable results. As shown for both GC-MS methods, all QC samples, represented by burgundy spheres, were strongly clustered on the PCA scores plot, indicating a good analytical reproducibility of methods **(Figure 12)**. The data obtained in all the groups was analyzed and the outliers detected in PCA data that were outside the Hoteling's T2 region were excluded. Here, according to **figure 12A**, some outliers can be detected. PCA plots for the different groups regarding the two protocols being done in this dissertation were also used to analyze group homogeneity **(Figures 13 and 14)** and showed good data profile.



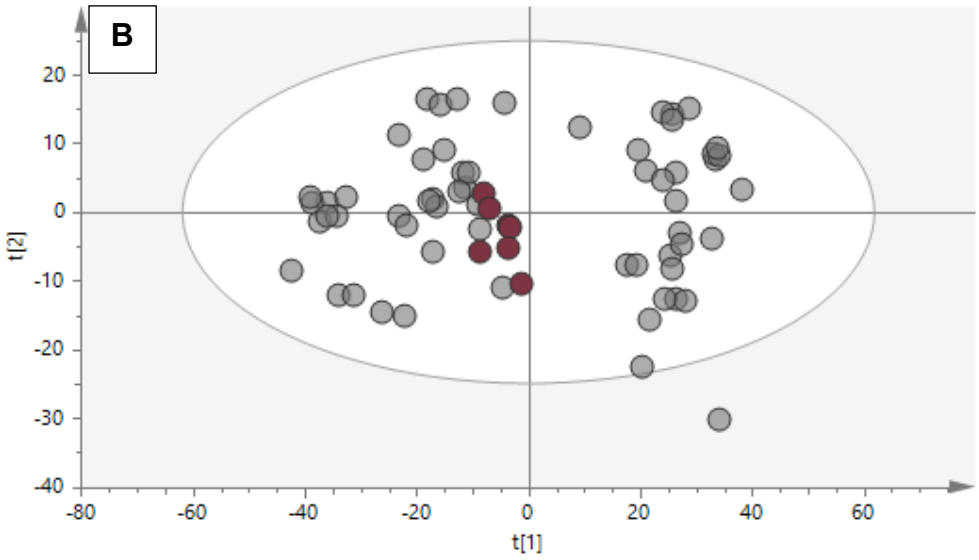


Figure 12. PCA scatter plots obtained through GC-MS data to evaluate the reproducibility of the methods for **(A)** Intracellular metabolic profiling and **(B)** Volatile carbonyl compounds (VCCs) profiling. Each sample is represented by a gray sphere as a single variable, while the QCs are represented in burgundy spheres.

Next, the PCA plots for all the groups (control, cells exposed to DMSO 0.05%, DMSO 0.25%, IMA, PAZ and SOR for 24h) of the intracellular metabolome profiling of differentiated AC16 cells were analyzed and are depicted in **Figure 13**, to remove outliers. PCA data was used to take out outliers and repeated samples with an initial sample size of 10 for all groups. In the case of control samples, the N6 control sample was not processed, so it was eliminated from the entire analysis. In detail, in DMSO 0.25% samples, although it seems that 3 groups are formed, the passages are grouped randomly as in all other groups. For all other groups, the distribution of all samples was homogeneous and none of the groups revealed outliers so, no samples were eliminated.

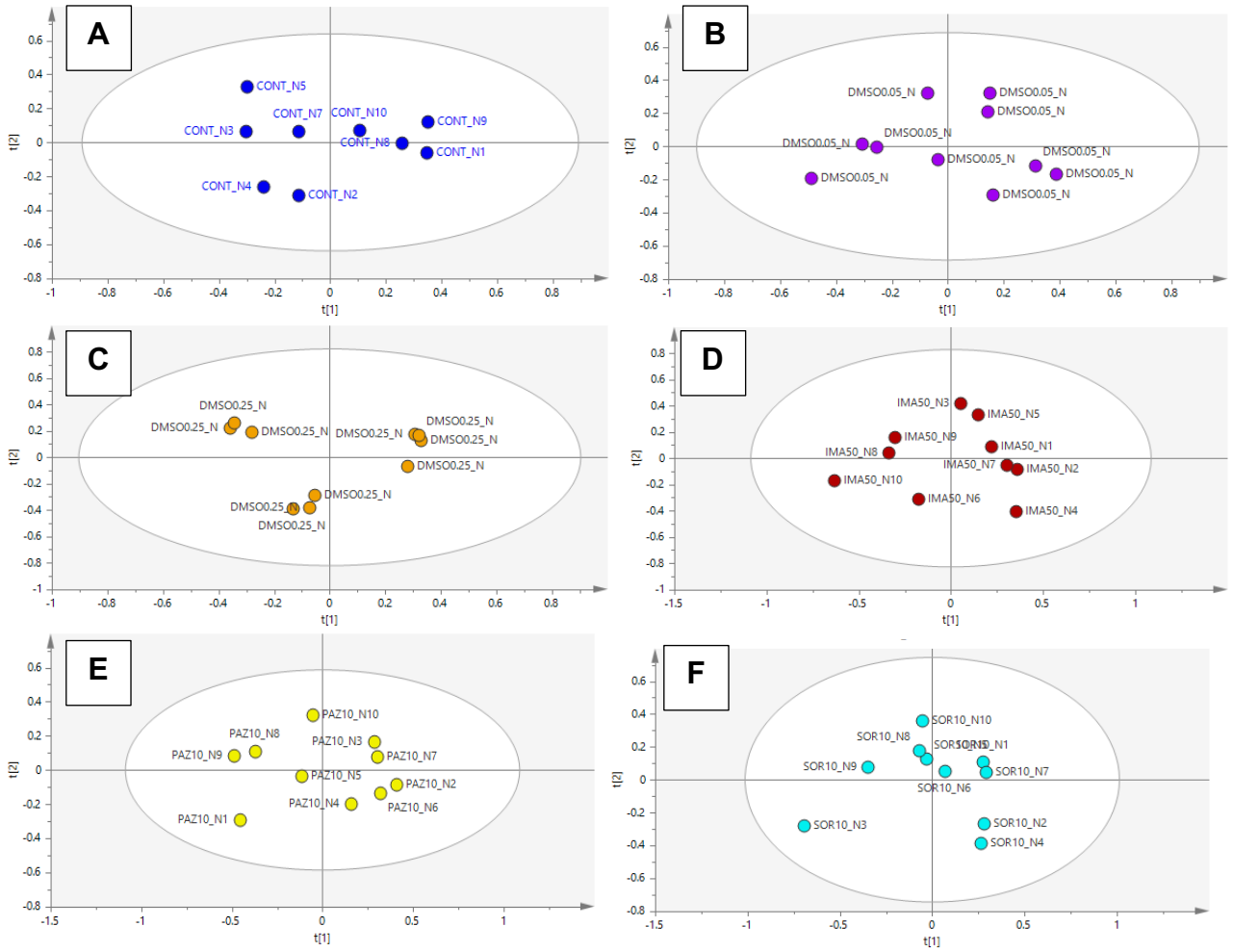


Figure 13. PCA scatter plots acquired from the analysis of the intracellular content of: **(A)** AC16 differentiated control cells (CONT n=9; PC2 R^2X=0.43); **(B)** exposed to DMSO 0.05 (n=10; PC2 R^2X=0.403); **(C)** DMSO 0.25 (n=10; PC2 R^2X=0.404); **(D)** imatinib (IMA n=10; PC2 R^2X=0.487)**; (E)** pazopanib (PAZ n=10; PC2 R^2X=0.568) or **(F)** sorafenib (SOR n=10; PC2 R^2X=0.468).

Similarly, the PCA plots for the VCC analysis with all the groups (control cells, and cells exposed to DMSO 0.5%, DMSO 0.25%, IMA, PAZ and SOR for 24h) of differentiated AC16 cells are depicted in **Figure 14**. PCA data was, once again, used to take out outliers with an initial sample size of 10 for all groups. In this case, samples CONT 6 and IMA 6 were eliminated as the chromatogram was not acquired in its entirety (analytical error). In this case, the reinjection of the samples is not correct since they had already been heated and injected a first time, so volatile compounds were lost which affect the analyze.

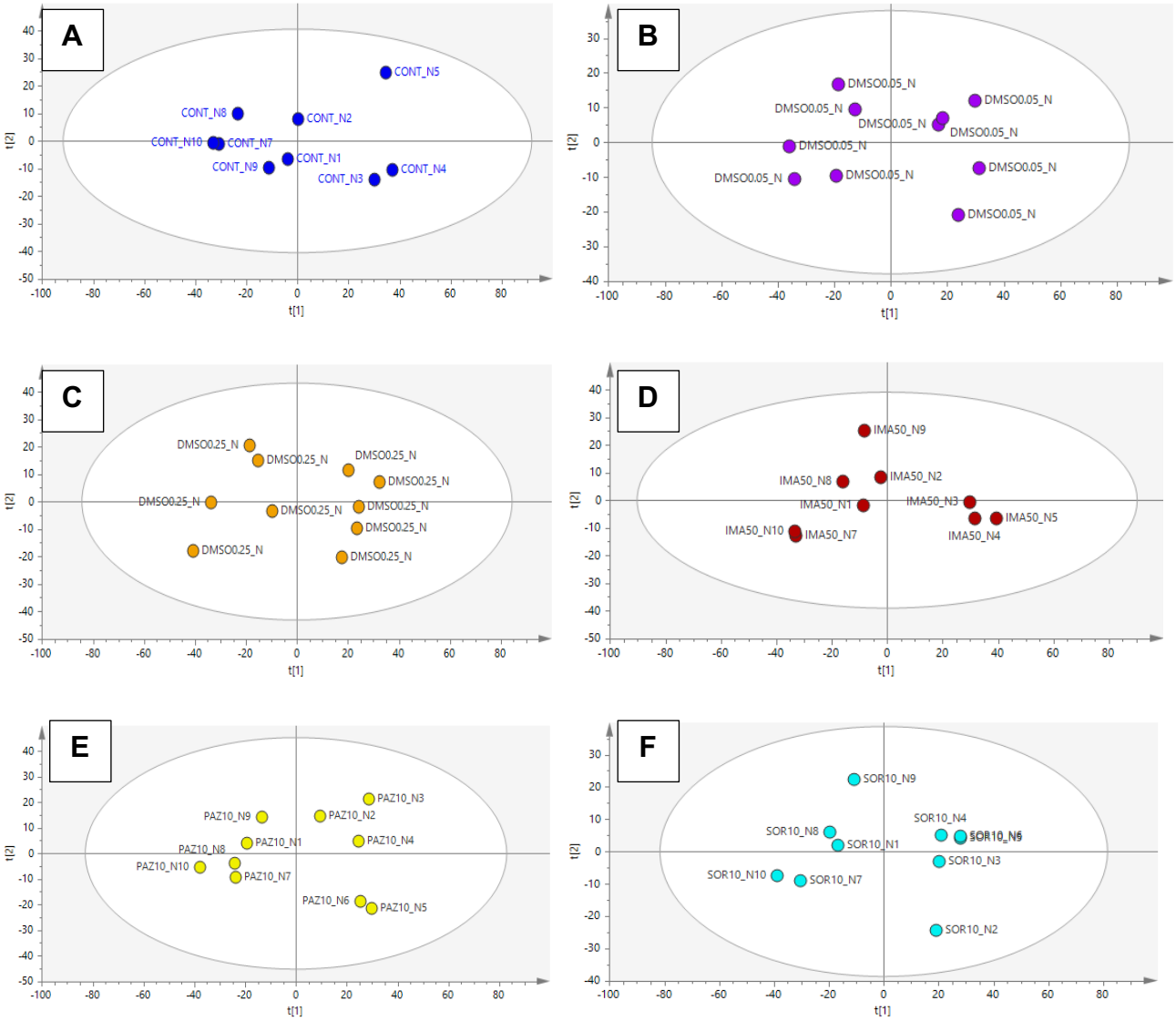


Figure 14. PCA scatter plots acquired from the analysis of the VCC content of: **(A)** AC16 differentiated control cells (CONT, n=9; PC2 R^2X=0.58); **(B)** exposed to DMSO 0.05% (n=10; PC2 R^2X=0.531); **(C)** DMSO 0.25% (n=10; PC2 R^2X=0.53); **(D)** imatinib (IMA, n=9; PC2 R^2X=0.561); **(E)** pazopanib (PAZ, n=10; PC2 R^2X=0.512) or **(F)** sorafenib (SOR, n=10; PC2 R^2X=0.495).

The next step refers to the PLS-DA pairwise analysis, where a panel of metabolites identified as potentially discriminant was selected for a univariate analysis. As recommended in the literature (93), a complete list with important characteristics of the potential discriminant metabolites (retention time, characteristic *m/z* ions, retention

indexes, match and reverse match, and their respective MSI level of identification (NIST14 and/or standards) is presented in Table 6 and 7.

Table 6. List of all intracellular metabolites TMS-derivatized detected from the PLS-DA models (data normalized by total area of the chromatogram) with VIP>1.

Metabolite	RT (minutes)	Characteristic ions (*m/z*) pairs	Match	R Match	RI Literature	RI Calculated	Level of Identification
Unknown RT 5.8	5.887	152 + 166 + 153 + 167 + 78	_	_	_	1038	L4
Lactic acid, 2TMS	6.090	73 + 117 + 147 + 75 + 191 + 66 + 148 + 190 + 74	946	963	1061	1055	L1
Unknown RT 6.1	6.150	147 + 75 + 190 + 73 + 66 + 100 + 148 + 149 + 221	_	_	_	1060	L4
Hexanoic acid, TMS	6.281	75 + 73 + 173 + 117 + 131 + 74	717	816	1074	1071	L2
L-Valine, TMS	6.503	72 + 55 + 73 + 75 + 74 + 146 + 56	652	789	1094	1089	L1
L-Alanine, 2TMS	6.594	116 + 73 + 147 + 117 + 75 + 74	789	842	1095	1097	L1
Unknown RT 6.7	6.776	73 + 258 + 116 + 77 + 75 + 74 + 147 + 89	_	_	_	1113	L4
Glycine, 2TMS	6.816	102 + 73 + 147 + 103 + 75 + 59 + 74 + 204	911	921	1105	1116	L1

Pyruvic acid, 2TMS	6.897	147 + 73 + 148 + 149 + 66 + 75 + 72	712	786	1099	1124	L2
Oxalic acid, 2TMS	7.028	73 + 147 + 148 + 72 + 59	700	787	1136	1135	L1
Phosphoric acid, 2TMS	7.413	241 + 73 + 133 + 75	720	794	1170	1170	L2
L-Isoleucine, TMS	7.494	86 + 75 + 73 + 69 + 87 + 146 + 74	780	847	1179	1177	L1
Unknown RT 7.6	7.625	70 + 75 + 73 + 147 + 79 + 52 + 172 + 69 + 103	_	_	_	1189	L4
L-Valine, 2TMS	7.827	144 + 73 + 218 + 145 + 147 + 100 + 146 + 74	920	928	1224	1208	L1
4-Aminobutanoic acid, 3TMS (GABA)	8.009	73 + 174 + 59 + 75 + 147 + 86 + 100	712	787	1260	1226	L2
Urea, 2TMS	8.080	147 + 189 + 73 + 148 + 171 + 74	860	881	1249	1233	L1
Unknown RT 8.2	8.222	192 + 191+ 163 + 123 + 177 + 95 + 136 + 173 + 70 + 193	_	_	_	1247	L4
L-Serine, 2TMS	8.282	116 + 132 + 73 + 75 + 147 + 103 + 57 + 144 + 133	841	872	1252	1253	L1

Phosphoric acid, 3TMS	8.363	299 + 73 + 300 + 314 + 301 + 133 + 147	892	907	1286	1261	L2
L-Isoleucine, 2TMS	8.605	158 + 73 + 218 + 159 + 147 + 75 + 74 + 100 + 160	896	947	1301	1285	L1
L-Threonine, 2TMS	8.646	73 + 117 + 130 + 147 + 75 + 57 + 219 + 146	911	926	1292	1289	L2
L-Proline, 2TMS	8.686	142 + 73 + 143 + 216 + 147 + 144 + 74 + 75	913	923	1305	1293	L1
Glycine, 3TMS	8.746	174 + 73 + 147 + 175 + 86 + 248 + 176 + 100	833	895	1315	1299	L1
Succinic acid, 2TMS	8.797	147 + 73 + 75 + 148	698	756	1321	1305	L1
Fumaric acid, 2TMS	9.130	245 + 73 + 147 + 75 + 246 + 143	712	920	1353	1340	L1
L-Serine, 3TMS	9.191	204 + 73 + 218 + 147 + 100 + 205 + 219 + 75 + 188	887	903	1368	1347	L1
Nonanoic acid, TMS	9.262	73 + 75 + 215 + 117 + 132 + 55 + 129	787	855	1355	1355	L2
L-Threonine, 3TMS	9.433	73 + 117 + 218 + 219 + 147 + 101 + 291	929	938	1367	1373	L2
L-Methionine, TMS	9.789	104 + 56 + 61 + 73 + 75 + 130 + 131	704	801	1416	1412	L2

L-Aspartic acid, 2TMS	9.840	73 + 160 + 130 + 75 + 117 + 116 + 147 + 74	748	805	1420	1418	L2
Aminomalonic acid, 3TMS	10.193	73 + 147 + 218 + 320 + 174 + 133	702	767	1485	1459	L2
Malic acid, 3TMS	10.314	73 + 147 + 233 + 245 + 133 + 189 + 75 + 148 + 190	921	926	1478	1472	L2
Pyroglutamic acid, TMS	10.546	84 + 75 + 73 + 158 + 157 + 186 + 56	761	819	1511	1499	L2
L-Aspartic acid, 3TMS	10.597	73 + 232 + 100 + 233 + 147 + 218 + 74 + 75	868	924	1522	1505	L2
L-5-oxoproline, 2TMS	10.688	156 + 73 + 147 + 157 + 258 + 230 + 75 + 158 + 74	930	936	1522	1517	L2
L-Cysteine, 3TMS	10.920	73 + 220 + 218 + 100 + 221 + 219 + 147	792	890	1568	1545	L2
Unknown RT 11.0	11.041	73 + 75 + 147 + 198 + 156 + 74 + 55 + 89 + 59 + 186	_	_	_	1560	L4
Unknown RT 11.1	11.162	147 + 73 + 75 + 84 + 186 + 142 + 79 + 148 + 52 + 156	_	_	_	1575	L4
L-Glutamic acid, 3TMS	11.395	246 + 73 + 128 + 147 + 247 + 75 + 156 + 248 + 230	931	933	1632	1604	L1
L-Tartaric acid, 4TMS	11.496	73 + 147 + 292 + 219 + 189 + 74 + 148 + 75	838	893	1622	1617	L2

Phenylalanine, 2TMS	11.546	73 + 218 + 192 + 147 + 100 + 219 + 91 + 193 + 75	879	890	1636	1624	L2
Pyrophosphate, 4TMS	11.688	73 + 451 + 452 + 453 + 299 + 75 + 74 + 466	888	903	1653	1642	L2
Taurine, 3TMS	11.849	326 + 73 + 147 + 327 + 174 + 188 + 100	803	869	1669	1663	L2
Suberic acid, 2TMS	12.021	73 + 75 + 55 + 187 + 169 + 129 + 147 + 117	726	838	1708	1685	L2
Glycerol-3-phosphate, 4TMS	12.425	73 + 357 + 299 + 147 + 358 + 315 + 300 + 103	934	942	1744	1740	L2
Nonanedioic acid, 2TMS	12.748	73 + 75 + 55 + 129 + 317 + 117 + 201 + 147 + 149	825	861	1806	1785	L2
Citric acid, 4TMS	12.849	273 + 73 + 147 + 363 + 375 + 347 + 274	889	897	1839	1799	L1
Unknown RT 12.9	12.960	73 + 147 + 75 + 217 + 218 + 117 + 204 + 191 + 84 + 79	_	_	_	1815	L3
Unknown RT 13.0	13.041	73 + 75 + 217 + 147 + 79 + 204 + 103 + 52 + 218 + 117	_	_	_	1827	L3
Myristic acid, TMS	13.132	73 + 75 + 117 + 285 + 132 + 129 + 55	707	877	1850	1840	L2

D-Fructose, 5TMS	13.203	73 + 103 + 217 + 147 + 307 + 133 + 74	872	893	1859	1851	L2
D-Glucose, 5TMS	13.385	73 + 147 + 319 + 205 + 160 + 103 + 217 + 320	895	899	1883	1877	L1
Unknown RT 13.4	13.455	205 + 73 + 147 + 179 + 189 + 273 + 206 + 117 + 75 + 207	_	_	_	1887	L3
D-Glucose, 5TMS	13.536	73 + 147 + 205 + 319 + 103 + 160 + 217	921	922	1901	1899	L1
D-Sorbitol, 6TMS	13.657	73 + 147 + 319 + 205 + 103 + 217 + 117	768	861	1920	1917	L2
L-Tyrosine, 3TMS	13.738	218 + 73 + 219 + 100 + 280 + 220 + 179 + 74 + 147	883	957	1959	1930	L1
Unknown RT 13.8	13.809	72 + 71 + 73 + 217 + 58 + 147 + 75 + 117 + 129 + 103	_	_	_	1941	L3
Unknown RT 13.9	13.890	217 + 73 + 147 + 218 + 129 + 246 + 219 + 191 + 204 + 75	_	_	_	1953	L3
Palmitic acid, TMS	14.465	117 + 73 + 313 + 75 + 132 + 129 + 145 + 55	914	917	2050	2037	L2

Unknown RT 14.5	14.516	73 + 217 + 147 + 75 + 129 + 218 + 246 + 318 + 191 + 79	_	_	_	2044	L3
Unknown RT 14.7	14.758	73 + 217 + 305 + 147 + 191 + 318 + 306 + 204 + 265 + 218	_	_	_	2077	L2
Unknown RT 15.6	15.688	73 + 147 + 299 + 75 + 342 + 211 + 227 + 79 + 315 + 243	_	_	_	2193	L3
Unknown RT 15.7	15.748	314 + 160 + 315 + 73 + 316 + 402 + 130 + 262 + 161 + 144	_	_	_	2200	L4
9-Octadecenoic acid, TMS	15.849	73 + 75 + 117 + 55 + 129 + 339	766	884	2222	2211	L2
Stearic acid, TMS	16.071	117 + 73 + 341 + 75 + 132 + 129 + 145 + 55 +342	877	887	2246	2236	L2
Oleamide	17.304	59 + 72 + 55 + 69 + 67	779	867	2386	2370	L1
1-Monomyristin, TMS	17.395	343 + 73 + 211 + 147 + 57 + 344 + 129	867	878	2382	2380	L2
D-Myo-inositol, 5TMS	17.546	73 + 318 + 315 + 299 + 147	778	797	_	2396	L2

2-Palmitoylglycerol, 2TMS	18.799	129 + 218 + 73 + 147 + 103 + 313 + 203 + 191	839	906	2558	2539	L2
1-Monopalmitin	19.112	371 + 73 + 372 + 147 + 129 + 205 + 57 + 203	926	946	2581	2576	L2
2-Monostearin, 2TMS	20.385	129 + 73 + 218 + 103 + 147 + 57 + 75	766	837	2772	2731	L2
Glycerol monostearate, 2TMS	20.678	399 + 73 + 147 + 400 + 129 + 55 + 103	917	918	2780	2769	L2
Uridine-5'-monophosphate	21.506	73 + 169 + 315 + 299 + 75 + 147 + 230 + 316	733	827	2896	2874	L2
Cholesterol, TMS	24.426	129 + 73 + 329 + 368 + 75 + 95 + 55 + 81	915	919	3150	3169	L2
Desmosterol, TMS	24.890	129 + 69 + 73 + 75 + 95 + 81 + 119 + 55	904	906	3202	3208	L1 (IS)

Foot note: Metabolite identification was performed according to the standards set by the Metabolomics Standard Initiative. Compounds were characterized by retention peak time (RT), relevant *m/z* ions, match and reverse match (R Match) factor from NIST, theoretical and calculated retention indexes (RI_{lit} and RI_{calc}, respectively), and level of identification when available. Note: L1 (Level 1) - Metabolites unequivocally identified by standards; L2 (Level 2) - Putatively annotated compounds (i.e. identification was based only in the mass spectrum similarity with commercial spectral libraries, retention indexes and reverse percentage of match); L3 (Level 3) - Putatively characterized compound classes (i.e. spectral and/or physicochemical properties are consistent with a particular class of compounds); L4 (Level 4) - Unknown compounds (although unidentified or unclassified metabolites can still be differentiated based upon mass spectrum data), IS – Internal Standard

Table 7. List of all VCCs PFBHA-derivatized metabolites detected from the PLS-DA models (data normalized by total area of the chromatogram) with VIP>1.

Metabolite	RT (minutes)	Base peak	Characteristic *m/z*	Match	R. Match	Level of Identification
Acetaldehyde oxime 1	14.446	181	182+209+161+117+195+99+167+93	915	927	L2
Acetaldehyde oxime 2	14.654	181	182+209+161+117+195+99+167+93+119	919	930	L2
Acetone	16.237	181	253+182+206+223+72+236+195	923	933	L2
Propanal oxime 1	16.842	181	236+182+161+195+117+167+99+223	886	892	L2
Propanal oxime 2	17.049	181	236+182+161+195+117+167+99+93+223	899	902	L2
Isobutanal	17.972	181	195+182+250+161+117+99	890	895	L1
2-Butanone oxime 1	18.357	181	56+250+42+41+182+58+195	841	842	L1

2-Butanone oxime 2	18.450	181	56+250+42+86+41+182+58+195	837	837	L1
Butanal oxime 1	19.305	181	239+41+182+43+195+161+117	847	847	L1
Butanal oxime 2	19.487	181	239+41+182+43+195+161+117	809	810	L1
3-Methyl-2-butanone	19.601	181	58+43+253+42+100+41	778	784	L2
2-Pentanone oxime 1	20.312	181	253+42+41+56+58+70	873	874	L2
Unknown_alkanal	20.405	181	239+57+41+182+44+195+55+161+167	_	_	L3
2-Pentanone oxime 2	20.532	181	253+42+41+56+72+182+58+70	883	883	L2
3-Methylbutanal	20.676	181	239+182+43+41+100	812	818	L2
2-Hexanone oxime 1	21.379	181	253+72+41+42+56+182+57	771	785	L2
2-Hexanone oxime 2	21.586	181	253+72+41+42+182+57	774	776	L2
Pentanal oxime 1	21.628	181	239+182+167+117+57	810	858	L2

Pentanal oxime 2	21.734	181	239+182+195+161+117+99	846	870	L2
3-Methylbutanal oxime 1	21.916	181	239+182+43+41+57+195	746	765	L2
3-Methylpentanal oxime 2	22.471	181	253+72+41+55+182	740	767	L2
4-hydroxy-2-butanone	24.016	181	57+41+72+56+253	719	736	L2
Hexanal oxime 1	24.151	181	239+182+41+114+43+207+55	880	880	L2
Hexanal oxime 2	24.287	181	239+182+41+43+55+195	827	827	L2
Cyclohexanone	26.019	181	82+67+293+81+41+112+276+54+55	847	847	L1
Heptanal oxime 1	26.459	181	239+182+43+41+207+55	820	830	L1
Heptanal oxime 2	26.544	181	239+182+43+55	733	756	L1
Unknown_alkenal oxime 1	28.051	181	250+41+44+57+182+195+55+43+117	_	_	L3

Unknown_alkenal oxime 2	28.220	181	250+41+44+57+182+195+55+99+56	_	_	L3
Octanal oxime 1	28.678	181	239+41+43+55	752	792	L2
Octanal oxime 2	28.750	181	239+41+43+55+182+69+57	732	757	L2
Benzaldehyde oxime 1	29.211	181	301+77+65+271+182+51	763	779	L2
Benzaldehyde oxime 2	29.385	181	301+77+65+271+182+51+89+300	866	866	L2
Nonanal	30.851	181	239+41+43+55+57+69+182	827	855	L2
Decanal	32.900	181	239+43+41+55+57+69	764	774	L2
Glyoxal oxime 1	34.586	181	182+161+195+167+117+99+448+119	897	912	L1
Glyoxal oxime 2	34.688	181	182+161+195	789	882	L1
Glyoxal oxime 3	34.755	181	182+448+161+195+167+117+99+119	919	970	L1
Methylglyoxal oxime 1	34.840	181	182+265+161+195+167+117+99+119	909	910	L1

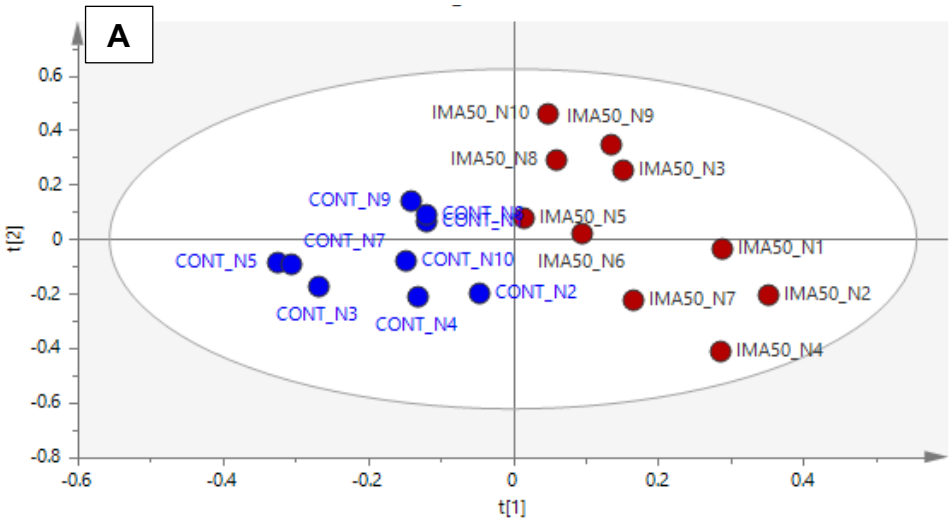
Methylglyoxal oxime 2	35.057	181	182+265+195+167+117+161+99+196	881	882	L1
Methylglyoxal oxime 3	35.357	181	182+265+161+195+167+117+99+119	938	939	L1
Dimethylglyoxal oxime 1	35.658	181	182+279+195+167+161+99+117	734	756	L2
Dimethylglyoxal oxime 2	35.818	181	182+195+167+161+99+117	742	757	L2
Dimethylglyoxal oxime 3	35.916	181	182+279+195+99+117	722	750	L2

Foot note: Metabolite identification was performed according to the standards set by the Metabolomics Standard Initiative. Compounds were characterized by retention peak time (RT), relevant *m/z* ions, match and reverse match (R Match) factor from NIST and level of identification when available. Note: L1 (Level 1) - Metabolites unequivocally identified by standards; L2 (Level 2) - Putatively annotated compounds (i.e. identification was based only in the mass spectrum similarity with commercial spectral libraries, retention indexes and reverse percentage of match); L3 (Level 3) - Putatively characterized compound classes (i.e. spectral and/or physicochemical properties are consistent with a particular class of compounds); L4 (Level 4) - Unknown compounds (although unidentified or unclassified metabolites can still be differentiated based upon mass spectrum data). O-2,3,4,5,6-PFBHA-oxime 1 correspond to cis or trans enantiomer; O-*2,3,4,5,6*-PFBHA-oxime 2 correspond to *cis* or *trans* enantiomer; *O-2,3,4,5,6*-PFBHA-oxime 3 correspond to another enantiomer corresponding to the second C=O group of the compound (glyoxal and methylglyoxal).

3.11. Imatinib caused a strong effect on the metabolome intracellular of AC16 cells

IMA induced a strong metabolic shift regarding the intracellular content of biochemical metabolites of AC16 cells **(Figure 15A)**. Group separation of control cells and cells incubated with IMA was supported by good validation parameters for the respective PLS-DA model (Q^2 > 0.51 and $p \leq 0.03$), as shown in **Table 8**. The permutations tests disclosed no overfitting of the model, as the permutated Q^2 and R^2 values are lower than the original classes **(Figure 15B).**

Furthermore, the signals considered potentially discriminative (VIP>1) and therefore important to group separation were selected for integration. Both statistical significance and effect magnitude are described in **Table 9**, where *p* values and effect sizes are represented. Of the 21 potentially discriminant metabolites, eleven (aminomalonic acid; citric acid; D-sorbitol; L-glutamic acid; pyrophosphate; taurine; unknown RT 6.1; unknown RT 12.9; unknown RT 13.0; unknown RT 13.9; unknown RT 14.7) were found to be significantly different from the control cells (**Table 9**). Among these 11 mentioned metabolites, all of them show a lower trend compared to control cells, except for the metabolite unknown RT 6.1, which is the only one with a higher trend. Those compounds belong to the class of amino acids, organic acids, sugars, among others, showing a diverse impact of IMA in metabolic pathways.



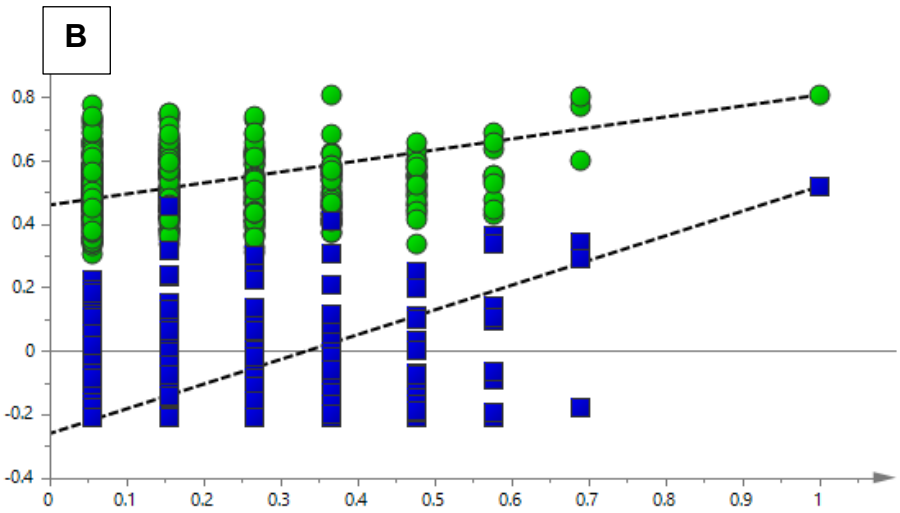


Figure 15. (A) PLS-DA score scatter plots of the differentiated control cells (CONT, n=9; blue circle), against the differentiated cells incubated with imatinib (IMA, n=10; red circle), in the intracellular metabolome; **(B)** PLS-DA models statistical validation by 500 permutations of the PLS-DA model of the differentiated AC16 cells incubated with imatinib.

Table 8. Parameters of cross-validation obtained for the PLS-DA models of the metabolome intracellular analysis of control differentiated AC16 cells and the respective cells incubated with imatinib.

PLS-DA Model	Component	R^2X	R^2Y	Q^2	Permutation tests		*p* [CV-ANOVA]
					R^2	Q^2	
IMA50 *vs* Control	2	0.504	0.808	0.519	0.46	-0.261	0.029315

Foot note: R^2X variance explained by the X matrix. i.e., GC–MS data; R^2Y variance explained by the Y matrix. i.e., sample class; Q^2 predictive power; R^2 and Q^2 (permutation tests) goodness of fit of the permuted model; p [CV-ANOVA]—*p* value to estimate the significance of PLS-DA models.

Table 9. Intracellular metabolites selected for integration of the PLS-DA model of differentiated AC16 cells incubated with imatinib (VIP>1).

Metabolite	ES±ESSE (a)	*p* value	Variation ± Uncertainty %	
1-Monopalmitin	0.96 ± 0.47	ns	23.14	± 9.06
Aminomalonic acid	-2.08 ± 0.55	0.0008	-47.66	± 13.74
Cholesterol	-0.49 ± 0.45	ns	-13.57	± 13.26

Citric acid	-1.35 ± 0.49	0.0105	-28.56	± 10.99
D-Sorbitol	-1.43 ± 0.50	0.0099	-28.89	± 10.72
Glycerol-3-phosphate	-0.89 ± 0.46	ns	-16.98	± 9.19
Glycerol monostearate	0.91 ± 0.46	ns	26.51	± 10.73
L-Glutamic acid	-1.98 ± 0.54	0.0005	-42.20	± 12.02
L-Isoleucine	-0.65 ± 0.45	ns	-22.32	± 16.52
L-Threonine	-0.80 ± 0.46	ns	-15.48	± 9.17
L-Tyrosine	-0.66 ± 0.45	ns	-15.91	± 11.39
Malic acid	0.77 ± 0.46	ns	28.82	± 14.14
Pyroglutamic acid	-0.52 ± 0.45	ns	-35.29	± 37.28
Pyrophosphate	-1.50 ± 0.50	0.0067	-36.52	± 13.50
Taurine	-1.21 ± 0.48	0.0175	-33.75	± 14.74
Unknown RT 6.1	0.97 ± 0.47	0.0496 (b)	29.97	± 11.59
Unknown RT 6.7	-0.57 ± 0.45	ns	-31.19	± 29.93
Unknown RT 12.9	-1.94 ± 0.54	0.0024	-46.50	± 14.53
Unknown RT 13.0	-1.74 ± 0.52	0.002	-38.76	± 12.39
Unknown RT 13.9	-1.11 ± 0.47	0.0385 (b)	-36.05	± 18.10
Unknown RT 14.7	-1.64 ± 0.51	0.0066	-53.37	± 20.69

Foot note: ES and *p* values are represented for all metabolites, eliciting the magnitude and statistical significance of group differences. A positive ES value shows that the metabolites increased in cells exposed to imatinib, while a negative ES value indicates a decrease comparatively to control. (a) ES were calculated as shown in the methods; (b) metabolites that lose the statistically significant difference after Benjamini-Hochberg correction – new cut-off *p* value for intracellular metabolome in differentiated AC16 cells incubated with imatinib: 0.018. ns - not significant

3.12. Pazopanib changed the metabolome intracellular of AC16 cells

PAZ caused a shift in the endometabolome of AC16 control cells compared to cells incubated with PBS **(Figure 16A).** Regarding the cells incubated with PAZ, group separation is supported by significant validation parameters obtained for the respective PLS-DA model (Q^2 0.6 and $p \leq 0.01$), as described in **Table 10**, along with the other validation parameters. The permutations test revealed no overfitting of the model, since all the permutated Q^2 and R^2 values were lower than the original classes **(Figure 16B).**

Next, the metabolites proposed as potentially discriminative (VIP>1), and consequently statistically responsible for group separation, were selected for integration. Once again, *p* values and effect sizes are described to reflect both statistical significance and effect magnitude in **Table 11**. Seventeen metabolites were identified as potentially discriminant, but only ten (citric acid; D-sorbitol; glycerol-3-phosphate; lactic acid; L-glutamic acid; L-proline; malic acid; phosphoric acid; pyrophosphate; unknown RT 12.9) were significantly different from the control cells. Of those all are present at significant lower levels compared to control cells, with the exception of malic acid which presents an upward trend also compared to the control. The significantly altered metabolites belong to a wide variety of biochemical classes.

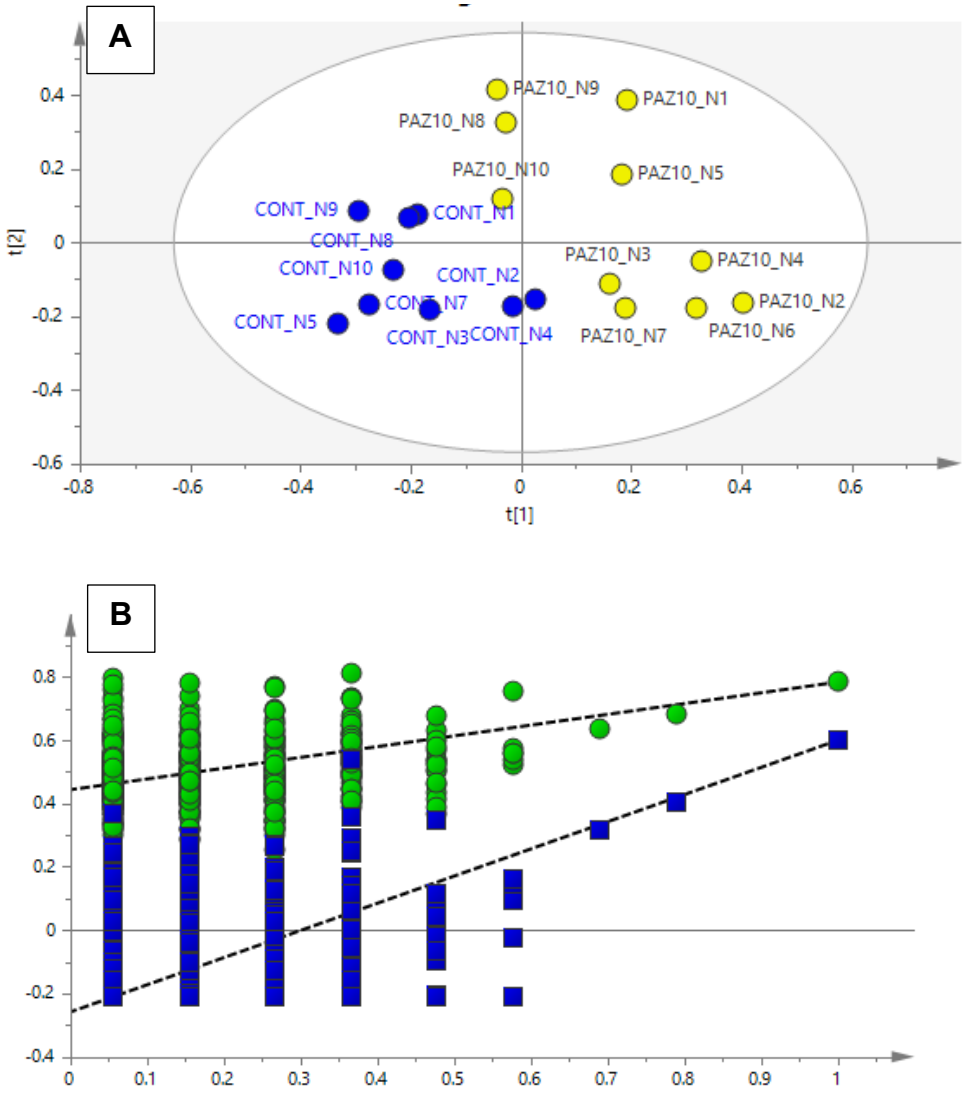


Figure 16. (A) PLS-DA score scatter plots of the differentiated control cells (CONT, n=9; blue circle), against the differentiated cells incubated with pazopanib (PAZ, n=10; yellow circle), in the intracellular metabolome; **(B)** PLS-DA models statistical validation by 500 permutations of the PLS-DA model of the differentiated AC16 cells incubated with pazopanib.

Table 10. Parameters of cross-validation obtained for the PLS-DA models of the endometabolome analysis of control differentiated AC16 cells and the respective cells incubated with pazopanib.

PLS-DA Model	Component	R^2X	R^2Y	Q^2	Permutation tests		*p* [CV-ANOVA]
					R^2	Q^2	
PAZ10 vs Control	2	0.590	0.784	0.600	0.444	-0.258	0.00733105

Foot note: R^2X variance explained by the X matrix. i.e., GC–MS data; R^2Y variance explained by the Y matrix. i.e., sample class; Q^2 predictive power; R^2 and Q^2 (permutation tests) goodness of fit of the permuted model; p [CV-ANOVA]—*p* value to estimate the significance of PLS-DA models.

Table 11. Intracellular metabolites selected for integration of the PLS-DA model of differentiated AC16 cells incubated with pazopanib (VIP>1).

Metabolite	ES±ESSE (a)	*p* value	Variation ± Uncertainty %
1-Monopalmitin	0.18 ± 0.44	ns	3.46 ± 7.94
Cholesterol	-0.92 ± 0.46	ns	-24.73 ± 13.88
Citric acid	-2.72 ± 0.62	<0.0001	-49.00 ± 10.92
D-Glucose	0.78 ± 0.46	ns	35.91 ± 16.41
D-Sorbitol	-1.37 ± 0.49	0.0091	-32.64 ± 12.63
Glycerol-3-phosphate	-2.07 ± 0.55	0.0003	-39.25 ± 10.47
Lactic acid	-1.09 ± 0.47	0.0294 (b)	-15.03 ± 6.49
L-Glutamic acid	-2.38 ± 0.58	0.0002	-44.42 ± 10.88
L-Isoleucine	-0.65 ± 0.45	ns	-22.62 ± 16.79
L-Proline	-1.34 ± 0.49	0.0094	-32.37 ± 12.52
Malic acid	2.39 ± 0.59	<0.0001	99.90 ± 11.77
Phosphoric acid	-1.47 ± 0.50	0.0075	-34.48 ± 12.81
Pyrophosphate	-1.11 ± 0.47	0.0302 (b)	-29.97 ± 14.17
Succinic acid	0.91 ± 0.46	ns	61.98 ± 21.72

Unknown RT 6.1	0.53 ± 0.45	ns	19.67	± 14.45
Unknown RT 12.9	-2.03 ± 0.55	0.0006	-58.06	± 18.36
Unknown RT 15.6	-0.47 ± 0.45	ns	-27.58	± 31.14

Foot note: ES and *p* values are represented for all metabolites, eliciting the magnitude and statistical significance of group differences. A positive ES value shows that the metabolites increased in cells exposed to pazopanib while a negative ES value indicates a decrease comparatively to control. (a) ES were calculated as shown in the methods; (b) metabolites that lose the statistically significant difference after Benjamini-Hochberg correction – new cut-off *p* value for intracellular metabolome in differentiated AC16 cells incubated with pazopanib: 0.017. ns - not significant

3.13. A clinically relevant concentration of sorafenib causes the strongest impact on the intracellular metabolites of AC16 cells

Similarly, to the two previous targeted drugs, SOR significantly impacted intracellular metabolome of AC16 cells **(Figure 17A)**. In fact, it had the strongest effect on the metabolome of all the drugs studied. The separation of control cell groups exposed to SOR is supported by good validation parameters (Q^2 0.79 and $p \leq 0.001$) of the PLS-DA models, as shown in **Table 12**. The permutated values of Q^2 and R^2 were lower than the original values, showing no over adjustment of the model **(Figure 17B)**.

The biochemical metabolites identified as possibly discriminating (VIP>1) and, as key for the separation of groups, were selected for integration and the values of *p* and effect sizes were calculated to express statistical significance and effect magnitude, respectively **(Table 13).** Of the 22 potentially discrepant compounds, 17 (2-palmitoylglycerol; aminomalonic acid; citric acid; glycerol-3-phosphate; L-5-oxoproline; L-glutamic acid; L-isoleucine; L-serine; L-threonine; L-tyrosine; L-valine; malic acid; phenylalanine; phosphoric acid; pyrophosphate; succinic acid; unknown RT 11.0) were significantly different from the control cells **(Table 13).** In this case only 7 metabolites (2-palmitoylglycerol; aminomalonic acid; citric acid; L-glutamic acid; phosphoric acid; pyrophosphate; unknown RT 11.0) have lower levels when compared with the control cells and the remaining 10 have a higher trend. Similarly, for this drug, altered biochemical metabolites belong to a broad group of biochemical classes. Moreover, SOR was the drug that presented a higher number of altered metabolites found.

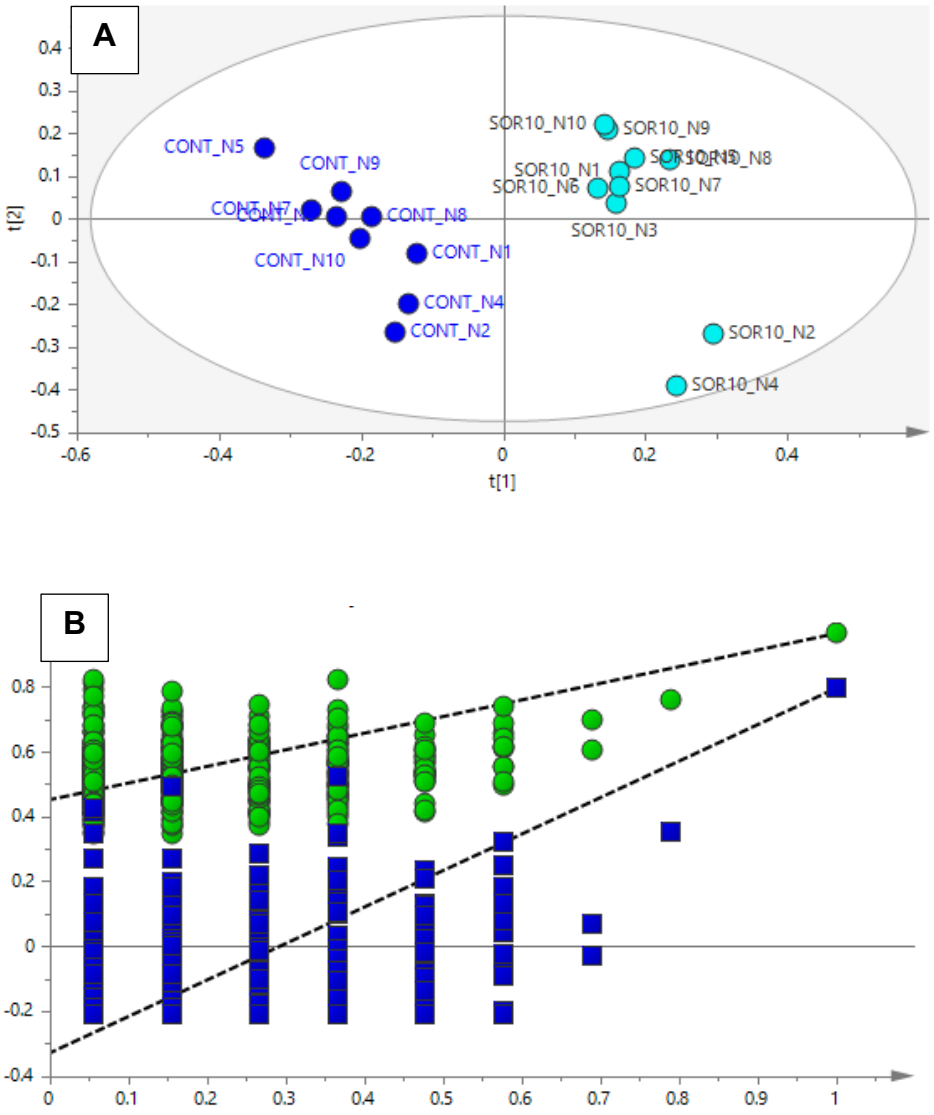


Figure 17. (A) PLS-DA score scatter plots of the differentiated control cells (CONT, n=9; blue circle), against the differentiated cells incubated with sorafenib (SOR, n=10; turquoise circle), in the intracellular metabolome; **(B)** PLS-DA models statistical validation by 500 permutations of the PLS-DA model of the differentiated AC16 cells incubated with sorafenib.

Table 12. Parameters of cross-validation obtained for the PLS-DA models of the endometabolome analysis of control differentiated AC16 cells and the respective cells incubated with sorafenib.

PLS-DA Model	Component	R^2X	R^2Y	Q^2	Permutation tests		*p* [CV-ANOVA]
					R^2	Q^2	
SOR10 vs Control	2	0.384	0.965	0.796	0.452	-0.329	0.000344015

Foot note: R^2X variance explained by the X matrix. i.e., GC–MS data; R^2Y variance explained by the Y matrix. i.e., sample class; Q^2 predictive power; R^2 and Q^2 (permutation tests) goodness of fit of the permuted model; p [CV-ANOVA]—*p* value to estimate the significance of PLS-DA models.

Table 13. Intracellular metabolites selected for integration of the PLS-DA model of differentiated AC16 cells incubated with sorafenib (VIP>1).

Metabolite	ES±ESSE (a)	*p* value	Variation ± Uncertainty %	
2-Palmitoylglycerol	-1.47 ± 0.50	0.0064	-37.07	± 13.84
Aminomalonic acid	-2.92± 0.65	<0.0001	-63.00	± 14.66
Cholesterol	-0.98 ± 0.47	ns	-27.07	± 14.35
Citric acid	-4.95 ± 0.92	<0.0001	-82.78	± 13.50
Glycerol-3-phosphate	1.45 ± 0.50	0.0079	79.47	± 16.17
Lactic acid	-0.94 ± 0.46	ns	-15.28	± 7.57
L-5-oxoproline	1.78 ± 0.53	0.003	50.36	± 9.51
L-Glutamic acid	-3.48 ± 0.72	<0.0001	-58.06	± 10.91
L-Isoleucine	1.89 ± 0.54	0.001	62.31	± 10.49
L-Serine	2.14± 0.56	0.0015	86.80	± 11.94
L-Threonine	2.37± 0.58	0.0001	68.14	± 8.95
L-Tyrosine	1.06 ± 0.47	0.0334 (b)	34.60	± 11.76
L-Valine	2.27 ± 0.57	0.0015	92.16	± 11.70

Malic acid	3.38 ± 0.70	<0.0001	164.22	± 11.09
Phenylalanine	2.09 ± 0.55	0.002	72.14	± 10.51
Phosphoric acid	-1.48 ± 0.50	0.0057	-39.05	± 14.65
Pyrophosphate	-1.10 ± 0.47	0.033 (b)	-28.39	± 13.48
Succinic acid	1.79 ± 0.53	0.0022	205.38	± 23.00
Unknown RT 6.1	0.88 ± 0.46	ns	34.55	± 14.16
Unknown RT 8.2	0.75± 0.46	ns	34.01	± 16.97
Unknown RT 11.0	-1.33± 0,49	0.0113	-27.83	± 10.80
Urea	0.65± 0.45	ns	107.73	± 44.44

Foot note: ES and *p* values are represented for all metabolites, eliciting the magnitude and statistical significance of group differences. A positive ES value shows that the metabolites increased in cells exposed to sorafenib while a negative ES value indicates a decrease comparatively to control. (a) ES were calculated as shown in the methods; (b) metabolites that lose the statistically significant difference after Benjamini-Hochberg correction – new cut-off *p* value for intracellular metabolome in differentiated AC16 cells incubated with sorafenib: 0.029. ns - not significant

3.14. The vehicle used did not caused relevant changes in the metabolome of cells

According to **Figure 18A**, no significant changes were observed between the intracellular metabolome of differentiated AC16 cells incubated with DMSO 0.05% and control cells, according to the validation parameters obtained for the respective PLS-DA model (Q^2 -0.21 and *p*-value of 1), as described in **Table 14**, along with the other validation parameters. The permutations test revealed an overfitting of the model, since all the permutated Q^2 and R^2 values were higher than the original classes (**Figure 18B**).

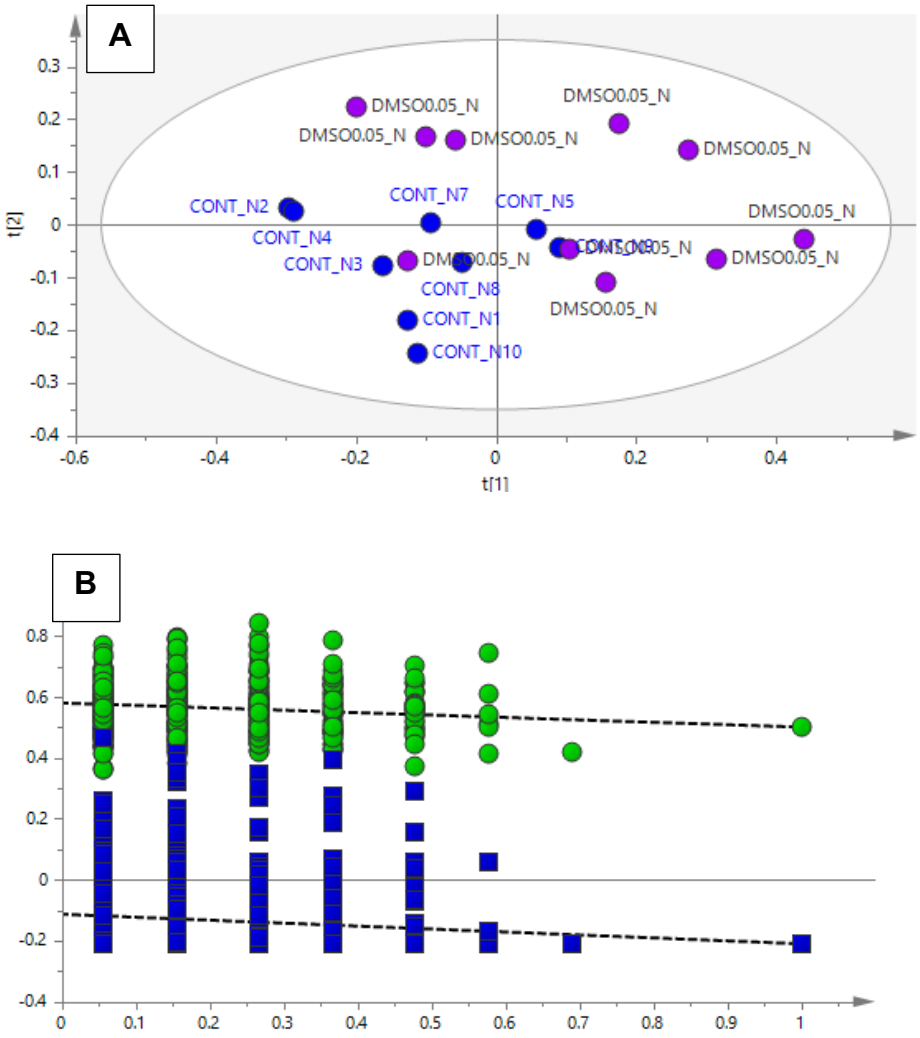


Figure 18. (A) PLS-DA score scatter plots of the differentiated control cells (CONT, n=9; blue circle), against the differentiated cells incubated with DMSO 0.05% (n=10; violet circle), in the intracellular metabolome; **(B)** PLS-DA models statistical validation by 500 permutations of the PLS-DA model of the differentiated AC16 cells incubated with DMSO 0.05%.

Table 14. Parameters of cross-validation obtained for the PLS-DA models of the endometabolome analysis of control differentiated AC16 cells and the respective cells incubated with DMSO 0.05%.

PLS-DA Model	Component	R^2X	R^2Y	Q^2	Permutation tests		*p* [CV-ANOVA]
					R^2	Q^2	
DMSO 0.05 vs Control	2	0.409	0.502	-0.21	0.581	-0.113	1

Foot note: R^2X variance explained by the X matrix. i.e., GC–MS data; R^2Y variance explained by the Y matrix. i.e., sample class; Q^2 predictive power; R^2 and Q^2 (permutation tests) goodness of fit of the permuted model; p [CV-ANOVA]—*p* value to estimate the significance of PLS-DA models.

After incubation with DMSO 0.25% for 24h, the intracellular metabolome was not significantly altered in relation to intracellular content of differentiated AC16 control cells **(Figure 19A)**. The validation parameters for the respective PLS-DA model (Q^2 -0.12 and *p*-value of 1), as displayed in **Table 15**, show that there is no good separation between the control cells and the cells incubated with DMSO 0.25%. As in the previous model, the permutation tests revealed excess of adjustment of the referred model, because the values of Q^2 and R^2 are higher than the original classes **(Figure 19B)**.

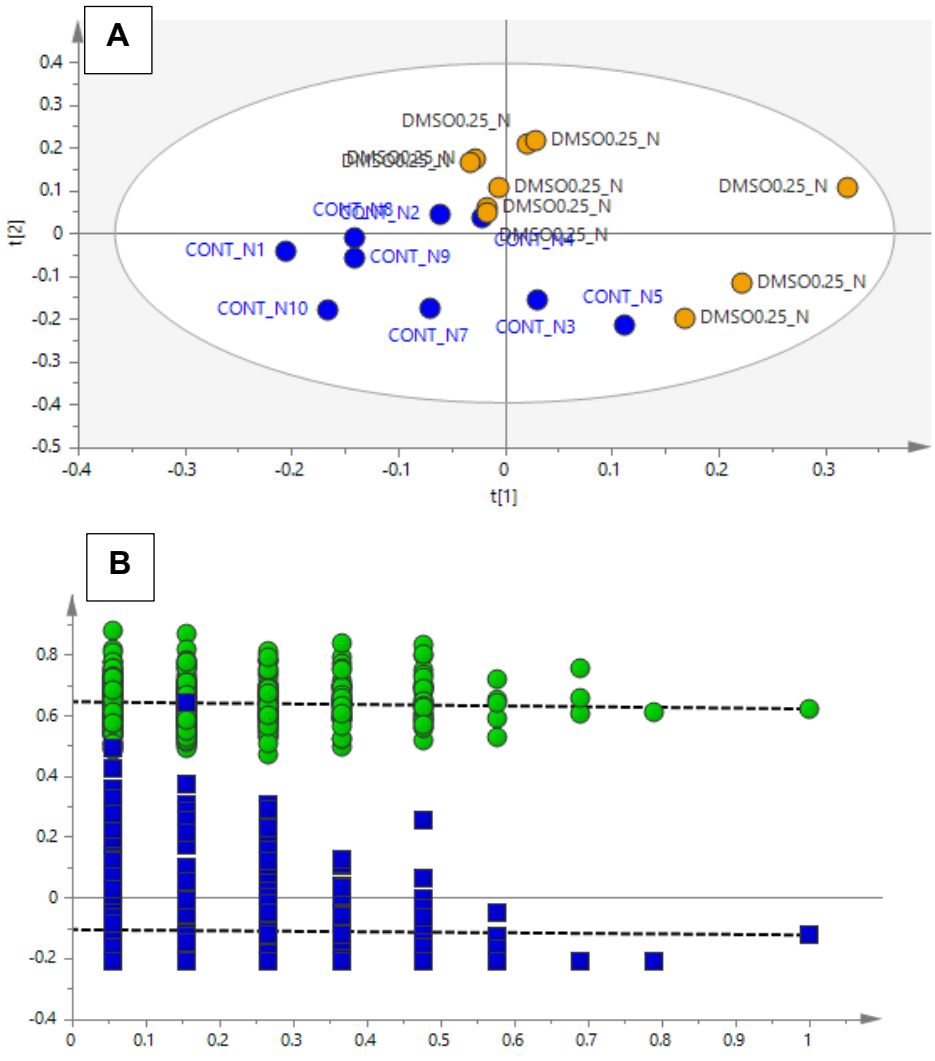


Figure 19. (A) PLS-DA score scatter plots of the differentiated control cells (n=9; blue circle), against the differentiated cells incubated with DMSO 0.25 (n=10; orange circle), in the intracellular metabolome; **(B)** PLS-DA models statistical validation by 500 permutations of the PLS-DA model of the differentiated AC16 cells incubated with DMSO 0.25.

Table 15. Parameters of cross-validation obtained for the PLS-DA models of the endometabolome analysis of control differentiated AC16 cells and the respective cells incubated with DMSO 0.25.

PLS-DA Model	Component	R^2X	R^2Y	Q^2	Permutation tests		*p* [CV-ANOVA]
					R^2	Q^2	
DMSO 0.25 vs Control	2	0.349	0.622	-0.123	0.645	-0.106	1

Foot note: R^2X variance explained by the X matrix. i.e., GC–MS data; R^2Y variance explained by the Y matrix. i.e., sample class; Q^2 predictive power; R^2 and Q^2 (permutation tests) goodness of fit of the permuted model; p [CV-ANOVA]—*p* value to estimate the significance of PLS-DA models.

3.15. Exometabolome of AC16 cells was significantly changed by imatinib but no discriminative metabolites were found

IMA induced a strong metabolic shift regarding the exometabolome, namely VCC content, of AC16 cells metabolites **(Figure 20A)**. Group separation of control cells and cells incubated with IMA was supported by good validation parameters for the respective PLS-DA model with $Q^2 > 0.63$, as shown in **Table 16**. The permutations tests disclosed no overfitting of the model, as the permutated Q^2 and R^2 values are lower than the original classes **(Figure 20B).** However, as can be seen by the *p*-value of 1, the separation was not robust, and the univariate analysis showed that none of the potentially discriminating metabolites had significant differences.

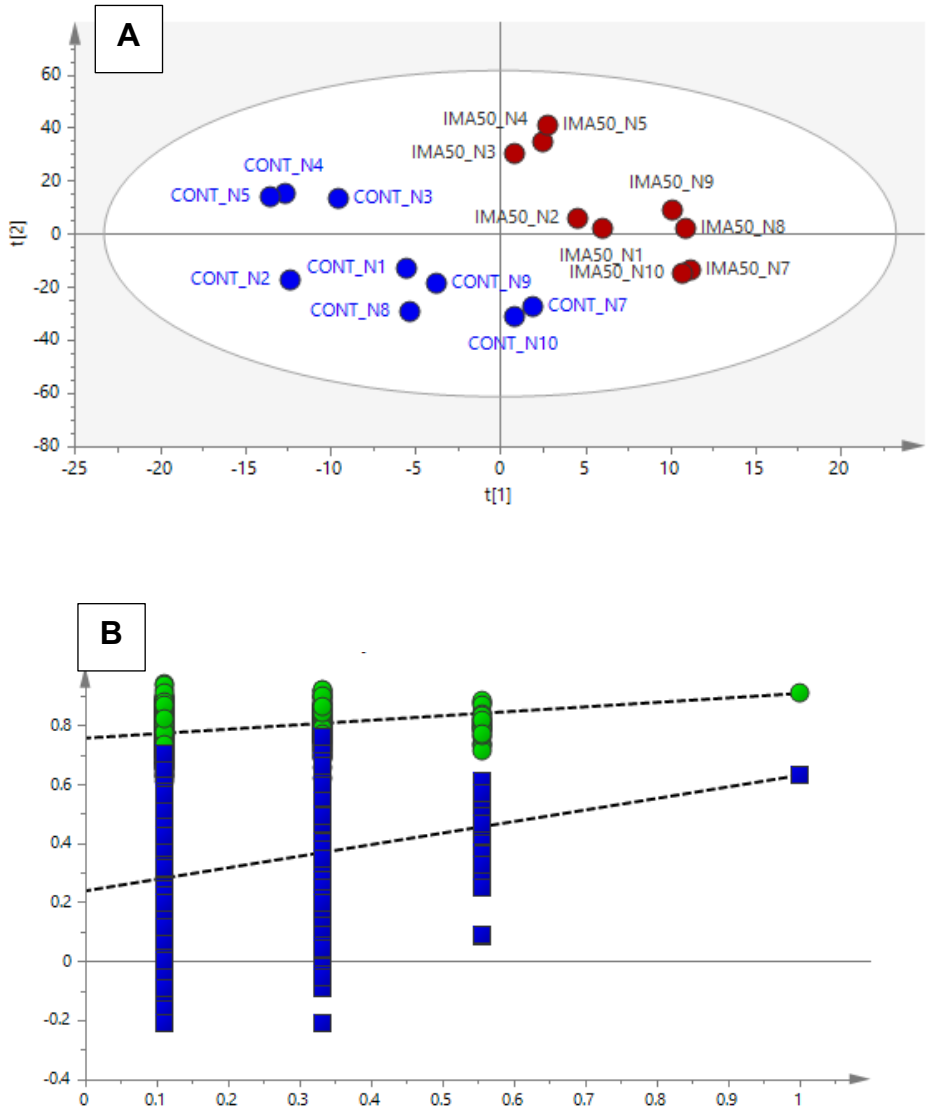


Figure 20. (A) PLS-DA score scatter plots of the differentiated control cells (CONT, n=9; blue circle), against the differentiated cells incubated with imatinib (IMA, n=9; red circle) after GC-MS analysis of VCCs; **(B)** PLS-DA models statistical validation by 500 permutation of the PLS-DA model of the differentiated AC16 cells incubated with imatinib.

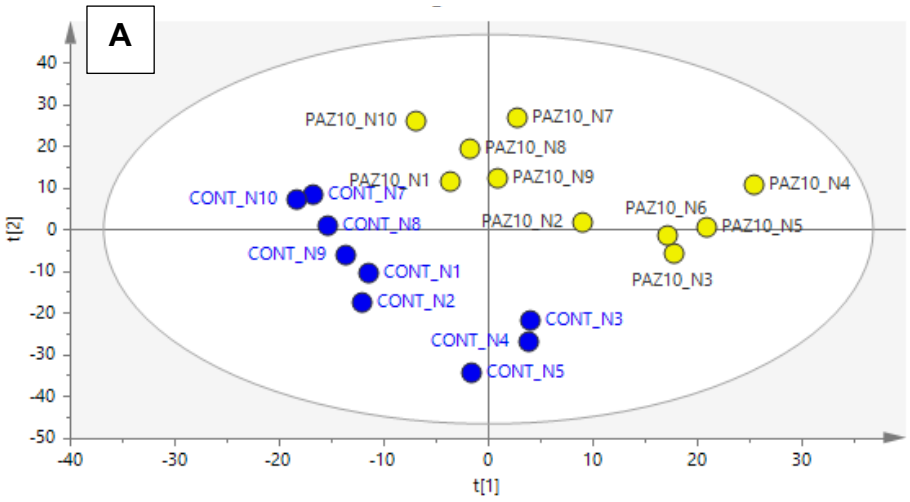
Table 16. Parameters of cross-validation obtained for the PLS-DA models regarding the VCC content, by comparison of control differentiated AC16 cells and the respective cells incubated with imatinib.

PLS-DA Model	Component	R^2X	R^2Y	Q^2	Permutation tests		*p* [CV-ANOVA]
					R^2	Q^2	
IMA 50 vs Control	2	0.565	0.908	0.631	0.757	0.238	1

Foot note: R^2X variance explained by the X matrix. i.e., GC–MS data; R^2Y variance explained by the Y matrix. i.e., sample class; Q^2 predictive power; R^2 and Q^2 (permutation tests) goodness of fit of the permuted model; p [CV-ANOVA]—*p* value to estimate the significance of PLS-DA models.

3.16. Pazopanib altered the exometabolome of AC16 cells

PAZ made a significant shift in the exometabolome of AC16 control cells **(Figure 21A).** Regarding the VCC analysis, group separation is supported by significant validation parameters obtained for the respective PLS-DA model, as described in **Table 17**. The permutations test revealed no over-fitting of the model, since all the permutated Q^2 and R^2 values were lower than the original classes **(Figure 21B).** In **Table 18**, the small number of metabolites considered potentially discriminant in the VCC content of differentiated AC16 cells incubated with pazopanib is described. Of the 10 potentially discrepant compounds, only acetaldehyde and benzaldehyde were significantly different and presented a higher level when compared with the control AC16 cells.



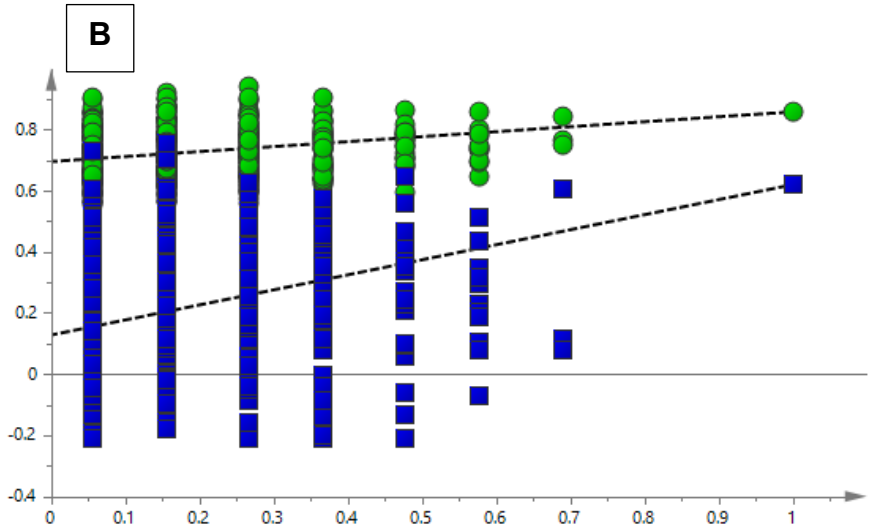


Figure 21. (A) PLS-DA score scatter plots of the differentiated control cells (n=9; blue circle), against the differentiated cells incubated with pazopanib (n=10; yellow circle), after GC-MS analysis of VCCs; **(B)** PLS-DA models statistical validation by 500 permutations of the PLS-DA model of the differentiated AC16 cells incubated with pazopanib.

Table 17. Parameters of cross-validation obtained for the PLS-DA models regarding the VCC content, by comparison of control differentiated AC16 cells and the respective cells incubated with pazopanib.

PLS-DA Model	Component	R^2X	R^2Y	Q^2	Permutation tests		*p* [CV-ANOVA]
					R^2	Q^2	
PAZ 10 vs Control	2	0.563	0.859	0.621	0.696	0.128	0.0298267

Foot note: R^2X variance explained by the X matrix. i.e., GC–MS data; R^2Y variance explained by the Y matrix. i.e., sample class; Q^2 predictive power; R^2 and Q^2 (permutation tests) goodness of fit of the permuted model; p [CV-ANOVA]—*p* value to estimate the significance of PLS-DA models.

Table 18. VCC metabolites selected for integration of the PLS-DA model of differentiated AC16 cells incubated with pazopanib (VIP>1).

Metabolite	ES±ESSE (a)	*p* value	Variation ± Uncertainty %	
4-hydroxy-2-butanone	-0.48 ± 0.45	ns	-14.94	± 14.83
Acetaldehyde	1.19 ± 0.48	0.0188 (b)	29.00	± 9.15

Benzaldehyde	1.05 ± 0.47	0.0345 (b)	59.02	± 18.19
Decanal	0.51 ± 0.45	ns	32.59	± 23.44
Glyoxal	-0.66 ± 0.45	ns	-24.94	± 19.21
Isobutanal	0.59 ± 0.45	ns	22.79	± 15.00
Methylglyoxal	0.56 ± 0.45	ns	21.48	± 15.35
Pentanal	-0.61 ± 0.45	ns	-23.95	± 20.09
Propanal	0.79 ± 0.46	ns	15.97	± 8.18
Unknown_alkanal RT 20.4	0.77 ± 0.46	ns	30.33	± 14.83

Foot note: ES and *p* values are represented for all metabolites, eliciting the magnitude and statistical significance of group differences. A positive ES value shows that the metabolites increased in cells exposed to pazopanib, while a negative ES value indicates a decrease comparatively to control. (a) ES were calculated as shown in the methods; (b) metabolites that lose the statistically significant difference after Benjamini-Hochberg correction – new cut-off *p* value for VCC metabolome in differentiated AC16 cells incubated with pazopanib: 0.003. ns - not significant

3.17. Sorafenib at pharmacological relevant concentrations caused significant differences on the volatile carbonyl compounds of AC16 cells

Regarding VCC content, when incubated with SOR, significant differences were detected in the cell culture medium of the differentiated AC16 cells (**Figure 22A**). Validation parameters for the PLS-DA models are depicted in **Table 19**. Since the permutated Q^2 and R^2 values were lower than the original ones, these demonstrate no overfitting of the model (**Figure 22B).** Moreover, the number of metabolites considered potentially discriminant in the VCC content of differentiated AC16 cells incubated with SOR are described in **Table 20**. In this case, 5 metabolites (benzaldehyde; heptanal; hexanal; propanal; unknown_alkenal RT 28.2) out of 16 potentially discrepant metabolites showed a significant difference and all had a higher content when compared to the control cells.

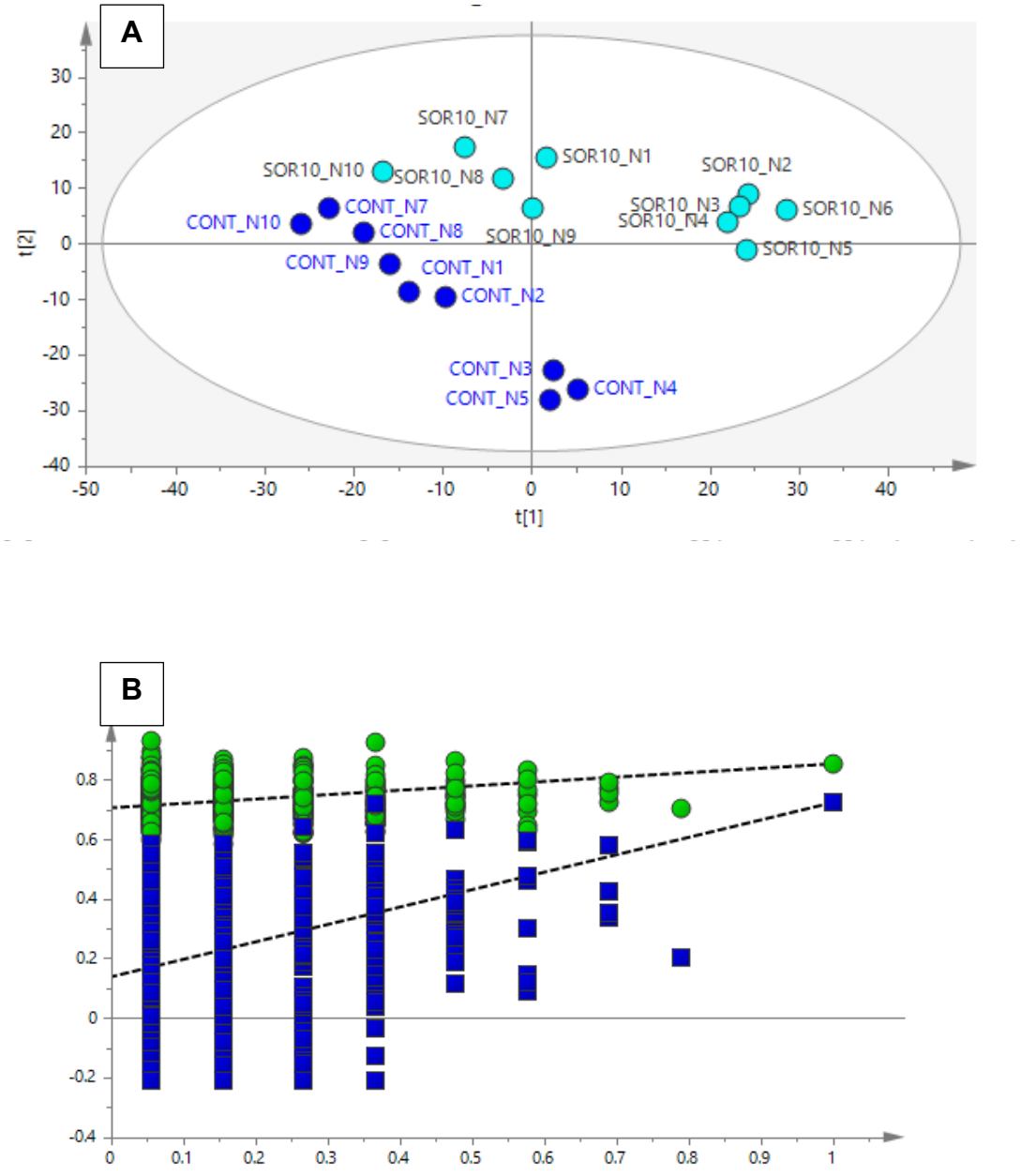


Figure 22. (A) PLS-DA score scatter plots of the differentiated control cells (n=9; blue circle), against the differentiated cells incubated with sorafenib (n=10; turquoise circle), after GC-MS analysis of VCCs; **(B)** PLS-DA models statistical validation by 500 permutations of the PLS-DA model of the differentiated AC16 cells incubated with sorafenib.

Table 19. Parameters of cross-validation obtained for the PLS-DA models regarding the VCC content, by comparison of control differentiated AC16 cells and the respective cells incubated with sorafenib.

PLS-DA Model	Component	R^2X	R^2Y	Q^2	Permutation tests		*p* [CV-ANOVA]
					R^2	Q^2	

SOR 10 vs Control	2	0.556	0.854	0.724	0.706	0.139	0.000982367

Foot note: R^2X variance explained by the X matrix. i.e., GC–MS data; R^2Y variance explained by the Y matrix. i.e., sample class; Q^2 predictive power; R^2 and Q^2 (permutation tests) goodness of fit of the permuted model; p [CV-ANOVA]—*p* value to estimate the significance of PLS-DA models.

Table 20. VCC metabolites selected for integration of the PLS-DA model of differentiated AC16 cells incubated with sorafenib (VIP>1).

Metabolite	ES±ESSE (a)	*p* value	Variation ± Uncertainty %	
2-Hexanone	-0.63 ± 0.45	ns	-38.67	± 34.19
2-Pentanone	-0.86 ± 0.46	ns	-44.60	± 30.75
3-Methylbutanal	0.54 ± 0.45	ns	21.12	± 15.47
3-Methylpentanal	-0.71 ± 0.45	ns	-21.62	± 15.17
4-Hydroxy-2-butanone	-0.87 ± 0.46	ns	-33.44	± 20.05
Benzaldehyde	1.50 ± 0.50	0.0056 (b)	104.86	± 19.05
Butanal	0.69 ± 0.45	ns	63.25	± 30.44
Dimethylglyoxal	0.91 ± 0.46	ns	39.56	± 15.62
Heptanal	1.02 ± 0.47	0.0267 (b)	43.05	± 14.88
Hexanal	1.17 ± 0.48	0.0205 (b)	57.14	± 16.20
Isobutanal	0.49 ± 0.45	ns	16.40	± 13.70
Methylglyoxal	0.65 ± 0.45	ns	49.64	± 25.50

Octanal	0.67 ± 0.45	ns	30.50	± 17.30
Propanal	1.14 ± 0.48	0.0235 (b)	23.76	± 8.03
Unknown_alkenal RT 28.0	0.98 ± 0.47	ns	43.53	± 15.88
Unknown_alkenal RT 28.2	1.06 ± 0.47	0.0338 (b)	62.87	± 19.33

Foot note: ES and *p* values are represented for all metabolites, eliciting the magnitude and statistical significance of group differences. A positive ES value shows that the metabolites increased in cells exposed to sorafenib, while a negative ES value indicates a decrease comparatively to control. (a) ES were calculated as shown in the methods; (b) metabolites that lose the statistically significant difference after Benjamini-Hochberg correction – new cut-off *p* value for VCC metabolome in differentiated AC16 cells incubated with sorafenib: 0.002. ns - not significant

3.18. The vehicle did not change the exometabolome of AC16 cells

The analysis of the exometabolome was performed with the vehicle, DMSO, and comprised the analysis of the VCC content, as mentioned in the methods section. Regarding VCC content, no significant differences were detected between the controls and the incubations with DMSO 0.05% (**Figure 23A**; validation parameters for the PLS-DA models are depicted in **Table 21**) and the permutations test revealed an overfitting of the model, since all the permutated Q^2 and R^2 values were higher than the original classes **(Figure 23B).**

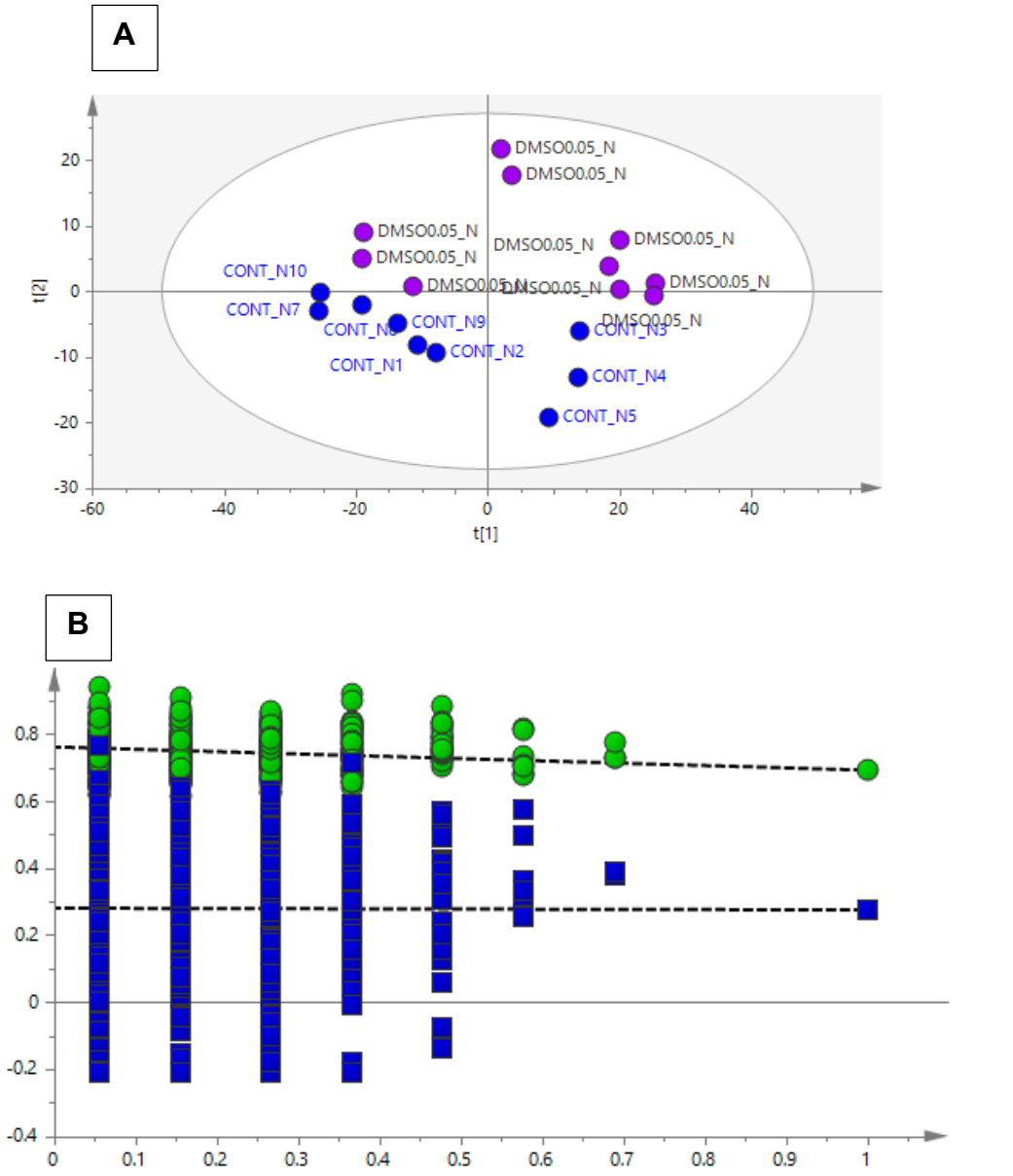


Figure 23. (A) PLS-DA score scatter plots of the differentiated control cells (n=9; blue circle), against the differentiated cells incubated with DMSO 0.05 (n=10; violet circle), after GC-MS analysis of VCCs ; **(B)** PLS-DA models statistical validation by 500 permutations of the PLS-DA model of the differentiated AC16 cells incubated with DMSO 0.05.

Table 21. Parameters of cross-validation obtained for the PLS-DA models regarding the VCC content, by comparison of control differentiated AC16 cells and the respective cells incubated with DMSO 0.05.

PLS-DA Model	Component	R^2X	R^2Y	Q^2	Permutation tests		*p* [CV-ANOVA]
					R^2	Q^2	
DMSO 0.05 % vs Control	2	0.576	0.693	0.275	0.762	0.281	0.324034

Foot note: R^2X variance explained by the X matrix. i.e., GC–MS data; R^2Y variance explained by the Y matrix. i.e., sample class; Q^2 predictive power; R^2 and Q^2 (permutation tests) goodness of fit of the permuted model; p [CV-ANOVA]—*p* value to estimate the significance of PLS-DA models.

Similarly, the VCCs of the differentiated AC16 cells when incubated with DMSO 0.25% did not induce significative alterations (**Figure 24A**; validation parameters for the PLS-DA models are depicted in **Table 22**). As in the previous model, the values of Q^2 and R^2 are higher than the original classes so, the permutation tests revealed excess of adjustment of the referred model **(Figure 24B)**.

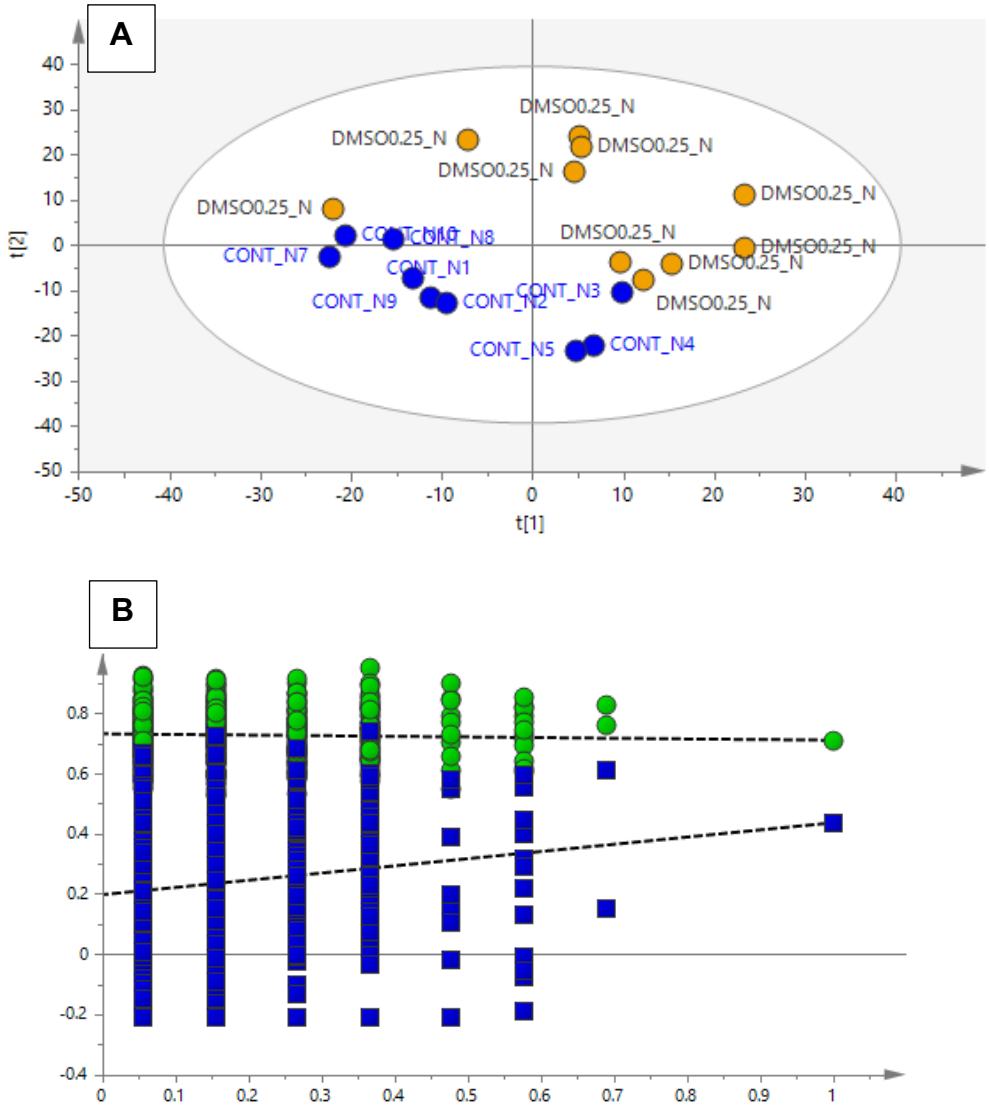


Figure 24. (A) PLS-DA score scatter plots of the differentiated control cells (n=9; blue circle), against the differentiated cells incubated with DMSO 0.25 % (n=10; orange circle), after GC-MS analysis of VCCs; **(B)** PLS-DA models statistical validation by 500 permutations of the PLS-DA model of the differentiated AC16 cells incubated with DMSO 0.25 %.

Table 22. Parameters of cross-validation obtained for the PLS-DA models regarding the VCC content, by comparison of control differentiated AC16 cells and the respective cells incubated with DMSO 0.25%.

PLS-DA Model	Component	R^2X	R^2Y	Q^2	Permutation tests		*p* [CV-ANOVA]
					R^2	Q^2	
DMSO 0.25% vs Control	2	0.588	0.711	0.437	0.732	0.198	0.144495

Foot note: R^2X variance explained by the X matrix. i.e., GC–MS data; R^2Y variance explained by the Y matrix. i.e., sample class; Q^2 predictive power; R^2 and Q^2 (permutation tests) goodness of fit of the permuted model; p [CV-ANOVA]—*p* value to estimate the significance of PLS-DA models.

4. Discussion

This dissertation aimed to disclosure the toxicity mechanisms of new targeted drugs in an *in vitro* heart model, AC16 cells. The new targeted drugs underlying cardiotoxic mechanisms were still barely studied. The dissertation was divided in classic cytotoxicity assays of cell culture paradigms and metabolomic sections. The discussion will follow the same paradigm for clarity purposes.

4.1. Cytotoxicity assays

All drugs were tested in differentiated human AC16 cells at concentrations lower than 100μM, which was in accordance to the range of plasma concentrations previously reported on patients, for the 3 targeted drugs, IMA, PAZ and SOR (74-76). Regarding the evaluation of IMA-induced cardiotoxicity by the MTT reduction assay, no significant cytotoxicity was detected up to 100μM after 24h. On the other hand, a time dependent cytotoxicity was observed at 48h. In the NR uptake assay, the cells exhibited a similar cytotoxic profile with a clear time-dependent cytotoxicity caused by IMA. However, unlike what was observed in the MTT assay, no dose-dependent toxicity was found. Surprisingly, according to the NR assay, the incorporation of NR in IMA 30μM was higher than those observed in IMA 20μM, which can be an adaptive response that needs disclosure. The time-dependent toxicity was confirmed with the results observed at 48h since cytotoxicity was increased for the double from IMA 30μM, reaching only 5% at the concentration of IMA 100μM. In a study featuring cardiac stem/progenitor cells, the cytotoxicity was assessed using a fluorescein diacetate assay, after a 24-h exposure to IMA (1-100μM) (98). In that study, cell viability, at levels equivalent to 'peak' (after 24h) plasma concentrations of treated patients, which was 10μM, was 91.5 ± 0.9%. In higher concentrations, the viability decreased in a dose-dependent manner, with 100μM being the most toxic (98). Comparing these results to the ones observed in this dissertation, in differentiated AC16 cells exposed to IMA for 24h, the toxicity of the compound was non-existent in the MTT assay, although at 10, 20 and 50μM, significantly cytotoxicity was observed, which could comprise an increase in mitochondrial activity after insult. However, at the same time point, in the NR assay, a significant cytotoxicity increased from IMA 20μM onwards was observed, which meets the results obtained by Smith and colleagues. On the study performed by Will and colleagues, the H9c2 cell line was grown in either high-glucose or galactose-containing medium and incubated for 24h with IMA up to 100μM. The test used to assess cytotoxicity was the CellTiter-Glo Luminescent cell viability assay that measures cellular ATP content. IMA was equally cytotoxic to both glucose and galactose-grown cells with an IC50 of 30.53

± 1.46μM and 29.17 ± 1.77μM, respectively (65). In comparison, that cell line and cytotoxicity assay was more sensitive towards IMA-cytotoxicity than MTT reduction assay and AC16 cells used in this dissertation. Moreover, in another study, neonatal rat ventricular myocytes were treated with doxorubicin 1mg/ml or IMA (2, 5 or 10μM) for 24h. The measurement of cell toxicity was done by quantifying the release of adenylate kinase (AK), a cytosolic protein that was released when membrane integrity was compromised. The data revealed that cell death was induced in a dose-dependent manner (43). Once again, these data showed that the cytotoxicity of IMA were not the same depending on the cells line that were used for the studies, but the concentrations being studied were similar between studies.

Similarly, in the case of PAZ, the drug led to a time-dependent toxicity, with no clear dose dependence, according to the MTT reduction assay. Indeed, at 24h, when compared with the control cells, a significantly impaired MTT reduction was found for 5, 10, 30 and 50μM, being that impairment significantly higher in the highest concentration tested. In this case, although there seems to be a dose dependence on the MTT results after 24h, when observing the 48h results, PAZ showed a significant impact on the ability to reduce MTT at concentrations of 1μM and above, but these, are relatively identical from PAZ 5μM to PAZ 100μM. These results confirmed the above described statement of a time and not dose dependent toxicity. Once again, the NR uptake was less sensitive to detect cytotoxicity, but the lysosomal damage induced by PAZ also presented a time-dependent profile. Another study was done in cultured neonatal rat cardiomyocytes with PAZ, using concentrations of 1 and 4mM for 48h. In that study PAZ, did not cause significant cytotoxicity, when assessed by the nuclear dye Hoechst 33342 (36), even with such high concentrations. Those differences can be due to the model, but most probably due to the test performed.

In contrast to the other drugs, the cytotoxic profile of SOR in differentiated cells was characterized by a concentration and time-dependent cytotoxicity, both clearly prominent. At 24h, this drug only caused mitochondrial dysfunction at the concentration of SOR 20μM, while at 48h incubation, a significant cardiotoxic effect was observed in all concentrations with the exception of the SOR 1μM condition. The MTT reduction assay data clearly demonstrate a time-dependent cytotoxicity for SOR in AC16 cells at the 48h time-point. Further, by measuring lysosome function, when exposed to several concentrations of SOR for 24h, AC16 cells ability to uphold NR was diminished at concentrations higher than 5μM. After 48h, a cytotoxic effect was also observed with all concentrations above SOR 2μM and increasing as the concentrations raised. In the study by Will and colleagues with the H9c2 cell line, SOR was incubated for 24h up to 100μM in media containing either glucose (glycolytic conditions) or galactose (mitochondrial-dependent conditions) and ATP was

measured as described earlier. SOR was significantly more toxic to galactose-grown cells than glucose-grown cells, demonstrating a greater than fourfold shift in the IC50 (10.1μM vs. 44.7μM, respectively) (65), showing metabolic preference and possibly mitochondrial involvement. Another study in this case using proliferative AC16 cells, investigated the cytotoxicity caused by SOR (99). Cell viability was assessed using CCK-8 viability assay, that measures the number of live cells, and the concentration range of SOR was 0.1 - 100μM over a period of 72h. SOR presented an IC50 on AC16 cells at 12.66 (± 2.9) μM and a cell viability was reduced to 0% at the highest concentration of 100μM at 72h (99). Then, time-dependent cytotoxicity was investigated by exposing cells to SOR (13.9μM and 24μM) during a period of 0, 24, 48 and 72h, using the same cell viability test assay. At 24μM, the time-course of cellular response data showed cell viability decreased compared to the control profile suggesting apoptosis, autophagy and cell growth inhibition as three different processes that affect the cellular response (99). In another study, the authors tested cellular viability in human myocardial samples using a fluorescein diacetate assay and the incubations used SOR (1-100μM) for 24h (98). The authors found a dose-dependent decrease in viability, illustrated with a 75.0 ± 1.6% cell viability at 10μM. When comparing this data to the literature, PAZ and IMA presented time-dependent cytotoxicity, with no clear dose dependence in both assays used, while SOR, in turn, caused in general higher toxicity at lower concentrations with a dose and time-dependent toxicity. Comparing to other studies, they used different models, time-points or cytotoxicity evaluation parameters, but, with the various examples reported above, it was unanimous that SOR was the drug that causes more toxicity in lower concentrations regardless of the models and assays tested. In fact, IMA and PAZ had a less toxic profile since higher concentrations are necessary to cause some toxicity in the models used.

To assess the effect of 3-MA, an autophagy inhibitor which blocks autophagosome formation via the inhibition of type III phosphatidylinositol 3-kinases (PI-3K), on the cytotoxicity of the drugs under study, relevant concentrations of IMA, PAZ and SOR were chosen and the NR uptake assay was used after a 24-h incubation. In relation to IMA, the autophagy inhibitor significantly increased its cytotoxicity at 30μM, when compared to IMA 30μM alone; however, 3-MA did not cause significant change when associated with IMA 50μM, when compared to IMA 50μM alone. On the other hand, 3-MA increased cytotoxicity in both PAZ concentrations tested, i.e., PAZ 30μM and PAZ 50μM. Finally, the results of SOR, presented concentration-dependent response since, 3-MA increased the cytotoxicity of SOR 10μM when compared to SOR 10μM isolated. Regarding to 3-MA partially prevented the cytotoxicity of SOR 20μM when compared to SOR 20μM alone. In conclusion, 3-MA gave no protection towards the majority of tested conditions, but it provided a small but meaningful protection towards SOR (at 20μM) in the NR uptake assay at 24h. Once

again, based in the NR uptake assay at 24h, the effect of chloroquine was tested. Chloroquine was another inhibitor of autophagy that blocks the binding of autophagosomes to lysosomes by altering the acidic environment of lysosomes, resulting in the accumulation of a large number of degraded proteins in cells (100). According to the results, chloroquine did not affect the cytotoxicity of IMA or PAZ at both concentrations of 30 and 50μM. On the other hand, chloroquine increased the cytotoxicity of SOR 10μM. These results suggested that, besides these inhibitors did not act in the same phases of autophagy, they had very different effects on drugs. The only similarity between them was relative to SOR 10μM, where both in the presence of 3-MA and chloroquine, the cells had a significant increase in toxicity, suggesting that autophagy could be protective in this condition. Previous data clearly demonstrated that autophagy was activated in human endogenous cardiac progenitor cells exposed to IMA (101). In this study, the cells were exposed to IMA 10μM and incubated for three time points (24, 48 and 72h). After a quantification of acridine-orange-positive cells, the authors observed a significant increase in the number of acidic organelles with a percentage of positive cells of 55.5%, 60% and 73.2% at the time points above indicated, respectively, when compared to control cells (that had only 9%). In addition, in the same conditions of IMA at 24h, the authors analyzed the expression of lysosomal Associated Membrane Protein 2 (LAMP2, a specific lysosomal protein marker) using the western blotting. An increase of 2.4-fold was seen in LAMP2 protein expression after IMA. Finally, using the marker of autophagosome LC3I to LC3II and the removal of the p62 protein, the authors measured autophagic flux with the same methods and exposure parameters as for the LAMP2. At 24h, an increase of 2.7 and 1.9-fold in LC3II and P62, respectively, was seen after IMA. Finally, a lysosomal inhibitor, bafilomycin A1, was used to prevent protein degradation and IMA further increased LC3II and P62 with bafilomycin A1 to 3.5 and 3.9-fold. However, after 48h, the results were 2.6 and 2.8-fold to LC3II and P62, respectively, with no significant increase after bafilomycin A1 co-treatment. The authors concluded that IMA induced accumulation of acidic vesicle organelles, indicative of autophagy and LAMP2 expression, while impaired the autophagic flux in human endogenous cardiac progenitor cells (101).

MMP was important for maintaining the physiological function of the respiratory chain to generate ATP, so a significant loss of ΔΨm caused cells to deplete energy with subsequent cell death, coinciding with the opening of the transition pores of mitochondrial permeability (102). In this dissertation, several concentrations of the drugs were tested in the measurement of MMP and there were chosen based on the clinical plasma levels and MTT and NR results, where the drugs did not present a very high cytotoxicity. Regarding the results of this dissertation, IMA only caused changes in MMP in the highest concentration tested, IMA 50μM, while all other conditions (PAZ, 10μM, 30μM or 50μM and

SOR 5, 10 or 20μM) caused a significantly mitochondrial depolarization compared to the values observed in control and healthy cells. Herein, SOR caused an impressive MMP depolarization being, once again, the most toxic drug used in this dissertation. The collapse of ΔΨm, observed in all drugs at both concentrations except for IMA 10 and 30μM, suggests that several mechanisms may be elicited thereafter. Thus, changes in mitochondrial permeability may be important for the generation of ROS, release of cytochrome c in the cytosol, which in turn triggers other events such as apoptotic cascade and nuclear DNA fragmentation (102). In this sense, according to the results obtained in the study by Will *et al*., described above, testing the effect of IMA (250nmol/mg mitochondrial protein) and SOR (100nmol/mg mitochondrial protein) on respiration was considered critical. That was measured in isolated rat heart mitochondria, but none of the two drugs caused had a statistically significant effect on basal respiration. In contrast, although IMA had no effect on respiration stimulated by ADP, it was inhibited more than 80% by SOR (65). Furthermore, IMA and SOR depleted ATP, both in glucose and galactose-grown cells but only SOR rendered the galactose-grown cells to be more sensitive to ATP depletion than glucose-grown cells, suggesting that SOR impaired mitochondrial function in H9c2 cells metabolism (103). Additionally, in neonatal rat ventricular myocytes (NRVMs), IMA at concentration of 2, 5 and 10μM produced dose-dependent collapse of the MMP determined by JC-1, followed by pronounced release of cytochrome *c* into the cytosol and a marked decline in cellular ATP content and in the ratio of ATP to ADP (43). On the other hand, no significant effect was detected on MMP of primary cultured neonatal (day 1) rat cardiomyocytes after a 48-h of exposure to PAZ and SOR (1 and 4mM) using tetramethylrhodamine methyl ester (TMRM) as the probe (36).

4.2. Metabolomic profiling

Drug-induced cardiovascular diseases in oncologic treatments have been widely studied since the early beginning of chemotherapy. Nevertheless, the data on new targeted drugs induced cardiotoxicity is scarce, but a prominent issue at present. Since the appearance of high throughput methods, like metabolomic, the use of this new tool can bring important and innovative information. Thus, the field of cardiovascular metabolomic aims to find what metabolic changes occur in cardiovascular diseases, identifying signaling pathways implicated in the elicited cardiotoxicity. In fact, metabolomic is defined as the systematic study of all metabolites (the metabolome) within a biological system (104). This '-omic' science involves the qualitative and quantitative analysis of a vast diversity of low molecular weight metabolites present in various biological matrices, such as cells, that would be the equivalent of exometabolome, tissues or biofluids. Metabolites are the end products of biochemical pathways and the change of their normal levels can affect the normal functioning of living entities (104). To unravel the adverse outcome pathways related to cardiotoxicity, it is critical to investigate the intrametabolome and relate it to changed pathways. Therefore, to evaluate possible metabolic disorders, as well as to have an overview of the cardiotoxic mechanisms of some TKIs, the metabolome of differentiated human cardiac cells AC16 was analyzed after incubation with IMA, PAZ and SOR, using an early time-point (24h) and clinically relevant concentrations. In fact, for an effective and viable evaluation, it was essential to determine low toxic concentrations of both compounds, so that it was possible to investigate early metabolic disorders or alterations before observing clear cytotoxic damage, where irreversible damage occurs. Thus, in this study, the cells were incubated for 24h with IMA 50μM, PAZ 10μM, SOR 10μM, and also with vehicle DMSO 0.25%, DMSO 0.05%. The gathered data were compared to control (PBS incubated) cells. Simultaneously, both the intracellular and extracellular metabolome was evaluated.

The analysis of the intracellular content revealed that IMA, PAZ and SOR induced a significant impact on the metabolome of differentiated AC16 cells, as seen in **figure 25**. Although the content of amino acids (AA) was altered when compared to controls, when comparing the three drugs they do not share any AA. Moreover SOR is the drug that had a higher number of AA altered. Moreover, while IMA decreased all the discriminant AA regarding control, as did PAZ **(Figure 24A and B)**, SOR increased all AA except one, the glutamic acid, having a higher influence on the pathway involving this AA. Also, regarding the levels of carbohydrates, comparing to the control, in IMA and PAZ there was a significant decrease in the levels of all discriminating carbohydrates, except for glucose,

whose levels were increased. The carbohydrate metabolites did not change after exposure of cells to SOR **(Figure 24C)**. Regarding carboxylic acids, all drugs had alterations in some metabolites with significant differences. In the case of IMA, it was possible to observe that the two acids showed significant decrease in their levels were aminomalonic and citric acid **(Figure 24A)**. In contrast, the exposure to both PAZ and SOR had dissimilar effects on the levels of carboxylic acids **(Figure 24B and C)**. In the case of PAZ exposure, malic acid had a significant increase while citric acid decreased **(Figure 24B).** The SOR condition impacted in the levels of four carboxylic acids, two revealed a significant increase (malic and succinic acid) in their levels compared to the control, while the other two (aminomalonic and citric acid) decreased **(Figure 24C)**. It was also possible to observe that in carboxylic acids, the IMA shares the same effect on aminomalonic acid with the SOR **(Figure 24A and C)**, while the SOR shares with the PAZ the malic acid **(Figure 24B and C)** and finally the citric acid was altered in both the IMA and PAZ, as discriminative metabolites **(Figure 24A and B)**. Levels of discriminant glycerolipids increased in IMA, but not in a meaningful way whereas SOR caused a significant decline in this group. PAZ did not alter any metabolite in this group. Although in all drugs, the levels of glycerophospholipid were altered, IMA and PAZ share the same glycerophospholipid. A significant decrease of the levels of glycerol-3-phosphate was found in PAZ condition **(Figure 24B)** despite this metabolite being also altered in IMA. In contrast, the glycerophospholipid present in the SOR increased significantly. It seems that this pathway was the most similar among groups. The inorganic compounds were present as discriminative in the medium of the three drugs, and the levels of the compounds always decreased in a significantly way, being phosphoric acid present in both SOR and PAZ and pyrophosphate also present as a discriminative metabolite in IMA and PAZ. Likewise, organic compounds were also discriminative in IMA, PAZ and SOR. Taurine levels decreased in IMA **(Figure 24A)**, whereas lactic acid levels decreased in PAZ and SOR **(Figure 24B and C)**. Finally, steroid (cholesterol) was discriminative in PAZ and SOR but not in IMA and its levels decreased in both drugs.

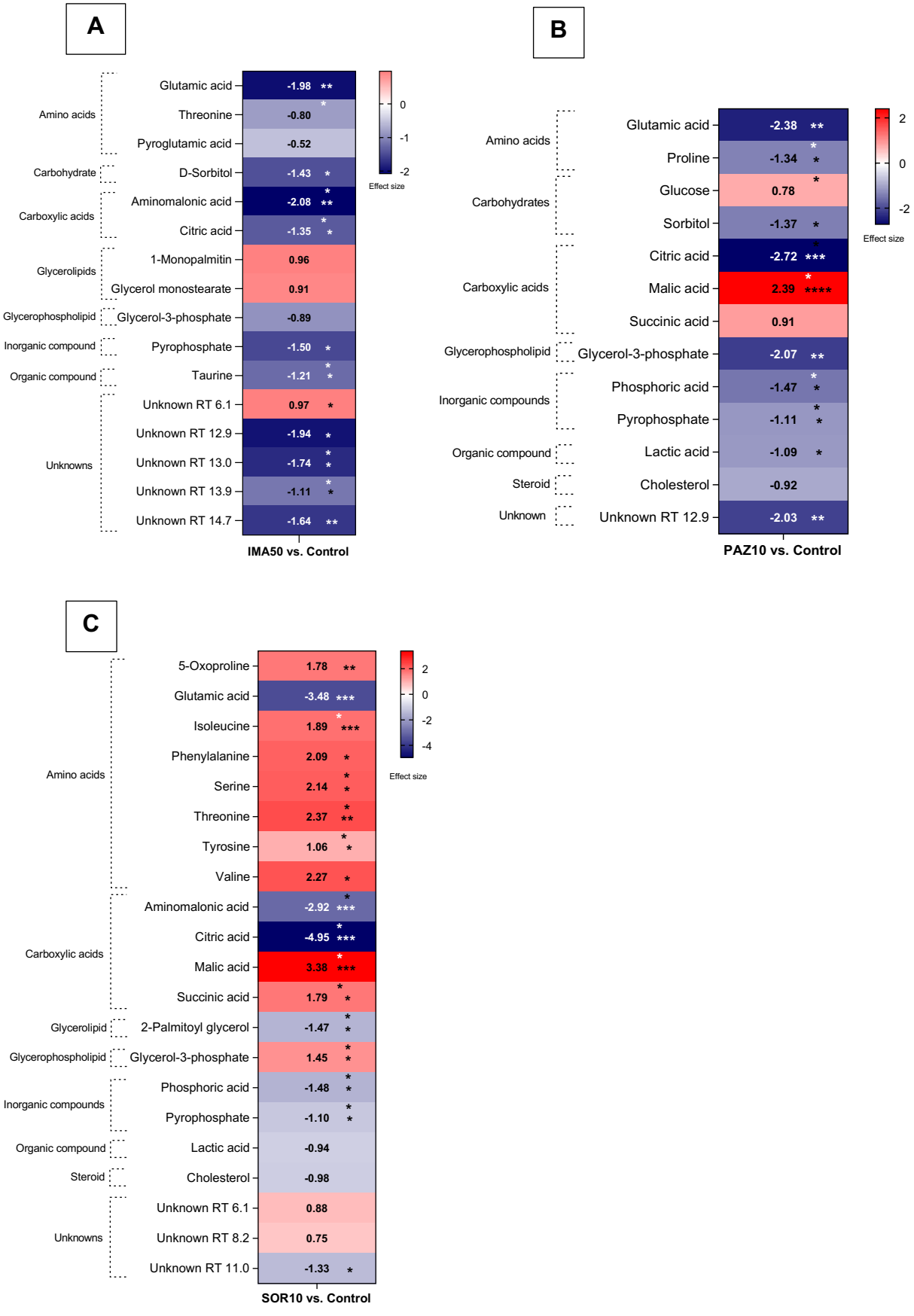
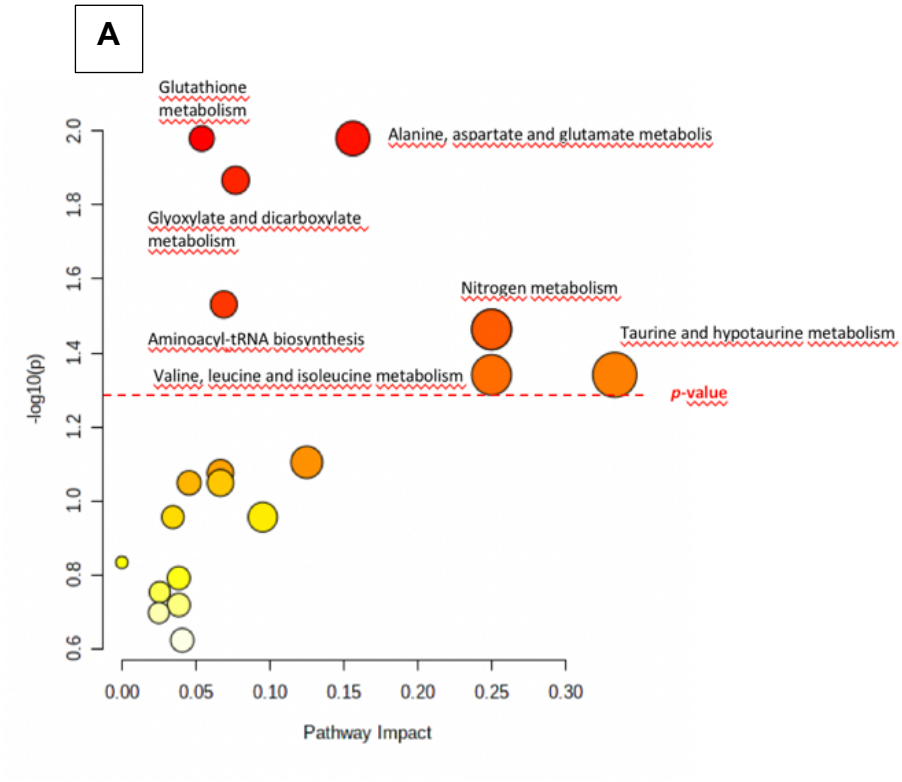
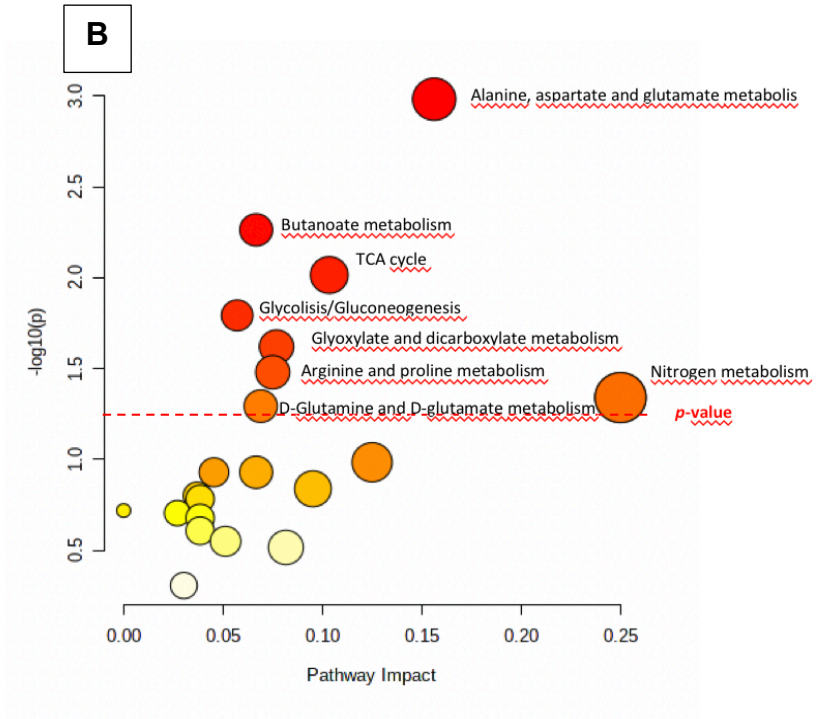

A
Amino acids
Carbohydrate
Carboxylic acids
Glycerolipids
Glycerophospholipid
Inorganic compound
Organic compound
Unknowns
Glutamic acid
Threonine
Pyroglutamic acid
D-Sorbitol
Aminomalonic acid
Citric acid
1-Monopalmitin
Glycerol monostearate
Glycerol-3-phosphate
Pyrophosphate
Taurine
Unknown RT 6.1
Unknown RT 12.9
Unknown RT 13.0
Unknown RT 13.9
Unknown RT 14.7
-1.98 **
-0.80 *
-0.52
-1.43 *
-2.08 * **
-1.35 * *
0.96
0.91
-0.89
-1.50 *
-1.21 * *
0.97 *
-1.94 *
-1.74 * *
-1.11 * *
-1.64 **
0
-1
-2
Effect size
IMA50 vs. Control
B
Amino acids
Carbohydrates
Carboxylic acids
Glycerophospholipid
Inorganic compounds
Organic compound
Steroid
Unknown
Glutamic acid
Proline
Glucose
Sorbitol
Citric acid
Malic acid
Succinic acid
Glycerol-3-phosphate
Phosphoric acid
Pyrophosphate
Lactic acid
Cholesterol
Unknown RT 12.9
-2.38 **
-1.34 * *
0.78 *
-1.37 *
-2.72 * ***
2.39 * ****
0.91
-2.07 **
-1.47 * *
-1.11 * *
-1.09 *
-0.92
-2.03 **
2
0
-2
Effect size
PAZ10 vs. Control
C
Amino acids
Carboxylic acids
Glycerolipid
Glycerophospholipid
Inorganic compounds
Organic compound
Steroid
Unknowns
5-Oxoproline
Glutamic acid
Isoleucine
Phenylalanine
Serine
Threonine
Tyrosine
Valine
Aminomalonic acid
Citric acid
Malic acid
Succinic acid
2-Palmitoyl glycerol
Glycerol-3-phosphate
Phosphoric acid
Pyrophosphate
Lactic acid
Cholesterol
Unknown RT 6.1
Unknown RT 8.2
Unknown RT 11.0
1.78 **
-3.48 ***
1.89 * ***
2.09 *
2.14 * *
2.37 * **
1.06 * *
2.27 *
-2.92 * ***
-4.95 * ***
3.38 * ***
1.79 * *
-1.47 * *
1.45 * *
-1.48 * *
-1.10 * *
-0.94
-0.98
0.88
0.75
-1.33 *
2
0
-2
-4
Effect size
SOR10 vs. Control

Figure 25. Heatmaps showing the metabolic alterations occurred on the endometabolome of AC16 differentiated cells after exposure to **A)** imatinib 50 μM; **B)** pazopanib 10 μM, **C)** sorafenib 10 μM, both compared to control cells. The scale is color-coded as a function of the ES, from maximum decrease (dark blue) to maximum increase (red). Statistically significant differences are indicated (*$p < 0.05$, **$p < 0.01$, ***$p < 0.001$, ****$p < 0.0001$).

The biological relevance of significantly altered metabolites was evaluated through the metabolic pathway analysis (MetaboAnalyst 5.0), in order to understand which metabolic pathways may be altered after exposure to IMA, PAZ and SOR. The results obtained after exposure to the individual compounds are represented in **Figure 26**. This graphic representation showed all matched pathways according to the *p* values from the pathway enrichment analysis and pathway impact values from the pathway topology analysis. For IMA 50μM exposure **(Figure 26A)**, the potentially altered metabolic pathways were the ones related to the glutathione metabolism (glutamic acid and 5-oxoproline), alanine, aspartate and glutamate metabolism (glutamic acid and citric acid), glyoxylate and dicarboxylate metabolism (glutamic acid and citric acid), aminoacyl-tRNA biosynthesis (threonine and glutamic acid), D-glutamine and D-glutamate metabolism (glutamic acid), nitrogen metabolism (glutamic acid), valine, leucine and isoleucine biosynthesis (threonine) and taurine and hypotaurine metabolism (taurine), where, potentially significantly altered pathways are in descending order of probability of being altered. In addition, the PAZ 10μM exposure **(Figure 26B)** may also induced alterations in alanine, aspartate and glutamate metabolism (glutamic acid, succinic acid, citric acid), butanoate metabolism (glutamic acid, succinic acid), citrate cycle (TCA cycle) (succinic acid, citric acid, malic acid), glycolysis / gluconeogenesis (lactic acid, glucose), glyoxylate and dicarboxylate metabolism (glutamic acid and citric acid), arginine and proline metabolism (glutamic acid and proline) and D-glutamine and D-glutamate metabolism (glutamic acid), according to the pathway enrichment analysis. Regarding the exposure to SOR 10μM, the most probable dysregulated metabolic pathways **(Figure 26C)** were the aminoacyl-tRNA biosynthesis (phenylalanine, serine, valine, isoleucine, threonine, tyrosine, glutamic acis), valine, leucine and isoleucine biosynthesis (threonine, isoleucine, valine), phenylalanine, tyrosine and tryptophan biosynthesis (phenylalanine, tyrosine), alanine, aspartate and glutamate metabolism (glutamic acid, citric acid, succinic acid), glyoxylate and dicarboxylate metabolism (serine, citric acid, glutamic acid), phenylalanine metabolism (phenylalanine and tyrosine), butanoate metabolism (glutamic acid and succinic acid), citrate cycle (TCA cycle) (succinic acid, citric acid, malic acid), glutathione metabolism (glutamic acid and 5-oxoproline) and glycine, serine and threonine metabolism (threonine and serine).


A
Glutathione metabolism
Alanine, aspartate and glutamate metabolis
Glyoxylate and dicarboxylate metabolism
Nitrogen metabolism
Aminoacyl-tRNA biosynthesis
Taurine and hypotaurine metabolism
Valine, leucine and isoleucine metabolism
p-value
-log10(p)
Pathway Impact


B
Alanine, aspartate and glutamate metabolis
Butanoate metabolism
TCA cycle
Glycolisis/Gluconeogenesis
Glyoxylate and dicarboxylate metabolism
Arginine and proline metabolism
Nitrogen metabolism
D-Glutamine and D-glutamate metabolism
p-value
-log10(p)
Pathway Impact

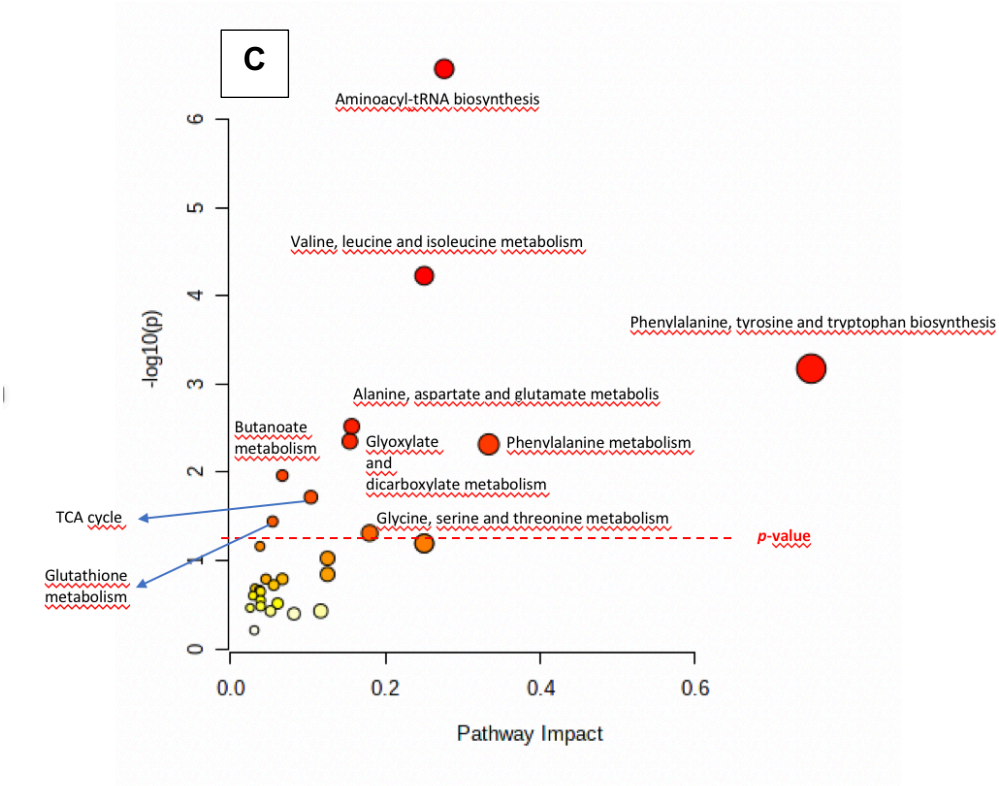


Figure 26. Overview of the dysregulated metabolic pathways of the intracellular metabolites alterations in differentiated AC16 cells after exposure to **A)** imatinib 50 μM; **B)** pazopanib 10 μM, **C)** sorafenib 10 μM, both compared to control cells. The node color is based on the *p* value, where a dark circle color indicates a more significant change of the pathway. The node radius corresponds to the pathway impact value. Pathways were annotated when $p < 0.05$ and pathway impact > 0.05.

In addition to intracellular analysis, extracellular medium analysis is also a powerful tool in the detection of metabolic disorders (105). Whereas, in the case of IMA, after multivariate analysis a meaningful difference was found, that was not enough to discover any discriminant metabolite in the univariate analysis. That has been described before and relates to the group differences when set together. Independent variables or abundances of metabolites could complement each other in the prediction of the dependent variable, meaning that, although there was a clear separation between classes when using all metabolites together, when performing univariate t tests for metabolites separately, no significant difference may be found between the metabolites. Thus, it was clear that the information depended on both variables, i.e., metabolite abundances themselves were not information rolling parameters, but complementary information in abundances of different metabolites (105). Although the IMA did not reveal significant metabolic differences, the PAZ and SOR groups had significant changes in the exometabolome evaluation. Regarding

the boxplots of the exometabolome evaluation, metabolite alterations were considered statistically significant when *p*-values < 0.05 (95% confidence). For PAZ 10µM *versus* controls (PBS) **(Figure 27A),** the drug induced a significant increase in acetaldehyde and benzaldehyde, while in the methylglyoxal statistically significance was not observed. The results obtained for SOR 10µM exposure were shown in **Figure 27B**. Regarding the boxplots, levels of benzaldehyde revealed significantly increase after SOR exposure comparing with the controls PBS. Finally, a significant increase was also observed in the levels of propanal, hexanal, heptanal and unknown_alkanal RT 28.2 at this concentration.

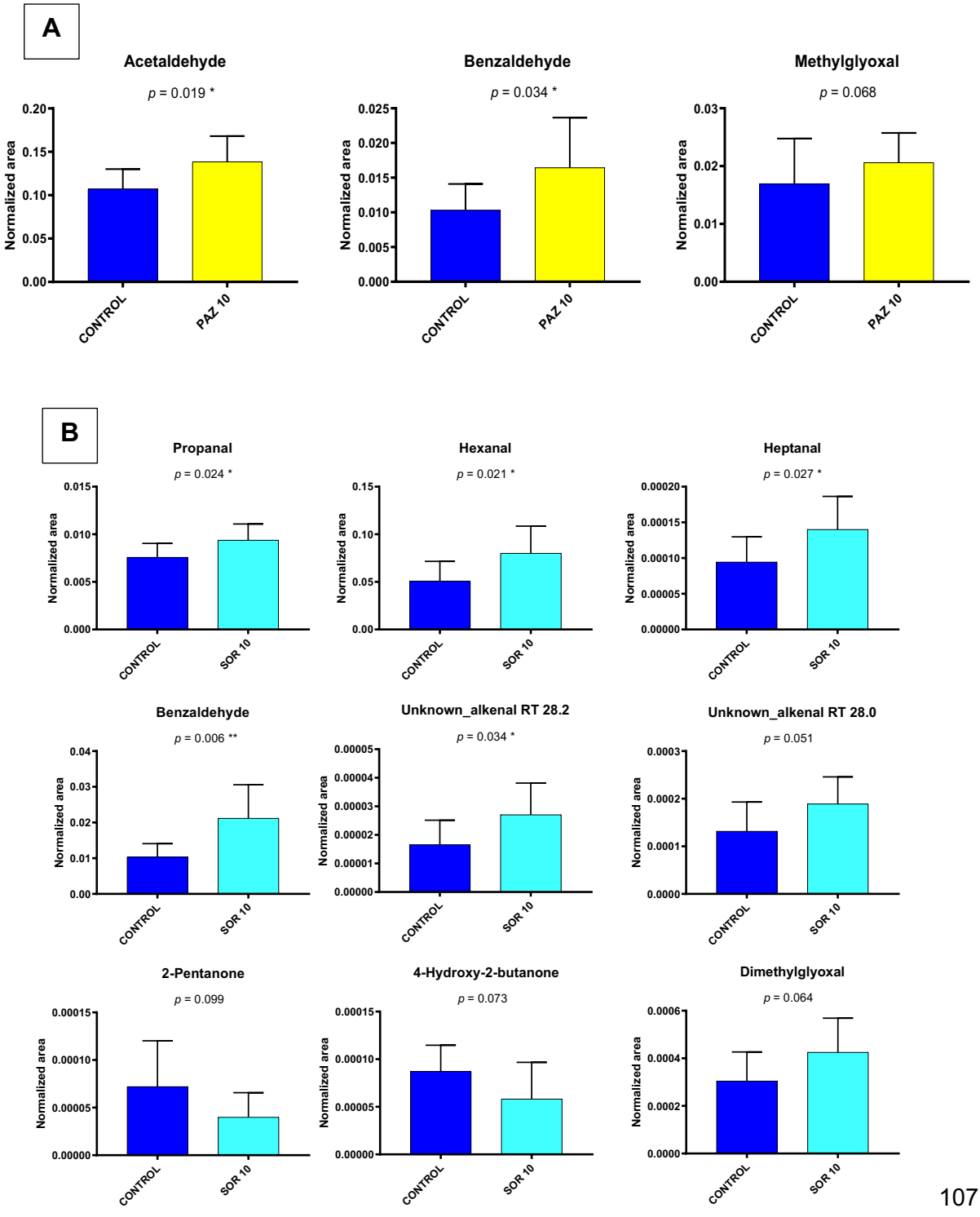


Figure 27 - Boxplots illustrating the metabolites changing in differentiated AC16 cells after exposure to **A)** pazopanib (PAZ) 10μM or **B)** sorafenib (SOR) 10μM both compared to control cells (*$p < 0.05$; **$p < 0.01$).

When addressing data present in the revised literature, no metabolomic data exists on IMA and heart models. Still, a study on patients was done to relate CVD after treatment with TKIs (106). In this study, Caocci and colleagues investigated the metabolic fingerprint of CML patients treated with TKIs who subsequently developed CVD. They divided 39 adult CML patients into two groups (with and without CVD) treated with IMA (n=16) and others TKIs. After that, all plasma samples from all patients were performed through GC-MS based metabolomic analysis. The parameters of the model were $R^2Y = 0.76$ and $Q^2 = 0.44$ and the main increased discriminant metabolites shown in plasma patients with CVD were: tyrosine, lysine, ornithine, glutamic acid, proline, citric acid, phenylalanine, mannitol, threonine, leucine, creatine, serine, 4-hydroxyproline, and alanine, while that the myristic acid, arabitol, oxalic acid, and 4-deoxyrithronic acid were decreased. In addition, after pathway analysis, several metabolic pathways were identified in both groups, such as: (a) transfer of acetyl groups to mitochondria, (b) amino sugar metabolism, (c) glycerolipid metabolism and (d) glycine and serine metabolism. However, in patients with CVD pathways like: (a) tyrosine and methionine metabolism, (b) sphingolipid metabolism, (c) tryptophan metabolism, (d) citric acid cycle, (e) beta-alanine metabolism and (f) glutathione metabolism were identified. These results showed that CML patients with CVD have a different metabolic profile when compared with patients with no history of CVD. The authors suggest probable mechanisms of endothelial damage facilitated by the increase of specific metabolites like tyrosine in those CVD patients (106). Comparing these results with the metabolomic study done in this dissertation, only two discriminant metabolites, citric acid and threonine, were in common with both studies. Additionally, only the glutathione metabolism pathway was potentially altered when compared to the IMA 50μM results gathered in AC16 cells herein.

Regarding PAZ, this was the first metabolomic study on cardiotoxicity or cardiotoxicity related that was done so far. However, in cancer cells like the human metastatic ccRCC cell line (Caki-1) and the non-malignant renal epithelial cell line (HK-2), PAZ 50μM disrupted several routes (107). In fact, compared with the control cells there were several metabolites significantly altered in the endometabolome of Caki-1 and HK-2: a) alanine, b) lactate, c) glutamate, d) isoleucine, e) ethanolamine and f) *myo*-inositol. Consequently, the altered metabolomic pathways were a) aminoacyl-tRNA biosynthesis, b) glutathione metabolism, c) glycerophospholipid metabolism, d) energy metabolism and e)

galactose metabolism, inositol phosphate metabolism, phosphatidylinositol signaling system. According to the heatmaps of the endometabolome of Caki-1 cells exposed to PAZ, significant alterations were seen with a decrease in myo-inositol and glutamate levels. In contrast, the endometabolome of HK-2 cells exposed to PAZ resulted in a significant decrease in alanine levels and a significant increase in ethanolamine and lactate levels (107). According to the results of our study, no metabolite or altered pathway corresponds or was similar to the results of the study described above. Although, the concentrations used with PAZ were different, and the study of Amaro and colleagues relates to cancer cells/renal cells and not cardiac cells. Therefore, these results were not surprising and in fact, it showed that toximetabolomic fingerprint is organ or tissue specific, which can be an interesting factor to be researched in the future as possible cardiac marker of toxicity.

Regarding SOR, there were some metabolomic data that tries to get a glimpse towards cardiotoxicity. On the study by Jensen and colleagues, they administrate by gavage SOR 30 mg/kg daily for two weeks to FVB/N mice. In that report, an undirected metabolomic analysis was performed through GC/MS using the heart as sample. In addition, plasma and skeletal muscle (quadriceps femoris) were analyzed in parallel since the objective would be to compare the changes between myocardial and striated muscle metabolism and if any of these observed changes could be monitored by any biomarker in plasma (108). The authors showed in the heart a total of 10 different significant metabolites and only glutamine was increased compared to vehicle-treated control hearts. The others 9 metabolites were significantly decreased. Pathway analysis of these 10 metabolites indicated that 3 were involved in taurine and hypotaurine metabolism including taurine, hypotaurine, and L-cysteine. In turn, 5 metabolites were significantly decreased in the skeletal muscle of SOR-treated animals. In the metabolic pathways there were 2 significantly affected: a) taurine and hypotaurine metabolism and b) cysteine and methionine metabolism. Finally, compared to vehicle controls, only 4 metabolites were significantly decreased in the plasma of SOR treated animals. They identified 2 affected metabolic pathways, such as, citrate (TCA) cycle and glyoxylate and dicarboxylate metabolism (108). Comparing these results with the study undertaken herein with SOR 10μM, in the case of the SOR treated heart, none shared common metabolites. This may be due to the fact that although different models were undertaken the toxicity of the drug may not manifest in the same way in both cases. In skeletal muscle levels of aminomalonic acid were decreased as it was herein in AC16 cells, whereas malic acid was increased in AC16 cells and decreased in the skeletal muscle. Finally, regarding the exposure to SOR and the dysregulated metabolic pathways, citrate cycle (TCA cycle) and glyoxylate and dicarboxylate metabolism were affected in both AC16 cells and skeletal muscle, however the metabolites involved in these changes were not the same.

Regarding another example of metabolomic applied to cardiotoxicity of SOR, Abdelgalil and colleagues, used healthy male Wistar rats weighting 250-350g. In these study, 3 groups with 6 rats each were used: a) group I received only water to serve as a control; b) group II was administered an oral single dose of SOR (20mg/kg) and c) group III, was administered oral single doses of SOR and losartan (20mg/kg and 10mg/kg; respectively) and the duration of the treatment was 4 weeks. The treatment with SOR induced cardiac toxicity whereas losartan seemed to revert the effect of SOR on the heart. In addition, the blood was collected at zero time and at the end of the treatment. GC-MS was used for the analysis of plasma (109). A total of 15 metabolites were identified and quantified in rat plasma, however, treatment with SOR alone significantly increased glycine and lactic acid metabolites levels. Moreover, co-administration of losartan with SOR restored these changes and resulted in a decrease of glycine, urea, *cis*-vaccenic acid, oleic acid, undecanoic acid and stearic acid. These findings indicated that losartan further reduced the levels of amino acids and fatty acids and had the potential to exert a protective effect against SOR-induced cardiotoxicity (109). Comparing these results with data gathered in this thesis, both studies had significant differences in lactic acid levels. However, while in the study by Abdelgalil and colleagues, lactic acid levels increased significantly, lactic acid decreased in the AC16 cells exposed to SOR. These significant differences can be due to different concentrations used with SOR but most likely because different models were being compared.

5. Conclusions

To conclude, the anticancer targeted drugs are cytotoxic at relevant clinical concentrations, according to the data gathered and the literature revised in this dissertation. The cardiotoxic profile of the tested drugs was different, being SOR the most cardiotoxic. Autophagy and mitochondria dysfunction are possibly involved in the cytotoxic effects, according to the preliminary data gathered so far. New data is urgent on the off-target toxicity of these new drugs, since they can bring serious consequences to the treated patients. Because of the enormous importance of cardiac metabolic flexibility, the determination of cardiac metabolome is crucial to determine the adverse pathway outcome as early as possible, because HF that can be elicited by these and other anticancer drugs is still with no pharmacological or non-pharmacological treatment. The metabolome was significantly changed in all drugs tested, with more affected pathways also in SOR revealing a cardiotoxic potential that only now the clinical studies are unveiling.

6. References

1. Organization WH. Who methods and data sources for country-level causes of death 2000-2019 2020, December [Available from: https://cdn.who.int/media/docs/default-source/gho-documents/global-health-estimates/ghe2019_cod_methods.pdf?sfvrsn=37bcfacc_5. [accessed on 25/09/2022]
2. Martel S, Maurer C, Lambertini M, Ponde N, De Azambuja E. Breast cancer treatment-induced cardiotoxicity. Expert Opin Drug Saf. 2017;16(9):1021-38.
3. Timmis A, Vardas P, Townsend N, Torbica A, Katus H, De Smedt D, et al. European Society of Cardiology: cardiovascular disease statistics 2021. Eur Heart J. 2022;43(8):716-99.
4. Ferlay J, Colombet M, Soerjomataram I, Parkin DM, Piñeros M, Znaor A, et al. Cancer statistics for the year 2020: An overview. Int J Cancer. 2021.
5. Siegel RL, Miller KD, Fuchs HE, Jemal A. Cancer statistics, 2022. CA Cancer J Clin. 2022;72(1):7-33.
6. Hong RA, Iimura T, Sumida KN, Eager RM. Cardio-oncology/onco-cardiology. Clin Cardiol. 2010;33(12):733-7.
7. Li T, Kang G, Wang T, Huang H. Tumor angiogenesis and anti-angiogenic gene therapy for cancer. Oncol Lett. 2018;16(1):687-702.
8. Paul MK, Mukhopadhyay AK. Tyrosine kinase - Role and significance in Cancer. Int J Med Sci. 2004;1(2):101-15.
9. Kamphuis JAM, Linschoten M, Cramer MJ, Gort EH, van Rhenen A, Asselbergs FW, et al. Cancer Therapy-Related Cardiac Dysfunction of Nonanthracycline Chemotherapeutics. JACC: CardioOncology. 2019;1(2):280-90.
10. Costa VM, Carvalho F, Duarte JA, Bastos Mde L, Remião F. The heart as a target for xenobiotic toxicity: the cardiac susceptibility to oxidative stress. Chem Res Toxicol. 2013;26(9):1285-311.
11. Totzeck M, Schuler M, Stuschke M, Heusch G, Rassaf T. Cardio-oncology - strategies for management of cancer-therapy related cardiovascular disease. Int J Cardiol. 2019;280:163-75.
12. Yu AF, Moskowitz CS, Chuy KL, Yang J, Dang CT, Liu JE, et al. Cardiotoxicity Surveillance and Risk of Heart Failure During HER2 Targeted Therapy. JACC CardioOncol. 2020;2(2):166-75.
13. Aleksey M. Chaulin OEA, Dmitry V. Duplyakov. Pathophysiological mechanisms of cardiotoxicity in chemotherapeutic agents. Russian Open Medical Journal. 2020, August 7;9(September 3).

14. Lenneman CG, Sawyer DB. Cardio-Oncology: An Update on Cardiotoxicity of Cancer-Related Treatment. Circ Res. 2016;118(6):1008-20.
15. Reis-Mendes AF, Sousa E, de Lourdes Bastos M, Costa VM. The Role of the Metabolism of Anticancer Drugs in Their Induced-Cardiotoxicity. Curr Drug Metab. 2015;17(1):75-90.
16. Institute NC. Targeted therapy to treat cancer 2022, May 31 [Available from: https://www.cancer.gov/about-cancer/treatment/types/targeted-therapies. [accessed on 02/09/2022]
17. Sculier JP, Berghmans T, Meert AP. Advances in target therapy in lung cancer. Eur Respir Rev. 2015;24(135):23-9.
18. Han X, Zhou Y, Liu W. Precision cardio-oncology: understanding the cardiotoxicity of cancer therapy. NPJ Precis Oncol. 2017;1(1):31.
19. Albini A, Pennesi G, Donatelli F, Cammarota R, De Flora S, Noonan DM. Cardiotoxicity of anticancer drugs: the need for cardio-oncology and cardio-oncological prevention. J Natl Cancer Inst. 2010;102(1):14-25.
20. Mayer DK, Nasso SF, Earp JA. Defining cancer survivors, their needs, and perspectives on survivorship health care in the USA. Lancet Oncol. 2017;18(1):e11-e8.
21. Paraskevaidis I, Dimopoulos M-A, Kastritis E, Repasos E, Ntalianis A, Koutsoukis A. Cardio-oncology: A Focus on Cardiotoxicity. European Cardiology Review. 2018;13(1).
22. Ghosh AK, Walker JM. Cardio-oncology. Br J Hosp Med (Lond). 2017;78(1):C11-c3.
23. Markman TM, Markman M. Cardio-Oncology: mechanisms of cardiovascular toxicity. F1000Res. 2018;7:113.
24. Adão R, de Keulenaer G, Leite-Moreira A, Brás-Silva C. Cardiotoxicity associated with cancer therapy: pathophysiology and prevention strategies. Rev Port Cardiol. 2013;32(5):395-409.
25. Lyon AR, Dent S, Stanway S, Earl H, Brezden-Masley C, Cohen-Solal A, et al. Baseline cardiovascular risk assessment in cancer patients scheduled to receive cardiotoxic cancer therapies: a position statement and new risk assessment tools from the Cardio-Oncology Study Group of the Heart Failure Association of the European Society of Cardiology in collaboration with the International Cardio-Oncology Society. Eur J Heart Fail. 2020;22(11):1945-60.
26. Society AC. How chemotherapy drugs work 2019, November 22 [Available from: https://www.cancer.org/treatment/treatments-and-side-effects/treatment-types/chemotherapy/how-chemotherapy-drugs-work.html. [accessed on 17/10/2022]

27. Australia C. Targeted therapies [Available from: https://www.canceraustralia.gov.au/impacted-by-cancer/treatment/targeted-therapy. [accessed on 17/10/2022]
28. Slamon DJ, Leyland-Jones B, Shak S, Fuchs H, Paton V, Bajamonde A, et al. Use of chemotherapy plus a monoclonal antibody against HER2 for metastatic breast cancer that overexpresses HER2. N Engl J Med. 2001;344(11):783-92.
29. Herceptin. Herceptin targets her2+ cancer [Available from: https://www.herceptin.com/patient/about-herceptin.html. [accessed on 12/10/2022]
30. Yang Y, Bu P. Progress on the cardiotoxicity of sunitinib: Prognostic significance, mechanism and protective therapies. Chem Biol Interact. 2016;257:125-31.
31. Chu TF, Rupnick MA, Kerkela R, Dallabrida SM, Zurakowski D, Nguyen L, et al. Cardiotoxicity associated with tyrosine kinase inhibitor sunitinib. Lancet. 2007;370(9604):2011-9.
32. Rini BI, Escudier B, Tomczak P, Kaprin A, Szczylik C, Hutson TE, et al. Comparative effectiveness of axitinib versus sorafenib in advanced renal cell carcinoma (AXIS): a randomised phase 3 trial. Lancet. 2011;378(9807):1931-9.
33. Ribeiro AL, Marcolino MS, Bittencourt HN, Barbosa MM, Nunes Mdo C, Xavier VF, et al. An evaluation of the cardiotoxicity of imatinib mesylate. Leuk Res. 2008;32(12):1809-14.
34. LAINO C. Cardiotoxicity of Sunitinib Greater than Expected. oncology times. 2008, september 25;30(18):15-7.
35. Joensuu H. Cardiac toxicity of sunitinib. Lancet. 2007;370(9604):1978-80.
36. French KJ, Coatney RW, Renninger JP, Hu CX, Gales TL, Zhao S, et al. Differences in effects on myocardium and mitochondria by angiogenic inhibitors suggest separate mechanisms of cardiotoxicity. Toxicol Pathol. 2010;38(5):691-702.
37. Abdelgalil AA, Alkahtani HM, Al-Jenoobi FI. Sorafenib. Profiles Drug Subst Excip Relat Methodol. 2019;44:239-66.
38. Tang W, Chen Z, Zhang W, Cheng Y, Zhang B, Wu F, et al. The mechanisms of sorafenib resistance in hepatocellular carcinoma: theoretical basis and therapeutic aspects. Signal Transduct Target Ther. 2020;5(1):87.
39. Mamoshina P, Rodriguez B, Bueno-Orovio A. Toward a broader view of mechanisms of drug cardiotoxicity. Cell Rep Med. 2021;2(3):100216.
40. Curigliano G, Cardinale D, Dent S, Criscitiello C, Aseyev O, Lenihan D, et al. Cardiotoxicity of anticancer treatments: Epidemiology, detection, and management. CA Cancer J Clin. 2016;66(4):309-25.

41. Damrongwatanasuk R, Fradley MG. Cardiovascular Complications of Targeted Therapies for Chronic Myeloid Leukemia. Curr Treat Options Cardiovasc Med. 2017;19(4):24.
42. Wu Q, Bai B, Tian C, Li D, Yu H, Song B, et al. The Molecular Mechanisms of Cardiotoxicity Induced by HER2, VEGF, and Tyrosine Kinase Inhibitors: an Updated Review. Cardiovasc Drugs Ther. 2022;36(3):511-24.
43. Kerkelä R, Grazette L, Yacobi R, Iliescu C, Patten R, Beahm C, et al. Cardiotoxicity of the cancer therapeutic agent imatinib mesylate. Nat Med. 2006;12(8):908-16.
44. Distler JH, Distler O. Cardiotoxicity of imatinib mesylate: an extremely rare phenomenon or a major side effect? Ann Rheum Dis. 2007;66(6):836.
45. Moslehi JJ, Deininger M. Tyrosine Kinase Inhibitor-Associated Cardiovascular Toxicity in Chronic Myeloid Leukemia. J Clin Oncol. 2015;33(35):4210-8.
46. Cirmi S, El Abd A, Letinier L, Navarra M, Salvo F. Cardiovascular Toxicity of Tyrosine Kinase Inhibitors Used in Chronic Myeloid Leukemia: An Analysis of the FDA Adverse Event Reporting System Database (FAERS). Cancers (Basel). 2020;12(4).
47. Schmidinger M, Zielinski CC, Vogl UM, Bojic A, Bojic M, Schukro C, et al. Cardiac toxicity of sunitinib and sorafenib in patients with metastatic renal cell carcinoma. J Clin Oncol. 2008;26(32):5204-12.
48. Ravaud A, Motzer RJ, Pandha HS, George DJ, Pantuck AJ, Patel A, et al. Adjuvant Sunitinib in High-Risk Renal-Cell Carcinoma after Nephrectomy. N Engl J Med. 2016;375(23):2246-54.
49. Escudier B, Eisen T, Stadler WM, Szczylik C, Oudard S, Staehler M, et al. Sorafenib for treatment of renal cell carcinoma: Final efficacy and safety results of the phase III treatment approaches in renal cancer global evaluation trial. J Clin Oncol. 2009;27(20):3312-8.
50. Rini BI, Quinn DI, Baum M, Wood LS, Tarazi J, Rosbrook B, et al. Hypertension among patients with renal cell carcinoma receiving axitinib or sorafenib: analysis from the randomized phase III AXIS trial. Target Oncol. 2015;10(1):45-53.
51. Shah RR, Morganroth J, Shah DR. Cardiovascular safety of tyrosine kinase inhibitors: with a special focus on cardiac repolarisation (QT interval). Drug Saf. 2013;36(5):295-316.
52. Rock EP, Goodman V, Jiang JX, Mahjoob K, Verbois SL, Morse D, et al. Food and Drug Administration drug approval summary: Sunitinib malate for the treatment of gastrointestinal stromal tumor and advanced renal cell carcinoma. Oncologist. 2007;12(1):107-13.

53. Choueiri TK, Schutz FA, Je Y, Rosenberg JE, Bellmunt J. Risk of arterial thromboembolic events with sunitinib and sorafenib: a systematic review and meta-analysis of clinical trials. J Clin Oncol. 2010;28(13):2280-5.
54. Qi WX, Min DL, Shen Z, Sun YJ, Lin F, Tang LN, et al. Risk of venous thromboembolic events associated with VEGFR-TKIs: a systematic review and meta-analysis. Int J Cancer. 2013;132(12):2967-74.
55. Kerkela R, Woulfe KC, Durand JB, Vagnozzi R, Kramer D, Chu TF, et al. Sunitinib-induced cardiotoxicity is mediated by off-target inhibition of AMP-activated protein kinase. Clin Transl Sci. 2009;2(1):15-25.
56. Telli ML, Witteles RM, Fisher GA, Srinivas S. Cardiotoxicity associated with the cancer therapeutic agent sunitinib malate. Ann Oncol. 2008;19(9):1613-8.
57. Motzer RJ, Hutson TE, Tomczak P, Michaelson MD, Bukowski RM, Rixe O, et al. Sunitinib versus interferon alfa in metastatic renal-cell carcinoma. N Engl J Med. 2007;356(2):115-24.
58. Motzer RJ, Hutson TE, Cella D, Reeves J, Hawkins R, Guo J, et al. Pazopanib versus sunitinib in metastatic renal-cell carcinoma. N Engl J Med. 2013;369(8):722-31.
59. van der Graaf WT, Blay JY, Chawla SP, Kim DW, Bui-Nguyen B, Casali PG, et al. Pazopanib for metastatic soft-tissue sarcoma (PALETTE): a randomised, double-blind, placebo-controlled phase 3 trial. Lancet. 2012;379(9829):1879-86.
60. Rini BI, Plimack ER, Stus V, Gafanov R, Hawkins R, Nosov D, et al. Pembrolizumab plus Axitinib versus Sunitinib for Advanced Renal-Cell Carcinoma. N Engl J Med. 2019;380(12):1116-27.
61. Hasinoff BB, Patel D. The lack of target specificity of small molecule anticancer kinase inhibitors is correlated with their ability to damage myocytes in vitro. Toxicol Appl Pharmacol. 2010;249(2):132-9.
62. Maayah ZH, Ansari MA, El Gendy MA, Al-Arifi MN, Korashy HM. Development of cardiac hypertrophy by sunitinib in vivo and in vitro rat cardiomyocytes is influenced by the aryl hydrocarbon receptor signaling pathway. Arch Toxicol. 2014;88(3):725-38.
63. Blanca AJ, Ruiz-Armenta MV, Zambrano S, Miguel-Carrasco JL, Arias JL, Arévalo M, et al. Inflammatory and fibrotic processes are involved in the cardiotoxic effect of sunitinib: Protective role of L-carnitine. Toxicol Lett. 2016;241:9-18.
64. Neves KB, Rios FJ, Jones R, Evans TRJ, Montezano AC, Touyz RM. Microparticles from vascular endothelial growth factor pathway inhibitor-treated cancer patients mediate endothelial cell injury. Cardiovasc Res. 2019;115(5):978-88.
65. Will Y, Dykens JA, Nadanaciva S, Hirakawa B, Jamieson J, Marroquin LD, et al. Effect of the multitargeted tyrosine kinase inhibitors imatinib, dasatinib, sunitinib, and

sorafenib on mitochondrial function in isolated rat heart mitochondria and H9c2 cells. Toxicol Sci. 2008;106(1):153-61.
66. Yang Y, Li N, Chen T, Zhang C, Liu L, Qi Y, et al. Trimetazidine ameliorates sunitinib-induced cardiotoxicity in mice via the AMPK/mTOR/autophagy pathway. Pharm Biol. 2019;57(1):625-31.
67. Cui G, Chen H, Cui W, Guo X, Fang J, Liu A, et al. FGF2 Prevents Sunitinib-Induced Cardiotoxicity in Zebrafish and Cardiomyoblast H9c2 Cells. Cardiovasc Toxicol. 2016;16(1):46-53.
68. Stuhlmiller TJ, Zawistowski JS, Chen X, Sciaky N, Angus SP, Hicks ST, et al. Kinome and Transcriptome Profiling Reveal Broad and Distinct Activities of Erlotinib, Sunitinib, and Sorafenib in the Mouse Heart and Suggest Cardiotoxicity From Combined Signal Transducer and Activator of Transcription and Epidermal Growth Factor Receptor Inhibition. J Am Heart Assoc. 2017;6(10).
69. Jensen BC, Parry TL, Huang W, Ilaiwy A, Bain JR, Muehlbauer MJ, et al. Non-Targeted Metabolomics Analysis of the Effects of Tyrosine Kinase Inhibitors Sunitinib and Erlotinib on Heart, Muscle, Liver and Serum Metabolism In Vivo. Metabolites. 2017;7(3).
70. Zhao Y, Xue T, Yang X, Zhu H, Ding X, Lou L, et al. Autophagy plays an important role in sunitinib-mediated cell death in H9c2 cardiac muscle cells. Toxicol Appl Pharmacol. 2010;248(1):20-7.
71. Rainer PP, Doleschal B, Kirk JA, Sivakumaran V, Saad Z, Groschner K, et al. Sunitinib causes dose-dependent negative functional effects on myocardium and cardiomyocytes. BJU Int. 2012;110(10):1455-62.
72. Matsui T, Shinozawa T. Spontaneous recovery from sunitinib-induced disruption of sarcomere in human iPSC-cardiomyocytes and possible involvement of the Hippo pathway. BMC Pharmacol Toxicol. 2021;22(1):55.
73. Davidson MM, Nesti C, Palenzuela L, Walker WF, Hernandez E, Protas L, et al. Novel cell lines derived from adult human ventricular cardiomyocytes. J Mol Cell Cardiol. 2005;39(1):133-47.
74. Toh YL, Pang YY, Shwe M, Kanesvaran R, Toh CK, Chan A, et al. HPLC-MS/MS coupled with equilibrium dialysis method for quantification of free drug concentration of pazopanib in plasma. Heliyon. 2020;6(4):e03813.
75. Guilhot F, Hughes TP, Cortes J, Druker BJ, Baccarani M, Gathmann I, et al. Plasma exposure of imatinib and its correlation with clinical response in the Tyrosine Kinase Inhibitor Optimization and Selectivity Trial. Haematologica. 2012;97(5):731-8.
76. Mai H, Huang J, Zhang Y, Qu N, Qu H, Mei GH, et al. In-vivo relation between plasma concentration of sorafenib and its safety in Chinese patients with metastatic renal cell carcinoma: a single-center clinical study. Oncotarget. 2017;8(26):43458-69.

77. Reis-Mendes A, Gomes AS, Carvalho RA, Carvalho F, Remião F, Pinto M, et al. Naphthoquinoxaline metabolite of mitoxantrone is less cardiotoxic than the parent compound and it can be a more cardiosafe drug in anticancer therapy. Arch Toxicol. 2017;91(4):1871-90.
78. van Tonder A, Joubert AM, Cromarty AD. Limitations of the 3-(4,5-dimethylthiazol-2-yl)-2,5-diphenyl-2H-tetrazolium bromide (MTT) assay when compared to three commonly used cell enumeration assays. BMC Res Notes. 2015;8:47.
79. Dionísio F, Araújo AM, Duarte-Araújo M, Bastos ML, Guedes de Pinho P, Carvalho F, et al. Cardiotoxicity of cyclophosphamide's metabolites: an in vitro metabolomics approach in AC16 human cardiomyocytes. Arch Toxicol. 2022;96(2):653-71.
80. Repetto G, del Peso A, Zurita JL. Neutral red uptake assay for the estimation of cell viability/cytotoxicity. Nat Protoc. 2008;3(7):1125-31.
81. Reis-Mendes A, Carvalho F, Remião F, Sousa E, Bastos ML, Costa VM. The Main Metabolites of Fluorouracil + Adriamycin + Cyclophosphamide (FAC) Are Not Major Contributors to FAC Toxicity in H9c2 Cardiac Differentiated Cells. Biomolecules. 2019;9(3).
82. Reers M, Smith TW, Chen LB. J-aggregate formation of a carbocyanine as a quantitative fluorescent indicator of membrane potential. Biochemistry. 1991;30(18):4480-6.
83. Cossarizza A, Baccarani-Contri M, Kalashnikova G, Franceschi C. A new method for the cytofluorimetric analysis of mitochondrial membrane potential using the J-aggregate forming lipophilic cation 5,5',6,6'-tetrachloro-1,1',3,3'-tetraethylbenzimidazolcarbocyanine iodide (JC-1). Biochem Biophys Res Commun. 1993;197(1):40-5.
84. Hompland I, Bruland Ø S, Ubhayasekhera K, Bergquist J, Boye K. Clinical implications of repeated drug monitoring of imatinib in patients with metastatic gastrointestinal stromal tumour. Clin Sarcoma Res. 2016;6:21.
85. Verheijen RB, Beijnen JH, Schellens JHM, Huitema ADR, Steeghs N. Clinical Pharmacokinetics and Pharmacodynamics of Pazopanib: Towards Optimized Dosing. Clin Pharmacokinet. 2017;56(9):987-97.
86. Tanaka H, Hiraga H, Takekuma Y, Harabayashi T, Nagamori S, Endo M, et al. Possibility for Dose Optimization of Pazopanib from Its Plasma Concentration in Japanese Patients with Cancer. Biol Pharm Bull. 2020;43(5):762-6.
87. Minami H, Kawada K, Ebi H, Kitagawa K, Kim YI, Araki K, et al. Phase I and pharmacokinetic study of sorafenib, an oral multikinase inhibitor, in Japanese patients with advanced refractory solid tumors. Cancer Sci. 2008;99(7):1492-8.
88. León Z, García-Cañaveras JC, Donato MT, Lahoz A. Mammalian cell metabolomics: experimental design and sample preparation. Electrophoresis. 2013;34(19):2762-75.

89. Chan EC, Pasikanti KK, Nicholson JK. Global urinary metabolic profiling procedures using gas chromatography-mass spectrometry. Nat Protoc. 2011;6(10):1483-99.
90. Araújo AM, Moreira N, Lima AR, Bastos ML, Carvalho F, Carvalho M, et al. Analysis of extracellular metabolome by HS-SPME/GC-MS: Optimization and application in a pilot study to evaluate galactosamine-induced hepatotoxicity. Toxicol Lett. 2018;295:22-31.
91. Pluskal T, Castillo S, Villar-Briones A, Oresic M. MZmine 2: modular framework for processing, visualizing, and analyzing mass spectrometry-based molecular profile data. BMC Bioinformatics. 2010;11:395.
92. Wheelock Å M, Wheelock CE. Trials and tribulations of 'omics data analysis: assessing quality of SIMCA-based multivariate models using examples from pulmonary medicine. Mol Biosyst. 2013;9(11):2589-96.
93. Sumner LW, Amberg A, Barrett D, Beale MH, Beger R, Daykin CA, et al. Proposed minimum reporting standards for chemical analysis Chemical Analysis Working Group (CAWG) Metabolomics Standards Initiative (MSI). Metabolomics. 2007;3(3):211-21.
94. Mastrangelo A, Ferrarini A, Rey-Stolle F, García A, Barbas C. From sample treatment to biomarker discovery: A tutorial for untargeted metabolomics based on GC-(EI)-Q-MS. Anal Chim Acta. 2015;900:21-35.
95. Aickin M, Gensler H. Adjusting for multiple testing when reporting research results: the Bonferroni vs Holm methods. Am J Public Health. 1996;86(5):726-8.
96. Yoav Benjamini YH. Controlling the False Discovery Rate: A Practical and Powerful Approach to Multiple Testing. Journal of the Royal Statistical Society. 1995;57(1):289-300.
97. Berben L, Sereika SM, Engberg S. Effect size estimation: methods and examples. Int J Nurs Stud. 2012;49(8):1039-47.
98. Smith AJ, Ruchaya P, Walmsley R, Wright KE, Lewis-McDougall FC, Bond J, et al. Receptor tyrosine kinase inhibitors negatively impact on pro-reparative characteristics of human cardiac progenitor cells. Sci Rep. 2022;12(1):10132.
99. Vaidya T, Kamta J, Chaar M, Ande A, Ait-Oudhia S. Systems pharmacological analysis of mitochondrial cardiotoxicity induced by selected tyrosine kinase inhibitors. J Pharmacokinet Pharmacodyn. 2018;45(3):401-18.
100. Jia B, Xue Y, Yan X, Li J, Wu Y, Guo R, et al. Autophagy inhibitor chloroquine induces apoptosis of cholangiocarcinoma cells via endoplasmic reticulum stress. Oncol Lett. 2018;16(3):3509-16.
101. Walmsley R, Steele DS, Ellison-Hughes GM, Papaspyros S, Smith AJ. Imatinib Mesylate Induces Necroptotic Cell Death and Impairs Autophagic Flux in Human Cardiac Progenitor Cells. Int J Mol Sci. 2022;23(19).
102. Skárka L, Ostádal B. Mitochondrial membrane potential in cardiac myocytes. Physiol Res. 2002;51(5):425-34.

103. Bouitbir J, Panajatovic MV, Krähenbühl S. Mitochondrial Toxicity Associated with Imatinib and Sorafenib in Isolated Rat Heart Fibers and the Cardiomyoblast H9c2 Cell Line. Int J Mol Sci. 2022;23(4).
104. Clish CB. Metabolomics: an emerging but powerful tool for precision medicine. Cold Spring Harb Mol Case Stud. 2015;1(1):a000588.
105. Saccenti E, Hoefsloot HCJ, Smilde AK, Westerhuis JA, Hendriks MMWB. Reflections on univariate and multivariate analysis of metabolomics data. Metabolomics. 2014;10(3):361-74.
106. Caocci G, Deidda M, Noto A, Greco M, Simula MP, Mulas O, et al. Metabolomic Analysis of Patients with Chronic Myeloid Leukemia and Cardiovascular Adverse Events after Treatment with Tyrosine Kinase Inhibitors. J Clin Med. 2020;9(4).
107. Amaro F, Pisoeiro C, Valente MJ, Bastos ML, Guedes de Pinho P, Carvalho M, et al. Sunitinib versus Pazopanib Dilemma in Renal Cell Carcinoma: New Insights into the In Vitro Metabolic Impact, Efficacy, and Safety. Int J Mol Sci. 2022;23(17).
108. Jensen BC, Parry TL, Huang W, Beak JY, Ilaiwy A, Bain JR, et al. Effects of the kinase inhibitor sorafenib on heart, muscle, liver and plasma metabolism in vivo using non-targeted metabolomics analysis. Br J Pharmacol. 2017;174(24):4797-811.
109. Abdelgalil AA, Mohamed OY, Ahamad SR, Al-Jenoobi FI. The protective effect of losartan against sorafenib induced cardiotoxicity: Ex-vivo isolated heart and metabolites profiling studies in rat. Eur J Pharmacol. 2020;882:173229.